Universidade de Aveiro Departamento de Engenharia de Materiais e Cerâmica
2015

Ishu Kansal

Diopside-Fluorapatite-Wollastonite Based Bioactive Glasses and Glass-ceramics

Vidros e Vitrocerâmicos Bioativos à Base de Diópsido-Fluorapatite-Wollastonite

Universidade de Aveiro
2015
Departamento de Engenharia de Materiais e Cerâmica

Ishu Kansal

Diopside-Fluorapatite-Wollastonite Based Bioactive Glasses and Glass-ceramics

Tese apresentada à Universidade de Aveiro para cumprimento dos requisitos necessários à obtenção do grau de Doutor em Ciência e Engenharia de Materiais, realizada sob a orientação científica do Doutor José Maria da Fonte Ferreira, Professor Associado com Agregação do Departamento de Engenharia Cerâmica e do Vidro da Universidade de Aveiro, e do Doutor Dilshat U. Tulyaganov, Professor Associado com Agregação da Universidade Politécnica de Turim em Tachkent, Uzbequistão.

Apoio financeiro da FCT e do FSE no âmbito do III Quadro Comunitário de Apoio.

Dedicated to my family

o júri

presidente

Doutor Carlos Fernandes da Silva
professor catedrático da Universidade de Aveiro

Doutor José Maria da Fonte Ferreira
professor associado com agregaçao da Universidade de Aveiro

Doutora Maria Clara Henriques Baptista Gonçalves
professora auxiliar do Instituto Superior Técnico da Universidade de Lisboa

Doutor Luís Filipe Santos
professor auxiliar do Instituto Superior Técnico da Universidade de Lisboa

Doutora Maria Ascensão Ferreira Silva Lopes
professora auxiliar da Universidade do Porto

Doutora Maria Elisabete Jorge Vieira da Costa
professora auxiliar da Universidade de Aveiro

agradecimentos

First and foremost, I would like to bow in full thankfulness and humbleness to the Almighty, God, who has given me the ability and strength to complete this research work. At this momentous occasion of compiling my Ph.D. dissertation, I would like to acknowledge the contribution of all those benevolent people; I have been blessed to associate with. The foundation for the successful completion of this research work, leading to my Ph.D. dissertation has been laid by a myriad of people whose help and contribution have made things successful. Since such a list can be prohibitively long, I may be excused for any omissions.

This Ph.D. dissertation came into being because of the immense faith shown by my supervisor, Professor José M.F. Ferreira, in me and my capabilities. It has been an honour to be his Ph.D. student. He was the person who gave me an opportunity to prove my potential and was always there by my side as a guiding torch during all odds. I appreciate all his contributions of time, ideas and funding to make my Ph.D. experience productive and stimulating. The joy and enthusiasm he has for his research was contagious and motivational for me, even during tough times in the Ph.D. pursuit. I am thankful for an excellent example he has provided as a successful scientist and professor.

I also wish to express my appreciation to my co-supervisor, Professor Dilshat U. Tulyaganov, who taught me the fundamentals of glass science and introduced me to the field of bioactive glasses. In the absence of his moral support and scientific guidance, it would have been really difficult to accomplish this arduous task with success.

Sincere thanks to Dr. Maria J. Pascual (CSIC-ICV, Madrid, Spain) and Prof. Hae-Won Kim (Dankook University, S. Korea) for their scientific collaboration.

The members of my research group have contributed immensely to my personal and professional time at Aveiro. I am especially thankful to Dr. Hugo R. Fernandes, Dr. Allu Amarnath Reddy, Mr. Raghu R. Rajagopal, Mr. Avito H.S. Rebelo, and Dr. Susana M.H. Olhero for their unconditional support. Words are inadequate to express my sincere gratitude for Dr. Saurabh Kapoor as without his support it would have been difficult to get my PhD accomplished. My keen appreciation goes to all the administrative and technical staff, especially Dr[a] Alexandra Vale, and Mrs. Célia Miranda for their support at both personal and professional level.

I gratefully acknowledge the financial support from CICECO, and Fundação para a Ciência e a Tecnologia (SFRH/BD/70917/2010) during my Ph.D. work.

Lastly, I would like to thank my family for all their love and encouragement. For my parents who raised me with love and supported me in all my pursuits. Most of all, I am thankful to my husband (Prof. Ashutosh Goel) and kids (Akul and Aadhya) for their support and encouragement in completing this odyssey.

palavras-chave bioactividade, vidros, vitrocerâmicos, diópsido, sinterização, estrutura

resumo

Os vidros e vitrocerâmicos bioactivos são uma classe de biomateriais que induzem uma resposta especial à sua superfície quando em contacto com fluidos biológicos que conduz a uma forte ligação ao tecido vivo. Esta característica particular conjugada com uma boa aptidão para a sinterização e elevada resistência mecânica torna estes materiais ideais para a fabricação de estruturas de suporte à regeneração óssea. O trabalho apresentado nesta tese pretende dar um contributo para uma melhor compreensão das relações entre composição-estrutura-propriedades em vidros potencialmente bioactivos com composições no sistema $CaO–MgO–P_2O_5–SiO_2–F$, em alguns casos com a adição de Na_2O. O estudo da influência exercida pela composição do vidro na estrutura molecular, capacidade de sinterização e nível de bioactividade dos vidros fosfosilicatados foi objecto de especial atenção. As composições vítreas foram concebidas no campo da cristalização primária do pseudo sistema ternário do diópsido ($CaO•MgO•2SiO_2$) – fluorapatite ($9CaO•3P_2O_5•CaF_2$) – wollastonite, e estudou-se o impacto das variações composicionais na estrutura, nas propriedades e na capacidade de sinterização destes vidros. Todos os vidros investigados neste trabalho foram preparados por fusão e fritagem e caracterizados quanto à sua estrutura molecular, capacidade de sinterização, degradação química e bioactividade, usando uma grande variedade de técnicas experimentais. Ficou demonstrado que em todas as composições de vidro investigadas a rede de silicato era dominada principalmente por unidades Q^2 enquanto o fosfato se encontrava coordenado em ambiente de ortofosfato. As composições de biovidros isentas de alcalinos do sistema diópsido–fluorapatite demonstram possuir excelente capacidade de sinterização e elevados níveis de bioactividade, atributos que os qualificam como materiais promissores para a fabricação de estruturas de suporte à regeneração de tecidos ósseos, enquanto os vidros bioactivos contendo alcalinos foram mais difíceis de densificar durante a sinterização e induziram citotoxicidade *in vitro*, não sendo candidatos ideais para a engenharia de tecidos. Uma das nossas composições de biovidro com um baixo teor de sódio foi testada com sucesso tanto *in vivo* como em ensaios clínicos preliminares. Mas este trabalho precisa de ser continuado e aprofundado. A dispersão de fritas moídas em meio aquoso ou outros solventes adequados, e o estudo dos factores mais relevantes que condicionam a reologia das suspensões são etapas essenciais para viabilizar o processo de fabrico de suportes porosos com estruturas hierárquicas de poros feitas por medida através de técnicas de processamento avançadas tais como o Robocasting.

keywords bioactivity, glasses, glass-ceramics, diopside, sintering, structure

abstract

Bioactive glasses and glass–ceramics are a class of biomaterials which elicit special response on their surface when in contact with biological fluids, leading to strong bonding to living tissue. This particular trait along with good sintering ability and high mechanical strength make them ideal materials for scaffold fabrication. The work presented in this thesis is directed towards understanding the composition-structure-property relationships in potentially bioactive glasses designed in $CaO–MgO–P_2O_5–SiO_2–F$ system, in some cases with added Na_2O. The main emphasis has been on unearthing the influence of glass composition on molecular structure, sintering ability and bioactivity of phosphosilicate glasses. The parent glass compositions have been designed in the primary crystallization field of the pseudo-ternary system of diopside ($CaO•MgO•2SiO_2$) – fluorapatite ($9CaO•3P_2O_5•CaF_2$) – wollastonite ($CaO•SiO_2$), followed by studying the impact of compositional variations on the structure-property relationships and sintering ability of these glasses. All the glasses investigated in this work have been synthesized via melt-quenching route and have been characterized for their molecular structure, sintering ability, chemical degradation and bioactivity using wide array of experimental tools and techniques. It has been shown that in all investigated glass compositions the silicate network was mainly dominated by Q^2 units while phosphate in all the glasses was found to be coordinated in orthophosphate environment. The glass compositions designed in alkali-free region of diopside – fluorapatite system demonstrated excellent sintering ability and good bioactivity in order to qualify them as potential materials for scaffold fabrication while alkali-rich bioactive glasses not only hinder the densification during sintering but also induce cytotoxicity in vitro, thus, are not ideal candidates for in vitro tissue engineering. One of our bioglass compositions with low sodium content has been tested successfully both in vivo and in preliminary clinical trials. But this work needs to be continued and deepened. The dispersing of fine glass particles in aqueous media or in other suitable solvents, and the study of the most important factors that affect the rheology of the suspensions are essential steps to enable the manufacture of porous structures with tailor-made hierarchical pores by advanced processing techniques such as Robocasting.

List of Tables

List of Figures

List of Publications

1. **I. Kansal**, A.A. Reddy, F. Muñoz, S.-J. Choi, H.-W. Kim, D.U. Tulyaganov, J. M.F. Ferreira, Structure, biodegradation behaviour and cytotoxicity of alkali-containing alkaline-earth phosphosilicate glasses, Materials Science and Engineering C 44 (2014) 159–165.
2. **I. Kansal**, D.U. Tulyaganov, M.J. Pascual, L. Gremillard, A. Malchere, J.M.F. Ferreira, Sintering behaviour of diopside ($CaO•MgO•2SiO_2$) – fluorapatite ($9CaO•3P_2O_5•CaF_2$) bioactive glass, Journal of Non-Crystalline Solids 380 (2013) 17–24.
3. **I. Kansal**, A. Goel, D.U. Tulyaganov, R.R. Rajagopal, J.M.F. Ferreira, Structural and thermal characterization of $CaO–MgO–SiO_2–P_2O_5–CaF_2$ glasses, Journal of the European Ceramic Society 32 (2012) 2739–2746.
4. **I. Kansal**, A. Goel, D.U. Tulyaganov, M.J. Pascual, H.Y.-Lee, H.W.-Kim, J.M.F. Ferreira, Diopside-fluorapatite glass-ceramics: Potential materials for bone tissue engineering, Journal of Materials Chemistry 21 (2011) 16247–16256.
5. **I. Kansal,** A. Goel, D.U. Tulyaganov, L.F. Santos, J.M.F. Ferreira, Structure, surface reactivity and physico-chemical degradation of fluoride containing phosphosilicate glasses, Journal of Materials Chemistry 21 (2011) 8074–8084.
6. **I. Kansal**, D.U. Tulyaganov, A. Goel, M.J. Pascual, J.M.F. Ferreira, Structure and thermal behaviour of diopside-fluorapatite-wollastonite based glasses and glass-ceramics, Acta Biomaterialia 6 (2010) 4380–4388.
7. **I. Kansal**, A. Goel, D.U. Tulyaganov, E.R. Shaaban, M.J. Ribeiro, J.M.F. Ferreira, The effect of fluoride ions on the structure and crystallization kinetics of diopside based oxyfluoride glasses, Ceramics International 35 (2009) 3489–3493.
8. **I. Kansal**, A. Goel, D.U. Tulyaganov, J.M.F. Ferreira, Effect of some rare-earth oxides on the structure and crystallization behaviour of diopside based glasses, Ceramics International 35 (2009) 3221–3227.

.....

Contents

List of symbols and notations

ρ	Density
Q^n	Degree of polymerization
V_e	Excess volume
M	Molar mass of glass
V_m	Molar volume
T_{dg}	Dilatometric glass transition temperature
T_s	Dilatometric softening temperature
T_g	Glass transition temperature
β	Heating rate
T_c	Temperature for onset of crystallization
T_p	Peak temperature of crystallization
T_{FS}	Temperature of first shrinkage
T_{MS}	Temperature of maximum shrinkage
ΔT	Thermal stability parameter
S_c	Sintering ability parameter
K_{ps}	Solubility product
χ^2	Goodness of fit in Rietveld refinement
R_{wp}	Weighted profile R- factor
R_p	Profile R- factor

List of abbreviations

AAS	Atomic absorption spectroscopy
AIMD	Ab initio molecular dynamic
ALP	Alkaline phosphatase
CTE	Coefficient of thermal expansion
DTA	Differential thermal analysis
EDS	Energy dispersive spectroscopy
FTIR	Fourier transform infrared spectroscopy
FBS	10% Foetal bovine serum
HSM	Hot stage microscope
ICP-OES	Inductive coupled plasma – optical emission spectroscopy
MAS	Magic angle spinning
MSC	Mesenchymal stem cells
MEM	α-Minimal essential medium
MTS	(3-(4,5-dimethylthiazol-2-yl)-5(3-carboxymethonyphenol)-2-(4-sulfophenyl)-2H-tetrazolium)
NC	Network connectivity
NMR	Nuclear magnetic resonance
SBF	Simulated body fluid
SEM	Scanning electron microscope
XRD	X-ray diffraction

Chapter 1. Introduction

A lot of advancement has been made in the field of glass science and as a result, glass materials have found applications in various technological domains, thus, improving the quality of human life. Some of the most common examples of glasses being used in different technological applications include: Float Glass (mainly soda-lime silica), Gorilla® (chemically strengthened, alkali-alkaline-earth aluminosilicate), Eagle® (alkaline-earth aluminosilicate), Pyrex® (low thermal expansion borosilicate) and, Borosil® (borosilicate). However, there also exist wide ranges of glass compositions which are used in various other important technological applications but are not known to common man. Some of the most prominent examples for such application include: radioactive waste immobilization, human biomedicine, specialty sealing and optical fibers.

The application of glasses as 'biomaterials' is one such area which has revolutionized the field of human biomedicine and has brought the concept of 'surface active' materials which have the ability to elicit a special response on its surface when in contact with biological fluids, leading to strong bonding to living bone or tissue [1]. The concept of 'bioactive' or surface active glasses/ceramics was introduced by Professor Larry L. Hench at University of Florida in late 1960s by the discovery of 45S5 Bioglass® with its chemical composition designed close to the eutectic of soda-lime silica ternary system (mol.%: 46.1SiO_2 – 26.9CaO – 24.4 Na_2O – 2.5 P_2O_5) (Figure 1.1) [2]. Since its discovery, 45S5 Bioglass® has been used in >650,000 human patients and is being marketed for various dental and orthopedic applications under different commercial brand names, for example: PerioGlass® and NovaBone® [1-3]. This has led to a considerable effort towards understanding the fundamental science governing the chemical, thermal and other properties of bioactive glasses based on – or – inspired by 45S5 Bioglass® so that novel glasses with enhanced biological efficacy can be designed [4-9].

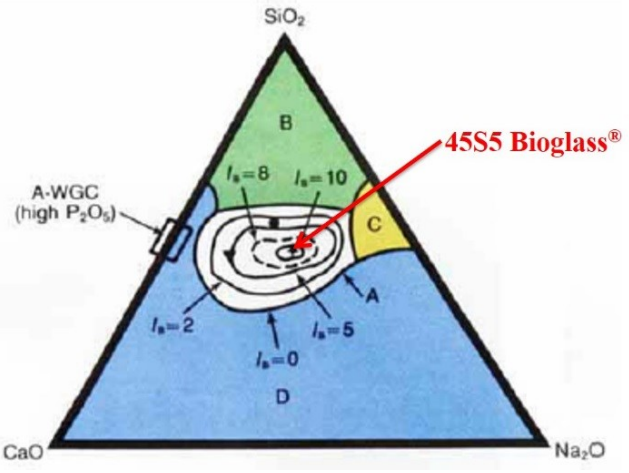

Figure 1.1. Ternary phase diagram of Na_2O-CaO-SiO_2 system depicting the glass forming region of 45S5 Bioglass® [2].

Despite its huge success, 45S5 Bioglass® (and other bioactive glasses with high alkali-content) has some inherent drawbacks which do not warrant its application in some of the most advanced areas of human biomedicine, for example: *in vitro* tissue engineering. *In vitro* tissue engineering involves the manipulation of cells *in vitro* on porous scaffolds, prior to implantation into the *in vivo* environment [10]. Accordingly, an ideal porous scaffold is expected to exhibit good biocompatibility with controlled dissolution behaviour and should be able to balance the temporary mechanical function with mass transport to aid biological delivery and tissue regeneration in three dimensions (3D) [11]. Interestingly, 45S5 Bioglass® does not meet the abovementioned pre-requisites due to its: (i) poor sintering ability and high crystallization tendency which convert it into a bio-inert glass-ceramic with poor mechanical strength [12, 13], (ii) high chemical dissolution in aqueous solutions and body fluids leading to sudden changes in pH environment (due to alkali outburst), thus, resulting in apoptosis *in vitro* [14].

Another potentially viable candidate for the task of scaffold fabrication is apatite-wollastonite (A/W) glass-ceramic (CERABONE® A-W) developed by Kokubo et al. [15], along the pseudo ternary system $3CaO{\bullet}P_2O_5 - CaO{\bullet}SiO_2 - MgO{\bullet}CaO{\bullet}2SiO_2$ and comprising of 38 wt.% apatite [$Ca_{10}(PO_4)_6(O, F_2)$], 24 wt.% wollastonite ($CaSiO_3$) and 28 wt.% residual glassy phase. The glass-ceramic is known to exhibit good sintering ability, high mechanical strength (flexural strength: 215 MPa and Young´s modulus: 118 GPa) and good bioactivity. Despite these salient features, the glass-ceramic scaffolds derived from this composition still are not suitable materials for scaffold fabrication mainly due to their slow degradation (owing to their high crystalline content, especially high apatite content with high chemical durability), often taking some years to disappear from the body [16]. The slow degradation of glass-ceramic scaffold may lead to reduction in its effective pore size by *in vivo* events such as the invasion of fibrous tissue into the pores and the nonspecific adsorption of proteins onto the material's surface.

Therefore, there is an exigent need to design low – or – negligible alkali content silicate glasses with controlled chemical dissolution, good sintering ability, high mechanical strength and excellent bioactive properties suitable for scaffold fabrication for their application in tissue engineering. However, the design of a multicomponent glass composition exhibiting the above-mentioned desired properties cannot be accomplished through trial-and-error approach as it needs an in-depth understanding of fundamental science governing the various macroscopic

properties of the potentially bioactive glass systems. Accordingly, the work reported in this dissertation has been directed towards fulfilment of the following aims:

1. To understand the glass forming region in alkali-free CaO – MgO – P_2O_5 – SiO_2 – F system.
2. To understand composition – structure – property relationships in phosphosilicate bioactive glasses.
3. To understand the sintering mechanism in alkaline-earth phosphosilicate bioactive glasses and its implications on the bioactivity of the resultant glass-ceramic.
4. To understand the impact of compositional variation on the structure, chemical durability, thermal stability and bioactivity of these glasses.

We hope that the work reported in this dissertation will be a good contribution to the growing knowledge base in the field of biomaterials and will be helpful in designing materials with novel applications in the field of human biomedicine.

References

[1] L. L. Hench, D. E. Day, W. Holand, and V. M. Rheinberger, "Glass and Medicine," *International Journal of Applied Glass Science,* vol. 1, pp. 104-117, 2010.

[2] L. L. Hench, "Bioceramics - from Concept to Clinic," *Journal of the American Ceramic Society,* vol. 74, pp. 1487-1510, 1991.

[3] L. Hench, "The story of Bioglass®," *Journal of Materials Science: Materials in Medicine,* vol. 17, pp. 967-978, 2006.

[4] A. Tilocca, "Structural models of bioactive glasses from molecular dynamics simulations," *Proceedings of The Royal Society A*, vol. 465, pp. 1003-1027, 2009.

[5] A. Tilocca, A. N. Cormack, and N. H. de Leeuw, "The formation of nanoscale structures in soluble phosphosilicate glasses for biomedical applications: MD simulations," *Faraday Discussions,* vol. 136, pp. 45-55, 2007.

[6] A. Tilocca, A. N. Cormack, and N. H. de Leeuw, "The structure of bioactive silicate glasses: New insight from molecular dynamics simulations," *Chemistry of Materials,* vol. 19, pp. 95-103, Jan 9 2007.

[7] L. Lefebvre, J. Chevalier, L. Gremillard, R. Zenati, G. Thollet, D. Bernache-Assolant, and A. Govin, "Structural transformations of bioactive glass 45S5 with thermal treatments," *Acta Materialia,* vol. 55, pp. 3305-3313, 2007.

[8] O. Bretcanu, X. Chatzistavrou, K. Paraskevopoulos, R. Conradt, I. Thompson, and A. R. Boccaccini, "Sintering and crystallisation of 45S5 Bioglass® powder," *Journal of the European Ceramic Society,* vol. 29, pp. 3299-3306, 2009.

[9] L. Lefebvre, L. Gremillard, J. Chevalier, R. Zenati, and D. Bernache-Assolant, "Sintering behaviour of 45S5 bioactive glass," *Acta Biomaterialia,* vol. 4, pp. 1894-1903, 2008.

[10] W. T. Godbey and A. Atala, "In Vitro Systems for Tissue Engineering," *Annals of the New York Academy of Sciences,* vol. 961, pp. 10-26, 2002.

[11] S. J. Hollister, "Porous scaffold design for tissue engineering," *Nature Materials,* vol. 4, pp. 518-524, 2005.

[12] D. C. Clupper and L. L. Hench, "Crystallization kinetics of tape cast bioactive glass 45S5," *Journal of Non-Crystalline Solids,* vol. 318, pp. 43-48, 2003.

[13] A. R. Boccaccini, Q. Chen, L. Lefebvre, L. Gremillard, and J. Chevalier, "Sintering, crystallisation and biodegradation behaviour of Bioglass®-derived glass-ceramics," *Faraday Discussions,* vol. 136, pp. 27-44, 2007.

[14] K. E. Wallace, R. G. Hill, J. T. Pembroke, C. J. Brown, and P. V. Hatton, "Influence of sodium oxide content on bioactive glass properties," *Journal of Materials Science: Materials in Medicine,* vol. 10, pp. 697-701, 1999.

[15] T. Kokubo, M. Shigematsu, Y. Nagashima, M. Tashiro, T. Nakamura, and T. Yamamuro, "Apatite and wollastonite containing glass-ceramics for prosthetic applications," *Bulletin of Institute of Chemical Research, Kyoto University,* vol. 60, pp. 260-268, 1982.

[16] M. Neo, T. Nakamura, C. Ohtsuki, T. Kokubo, and T. Yamamuro, "Apatite formation on three kinds of bioactive material at an early stage in vivo: A comparative study by transmission electron microscopy," *Journal of Biomedical Materials Research,* vol. 27, pp. 999-1006, 1993.

Chapter 2. State of the art

2.1 Biomaterials

A biomaterial is a natural or synthetic material to be used in intimate contact with living tissue. In 1986, at the Consensus Conference of the European Society for Biomaterials, biomaterial was defined as "a nonviable material used in a medical device, intended to interact with biological systems" [1]. Synthetic biomaterials have been broadly classified into three separate categories, on the basis of the strength of the response that the exposure of the implant to a biological medium elicits in the living environment (Figure 2.1) [2, 3].

Bio-inert or First-generation biomaterials, developed during the 1960s and 1970s, are metals or alloys (titanium, stainless steel, cobalt–chrome) and dense or porous ceramics (Al_2O_3 or alumina and ZrO_2 or zirconia). They are *bioinert*, owing to their absent or weak interaction with living tissues upon implant: in the past, the minimal response from the host was in fact considered a desirable feature of any biomaterial for use inside the human body. Following contact with biological fluids, inert biomaterials are encapsulated within a non-adherent, fibrous layer of variable thickness. The implant–tissue interaction is essentially of mechanical nature, as the material can be cast and pressed in place to yield a suitably tight fit: this result in a very thin fibrous layer, which is crucial for the success of inert implants, as it reduces relative movement at the implant–tissue interface. Interfacial movement under external stress leads to loosening and deterioration of the mechanical fit, which causes pain and eventually leads to clinical failure of bioinert implants [2]. While porous ceramics can achieve a better mechanical fit thanks to tissue in-growth in the micropores [4], the absence of a real chemical adhesion with the tissues, combined with the reduction in strength inherent to the porous structure, limits their long-term durability in porous ceramic implants as well, and they have found applications mostly as bone spacers and scaffolds.

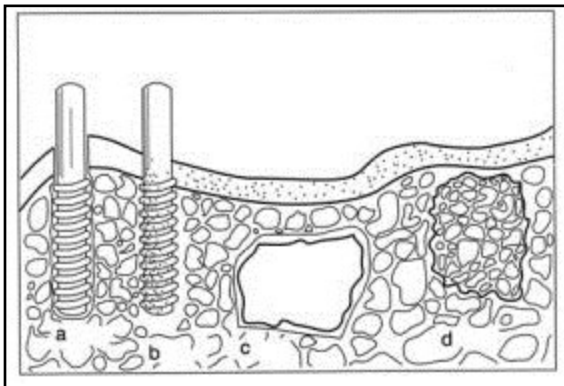

Figure 2.1 Classification of biomaterials according to their bioactivity (a) bioinert alumina dental implant, (b) bioactive hydroxyapatite [$Ca_{10}(PO_4)_6(OH)_2$] coating on a metallic dental implant, (c) surface active bioglass and (d) bioresorbable tricalcium phosphate ([$Ca_3(PO_4)_2$] [3]

The opposite case of bio-inert materials is represented by ***resorbable or completely biodegradable materials***, such as calcium phosphates, either crystalline or amorphous, which are rapidly dissolved upon exposure to physiological fluids, and gradually replaced with living tissues [5, 6]. This procedure is, in principle, ideal, being based on the natural ability of bone and muscles to self-heal and regenerate, but is complicated by the need to match the rates of implant dissolution and tissue growth; while the implant is being replaced by new tissue, its strength will progressively decrease, and a very unstable interface will result, requiring immobilization of the patient for long periods.

Surface-active or bioactive materials represent an ideal compromise between these two limits: after implant, a bioactive material rapidly forms a stable bond with the tissues through a reactive surface layer. The chemical nature of this bond considerably enhances the interfacial adhesion of the implant; at the same time, the reactivity of bioactive materials is limited to their surface, owing to progressive passivation by the surface layer, which does not allow further degradation to progress rapidly to the bulk material, and therefore a stable interface is maintained long enough to favour further cellular interaction and induce controlled growth of mature tissues. Several biomaterials belong to this category: the first bioactive materials were discovered by Hench *et al*. (1971) *ca* 40 years ago [7]; they showed that specific compositions of melt-derived Na_2O–CaO–SiO_2–P_2O_5 glasses can form a strong bond with hard (bone) and in some cases soft (muscle and tendons) connective tissues, through a sequence of rapid chemical processes that follow their implant *in vivo* or the *in vitro* contact with a physiological test solution. Until few years back, it was well accepted and agreed that the key feature which leads to the bone-bonding ability of bioactive glasses (and of bioactive materials in general), is the formation of a film of crystalline hydroxyapatite (HA) on their surface. Since HA is the mineral component of bone, its presence on the glass surface was considered to promote further cellular steps, such as incorporation of collagen and interaction with other biomolecules and tissue growth factors, which then favour the development of a biological bond with the tissues [2, 8-10]. However, recent literature suggests that formation of HA layer on the glass surface is not critical for the bioactivity of the material [11] as the ionic dissolution products from the bioactive glasses/ceramics appear to stimulate the growth and differentiation of cells at the genetic level [12], an effect which has been considered to be dose dependent [13, 14]. Despite the controversy surrounding the importance of HA layer formation on the surface of bioactive glasses/ceramics,

it still enjoys the support of the scientific community and is considered to be the marker of bioactivity during initial screening of biomaterials [15]. Therefore, we shall follow this protocol for the work reported in this dissertation.

2.2 Bioactive materials

Bioactive materials have been classified in two different sets namely, 'Class A' and 'Class B'. Class A bioactivity is 'The process whereby a biological surface is colonized by osteogenic stem cells free in the defect environment as a result of surgical intervention'. An extra- as well as intracellular response is elicited by a 'Class A' bioactive material at the interface. Such materials are said to be osteoproductive. 'Class B' bioactivity is a bioinductive pathway that allows bone to grow along it, thus, the material only exhibits an extracellular response at the interface. Such materials are known as osteoconductive [16]. Bioactive glasses and glass-ceramics are typical examples of 'Class A' biomaterials. The development in the field of bioactive glasses has not yet reached its potential and research activity in this field if still growing as is evident from these recent review articles [9, 14, 17-20]

2.3 Compositional and structural design of bioactive glasses

Glass network former

Until today, bioactive glasses have been designed in borate [21-23], phosphate [6, 24] and silicate [7, 25, 26] glass systems. However, silicate glasses have always received considerable attention in comparison to the other two systems mainly due to their higher chemical and thermal stability which allows easy synthesis and processing of these glasses and provides flexibility to tailor their chemical compositions

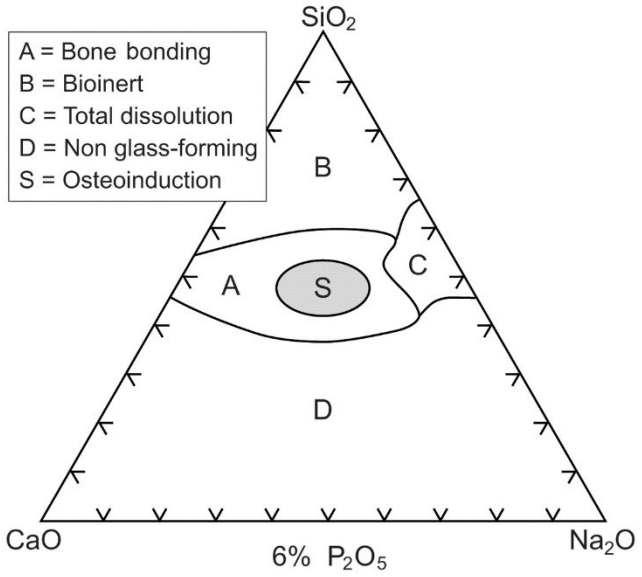

Figure 2.2 Compositional dependence of bioactivity in Na_2O-CaO-SiO_2-P_2O_5 glass system.

in order to achieve desired properties. Also it has been reported that release of silica species from the bioactive glasses in the range of 0.1 ppm to 100 ppm exhibits stimulatory effects on the osteoblasts and the expression of TGF-β mRNA in human osteoblast-like cells [27].

Several studies on the chemical dissolution and bioactivity of different glass compositions in the silicate glass system have led to the establishment of an empirical model describing the relationship between the chemical composition and bioactivity of silicate glasses wherein a glass with SiO_2 content varying between 45 – 52 wt.% exhibits highest bioactivity. In this compositional range, a bonding both to soft and hard connective tissue occurs within 5-10 days. Bioactive glasses and glass-ceramics containing 55 – 60 wt.% SiO_2 require a longer time to form a bond with bones and do not bond to soft tissues. Glass compositions with >60 wt.% SiO_2 do not bond either to bone or soft tissues, and elicit formation of a non-adherent fibrous interfacial capsule [28]. Figure 2.2 exhibits the compositional dependence of bioactivity in the silicate glasses designed in soda-lime silica system. It is noteworthy that this composition-bioactivity relationship has been established for glasses synthesized through melt-quenched route and may not be considered valid for sol-gel glasses as HA formation on the surface of glasses with 90 mol% SiO_2 content has been observed in this case when in contact with SBF solution [29]. These differences in bioactivity of melt-quenched glasses versus sol-gel glasses are due to different surface chemistry of the two systems considering the high amount of inherent porosity and molecular water present in the sol-gel glasses [29].

From the structural viewpoint, it has been well established that molecular structure of glasses plays a crucial role in deciding their bioactivity. For example, the high level of bioactivity in 45S5 Bioglass® is known to arise from a structure dominated by chains of Q^2 metasilicates, which are occasionally cross-linked through Q^3 units, whereas Q^1 species terminate the chains, where Q^n species distribution furnishes a measure of the connectivity of the glass network and the index n refers to the number of bridging oxygens (BOs) surrounding network former ions [30]. Similarly, the enhanced dissolution of silica in highly bioactive compositions has also been found to be closely related to the significant fraction of Q^1 *(Si)* chain terminators while moderate bioactivity can be achieved when Q^3 *(Si)* structures predominate [30].

The incorporation of P_2O_5 in silicate-based bioactive glasses induces significant structural changes as has been elucidated by experimental [31, 32] as well as computational studies [33],

thus, impacting the overall bioactivity of the glass system. The physiological response of silicate-based bioactive glasses is known to depend critically on both the P_2O_5 content and silicate network connectivity (NC). Since network modifying cations have higher affinity for phosphate groups, incorporating P_2O_5 in bioactive glasses strips the network modifying cations out of silicate glass network, thus inducing re-polymerization. Therefore, substantial fraction of P_2O_5 in bioactive glass may increase its network connectivity (NC), thus exhibiting negative impact on its bioactivity. On the other hand, P_2O_5 when added in small concentrations (2 – 10 mol.%) coordinates itself predominantly in orthophosphate environment (Q^0 *(P)*) and does not participate to form the part of actual glass network backbone [34, 35]. Structural studies on compositionally complex bioactive glasses are yet to be reported. While the bioactivity generally displays a non-monotonic dependence of P_2O_5 concentration, literature suggests that it is merely the net orthophosphate content that directly links to the bioactivity [34-36].

Glass network modifier

The choice of glass network modifiers for the design of bioactive glasses has been mainly confined to alkali and alkaline-earth oxides because of their ability to tailor the molecular structure of glasses to achieve desired properties and more importantly owing to their biological significance. For example: calcium is the main component of human bone and its importance in bone mineralization process and effect on cell specific responses has been well established [37]. It is due to this reason that CaO has become an integral component of bioactive glasses. However, it is difficult to obtain a stable melt-quenched glasses from $CaO–SiO_2$ binary system due to their higher tendency towards crystallization. This problem has been overcome by incorporation of alkali oxides in the glasses which not only create non-bridging oxygens in the silicate glass structure but also expand the glass forming region from $CaO–SiO_2$ binary system to soda-lime-silica ternary system as shown in Fig. 2.2. As mentioned in *Chapter 1: Introduction*, the 45S5 Bioglass® composition has been designed near the eutectic of soda-lime silica system (which was the original basis of selecting this composition for investigation by Hench et al. [16]) but far from the typical compositions of soda-lime glasses, which contain much more silica.

Despite being the primary cation in extracellular fluids in animals and humans (sodium: 135-145 mmol l^{-1} and potassium: 3.6 – 5.1 mmol l^{-1}) and their importance in generation of nerve

impulses, finer regulation of the fluid balance, regulating blood volume, blood pressure, osmotic equilibrium and pH, the influence of alkali-ions on the bioactivity of silicate glasses has been rarely studied. According to Wallace et al. [38], incorporating sodium ions in silicate glasses induces cytotoxicity *in vitro* thus, resulting in apoptosis. Similar observations have also been reported in our recent study where sodium-free glass composition exhibited the highest cell viability and proliferation on its surface while incorporation of 2-10 mol.% Na_2O in silicate glasses resulted in apoptosis over a duration of 7 – 14 days [39]. The reason for this behavior has been explained on the basis of Na:Ca ratio and their mutual interaction in glasses in Chapter 4. Interestingly, 45S5 Bioglass® contains 24-25 mol.% Na_2O, still it has been used in >650,000 human patients [9] owing to the ability of the human renal system to get rid of all the excess sodium in order to maintain osmo-regulation. However, these observations raise serious concerns for application of alkali-containing bioactive glasses in *in vitro* tissue engineering. Further, the fast dissolution behavior [40] and poor sintering ability [41] of glasses with high alkali-content (>10 mol.%), for example: 45S5 Bioglass, renders them unfit for their aqueous processing and scaffold fabrication. Therefore, in order to design glasses with controlled dissolution behavior, good sintering ability and minimal cytotoxicity *in vitro*, their alkali content needs to be well optimized.

Apart from sodium and calcium, another cation which though is non-essential for the bioactive glass design but plays crucial role in enhancing their biological efficacy is magnesium (Mg^{2+}). Magnesium is the fourth most abundant cation in human body with an estimated 1 mole of magnesium stored in the body of a normal 70 kg adult, with approximately half of the total physiological magnesium stored in bone tissue [42]. It is essential to bone metabolism and has been shown to have stimulating effects on new bone formation [43]. Magnesium is a co-factor for many enzymes, and stabilizes the structures of DNA and RNA. Rude et al. [44, 45] observed that magnesium depletion results in impaired bone growth, increased bone resorption and loss in trabecular bone underlining the significant role that magnesium plays in bone metabolism. The level of magnesium in the extracellular fluid ranges between 17 ppm and 25.5 ppm, where homeostasis is maintained by the kidneys and intestine [42, 46]. Although magnesium levels exceeding 25.5 ppm can lead to muscular paralysis, hypotension and respiratory distress and cardiac arrest occurs for severely high serum levels of 145–170 ppm, the incidence of hyper-magnesium is rare due to the efficient excretion of the element in the urine [42, 46, 47]. One

important factor that leads to the incorporation of magnesium in bioactive glasses is its ability to increase their fracture toughness and lower their Young's modulus [48, 49].

From structural viewpoint, the influence of magnesium on structure of glasses has been well described in literature [36, 48, 50-54]. MgO is considered to behave like CaO (i.e. network modifier) within a silicate glass structure [54] but its elemental properties such as charge to size ratio and Pauling electronegativity suggest that Mg^{2+} falls on the boundary between being a network modifier and an intermediate oxide [51]. Accordingly, the structural coordination of magnesium in silicate glasses has been shown to depend on glass chemistry as it has been found to exist in 4-, 5- and 6- fold coordination in these glasses. Pedone et al. (using molecular dynamic simulations) found magnesium to exist in four-coordination in a silica-rich (SiO_2 = 75 mol.%) soda lime silica glass [49] while it was found to exist in five-coordination in 45S5 Bioglass® [48] and also in alkali-free bioactive glasses [55]. The overall network connectivity and number of non-bridging oxygens (NBOs) remained unchanged with varying CaO/MgO ratio. Similar results have been obtained by Watts et al. [51] while experimentally investigating the influence of CaO/MgO ratio on the structure and thermal properties of soda-lime silica based bioactive glasses. Further, it has been reported that among sodium, calcium and magnesium ions, Mg^{2+} has the least affinity to associate with phosphate component in a bioactive glass possibly due to its role as an intermediate [48, 55].

The influence of magnesium on the *in vitro* bioactivity has been reported for both melt-quenched and sol-gel derived glasses [52, 53, 56-61]. Magnesium is known to associate preferentially to phosphorus at the glass surface thus, making the surface of glass poorer in calcium (in comparison to bulk) which slows down (but not hinder) the apatite forming ability of glasses when immersed in SBF solution due to lack of apatitic nucleation domains [52, 53, 56]. However, considering the influence of ionic dissolution products at the genetic level and importance of magnesium in bone regeneration and tissue engineering, the retardation in the HA layer formation on bioactive glass surface may be ignored. Similar observations have been reported for strontium and zinc incorporation in the bioactive glasses [55, 62].

Intermediates

Al_2O_3 and TiO_2 are the two most common intermediate oxides that have been used in design of bioactive glass compositions [63-66]. Since both these oxides have been shown to

increase the chemical durability of glasses (thus, decreasing their bioactivity), their usage (if any) in bioactive glass compositions has been confined to small amounts i.e. 1 – 2 mol.%. It is noteworthy that apatite-mullite glass-ceramics (containing significant amount of Al_2O_3) have been found biocompatible *in vivo* (not *in vitro*) [67]. However, most of the Al_2O_3 in these glass-ceramics is concentrated in crystalline regions of the final product and these materials exhibit very slow chemical degradation behaviour. Similarly, TiO_2 has been used in significant amounts in phosphate based bioactive glasses as it slows down their chemical degradation in body fluids and tailor bioactivity [68-70]. All the glasses studied in our work are Al_2O_3- and TiO_2- free.

Additives

Several inorganic functional ions (for example, Sr^{2+}, Zn^{2+}, Cu^{2+}, F^-, etc.) might be added to the glass compositions in trace quantities in order to design gene-activating bioactive glasses with controlled release of functional ions tailored for specific patients and disease states. For example, although the amount of strontium in the skeleton is only 0.335% of its calcium content [71], its important role in treatment of osteoporosis by promoting bone regeneration through osteoblast replication has resulted in development of strontium containing bioactive glasses for orthopaedic applications [62, 72-76]. Similarly, owing to their favourable attributes, fluoride-releasing biomaterials are being considered for their potential applications in various fields of biomedicine, especially dentistry and orthopaedics [77, 78]. Fluoride is known to increase bone density and also acts as an anti-carcinogenic agent [78-80]. Also, intracellular or plaque-associated enzymes have been reported to be affected by fluoride ions [77].

There are several challenges that need to be addressed while incorporating fluoride in silicate glasses including their high volatility during glass melting [81] and lower solubility in silicate glasses. Brauer et al. [81] synthesized soda-lime phosphosilicate based bioactive glasses containing 0 – 17.76 mol% CaF_2 and found that 5 – 23% CaF_2 is lost during synthesis of glasses *via* melt-quench route (higher the fluoride content, more is the loss). At molecular level, the structural role of fluoride in silicate glasses depends mainly on the local environment in glasses. For example, in fluorinated silica (SiO_2) glass, fluoride tends to bond only to silicon (≡Si-F) to form SiO_3F tetrahedra with no evidence for the formation of oxyfluorides [82-84]. In silicates, the acidic environment in these glasses induces greater amount of Si–F bonds while basic environments favour the formation of M–F (where, M is a network modifier cation) aggregates

as has been shown by Hayakawa et al. [85]. Since the overall environment in silicate/phosphosilicate bioactive glasses is basic in nature (due to the presence of Na^{+}, Ca^{2+}, Mg^{2+}, Sr^{2+}, etc.), fluoride is mainly found associated with alkali/alkaline-earth cations forming ionic aggregates (CaF^{+}, SrF^{+}) as has been shown by Kapoor et al. [86] and Lusvardi et al. (Figure 2.3) [87]. The ability of fluoride ion to strip network modifying cations (from the glass network may force the silicate network to re-polymerize by forming Si–O–Si or Si–O–P bonds (depending on the fluoride and phosphate concentration in the glass), thus, increasing the network connectivity.

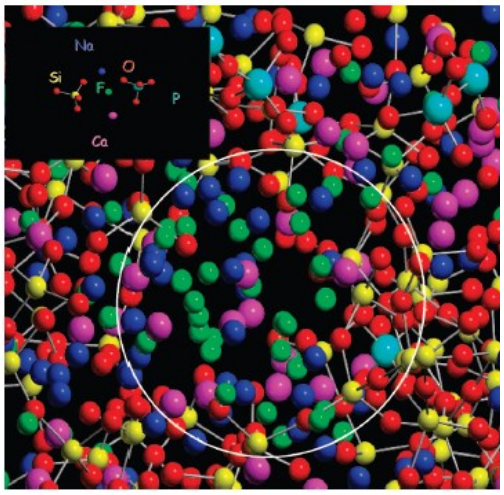

Figure 2.3 Snapshot of the glass structure for fluorinated-45S5 Bioglass® where 15 mol.% CaO has been substituted by equivalent concentration of CaF_2. The micro-segregation zone of network modifiers (Ca and Na) with fluoride ion can be seen in white circle. [87]

Although considerable amount of literature is available describing the influence of fluoride on molecular structure and chemical dissolution behaviour of silicate and phosphosilicate glasses [26, 81, 87-90], there is no consensus on its impact on hydroxyapatite formation and *in vitro* bioactivity of glasses. All the glasses investigated studied in this work contain fluoride in minor amounts.

2.4 Sintering behaviour of bioactive glasses – Its implications on scaffold fabrication for tissue engineering

Tissue engineering is an interdisciplinary field that applies the principles of engineering and life sciences toward the development of biological substitutes that restore, maintain, or improve tissue function or a whole organ [91]. Tissue engineering involves the expansion of cells from a small biopsy followed by the culturing of cells in temporary three-dimensional (3D) scaffolds to form a new organ or tissue. The primary function of a scaffold for hard tissues engineering is its role as the substratum that allows cells to attach, proliferate, differentiate (i.e., transform from a non-specific or primitive state into cells exhibiting the bone specific functions), and organize into normal, healthy bone as the scaffold degrades. Therefore, this new paradigm

requires scaffolds that balance temporary mechanical function with mass transport to aid biological delivery and tissue regeneration in three dimensions (3D) [92]. The synthetic scaffold, once seeded with cells, should be as short lived as possible; however, the scaffold must maintain its viability and integrity long enough for the cells to produce their own extracellular matrix. Therefore, a major consideration when designing a scaffold for tissue engineering is the scaffold material.

During fabrication of glass-ceramic scaffolds, the success of the fabrication process depends mainly on the sintering ability of glass powders as, in order to obtain a mechanically strong glass-ceramic scaffold, viscous flow sintering should precede crystallization. Furthermore, although crystallization in glasses might be required to enhance the mechanical strength of scaffolds, too high crystalline content (> 90 wt.%) in glass-ceramics can turn the material to be bio-inert [93]. Thus, it becomes highly crucial to optimize the sintering conditions of the glass powder so as to achieve equilibrium in the midst of biological and mechanical properties of the final material.

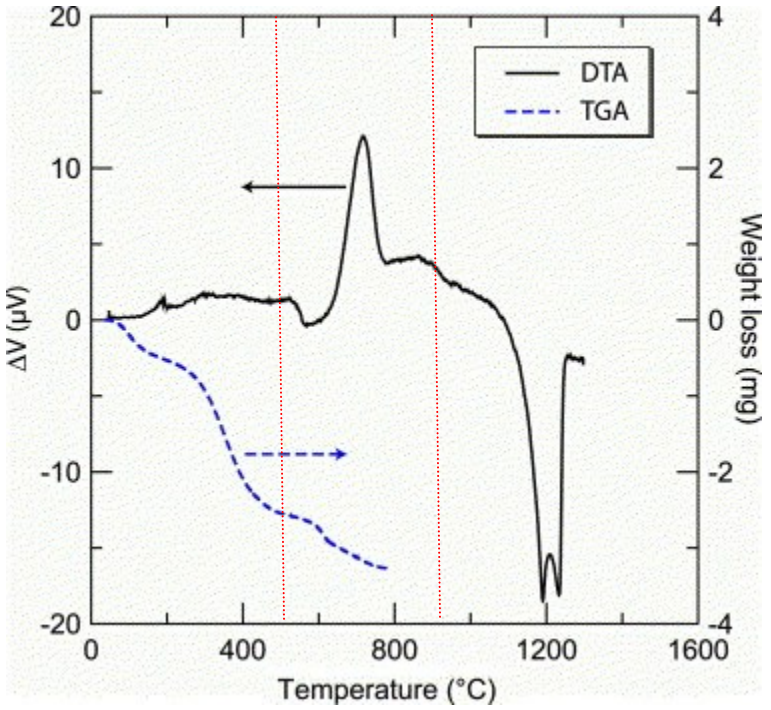

Figure 2.4. Differential thermal analysis (DTA) scan of 45S5 Bioglass at 5 ºC min^{-1} [101].

Most of the studies on sintering of bioactive glasses have focused on understanding the thermal transformations in 45S5 Bioglass® [94-101]. According to Lefebvre et al. [100], five successive transformations occur during heating of 45S5 Bioglass® powder from room temperature to 1000 ºC at a heating rate of 5 ºC min^{-1}: (1) Glass transition (T_{g1}) at 550 ºC [101] (Figure 2.4), (2) glass-in-glass phase separation at 580 ºC, (3) surface crystallization of $Na_2CaSi_2O_6$ at 610 ºC from silica rich phase, (4) crystallization of $Na_2Ca_4(PO_4)_2SiO_4$ from

phosphate rich phase at 800 ºC, (5) second glass transition (T_{g2}) of the remaining glassy phase. The sintering of 45S5 Bioglass® exhibits two main shrinkage stages associated with two glass transition temperatures. The crystallization of $Na_2CaSi_2O_6$ at 610 ºC immediately after glass-in-glass phase separation completely inhibits the sintering of this glass, thus, leading to the formation of a non-sintered, porous, mechanically weak and crystalline glass powder compact. In fact it has been reported that crystallization of 45S5 Bioglass® turns this glass into an inert material [99, 102]. Although three-dimensional porous, fully crystallized glass-ceramic scaffolds have been obtained from 45S5 Bioglass® after sintering at 1000 ºC for 1 h, the compressive and bending strength of the as produced scaffolds has been reported to be 0.3–0.4 and 0.4–0.5 MPa, respectively [98]. These values are significantly lower than the compressive strength of apatite-wollastonite based glass-ceramics scaffolds i.e. 5 MPa for a scaffold with 75% total porosity [103]. The 45S5 Bioglass® glass-ceramic scaffolds have been shown to exhibit hydroxyapatite formation on their surface after 28 days of immersion in simulated body fluid (SBF) [98, 99] which in itself is a marker of their low bioactivity level. Further attempts are being made to optimize the recipe for fabrication of mechanically strong but amorphous scaffolds from 45S5 Bioglass® by solid freeform fabrication techniques [104, 105], the small sintering window of this glass poses a big challenge in this arduous task.

Another glass composition that has been most widely and successfully used as a glass-ceramic biomaterial is CERABONE® A-W developed by Kokubo et al. [106] along the pseudo ternary system $3CaO{\cdot}P_2O_5$ - $CaO{\cdot}SiO_2$ - $CaO{\cdot}MgO{\cdot}2SiO_2$ and comprising 38 wt.% apatite [$Ca_{10}(PO_4)_6(O, F_2)$], 24 wt.% wollastonite ($CaSiO_3$) and 28 wt.% residual glassy phase. The glass-ceramic exhibits good bioactivity *in vivo*, and high mechanical strength (flexural strength: 215 MPa and Young´s modulus: 118 GPa) [107]. Since 1983, this glass-ceramic has been used in spine and hip surgeries of patients with extensive lesions and bone defects [107]. It is due to these reasons that even after more than 3 decades of its discovery; CERABONE® A-W glass-ceramic still enjoys an immense attention from biomaterials community. However, despite all the salient features exhibited by this material, the scaffolds derived from this glass-ceramic still cannot be used in load-bearing applications [108]. Also, there are questions raised related to the long term effect of silica, and slow degradation of this glass-ceramic (apatite crystals have very high chemical durability) [109], often taking some years to disappear from the body [110, 111]. The slow degradation of glass-ceramic scaffold may lead to reduction in its effective pore size by

in vivo events such as the invasion of fibrous tissue into the pores and the nonspecific adsorption of proteins onto the material's surface. Therefore, there is an exigent need to design novel bioactive glasses with good sintering ability and optimized amorphous/crystalline ratio so as to achieve equilibrium between their mechanical properties, chemical degradation and bioactivity.

2.5 Design of glass compositions for the present study

Diopside based materials have generated significant interest in biomedicine due to their good sintering behaviour resulting in mechanically strong ceramics/glass-ceramics (diopside based glass-ceramics have higher mechanical strength than their wollastonite based analogues) [112, 113] with no general toxicity in cell cultures [114, 115] and ability to enhance bone regeneration [116-118]. Further, incorporation of phosphate and fluoride component to these glass-ceramics will not only enhance their bioactivity (as discussed in section 2.3) but might also aid in sintering of diopside-rich glass-ceramics. Therefore, the parent series of glasses in this study has been designed along diopside ($CaO•MgO•2SiO_2$) – fluorapatite ($9CaO•3P_2O_5•CaF_2$) system.

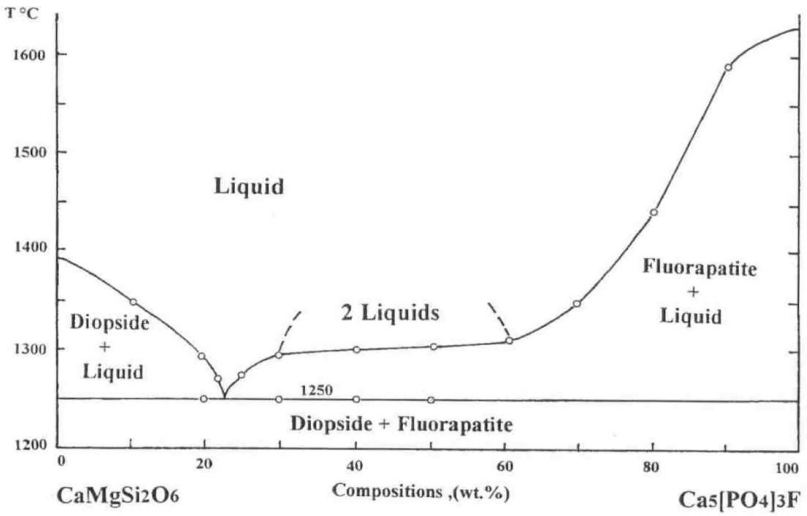

Figure 2.5 Phase diagram of diopside – fluorapatite system [119]

The phase equilibrium along diopside – fluorapatite join (Figure 2.5) has been studied by Tulyaganov [119, 120] and is characterized by the absence of any solid solutions. From the viewpoint of developing biomaterials, apatite-rich glass-ceramics were produced by controlled nucleation and crystallization along diopside – fluorapatite join by Hobo and Takoe with an objective of producing biomaterials for restorative dental applications under the commercial name of Cerapearl® [107]. Special optical properties, such as high translucency, as well as excellent chemical resistance and strength, were required. These goals, however, were not

always met and due to these reasons, this glass-ceramic was produced only for a limited time by Kyocera, Japan [107]. Few more attempts have been made to design diopside and fluorapatite containing bioactive glass-ceramics but mainly in ternary systems, for example, diopside – fluorapatite – mica [121] and diopside – Ca-Tschermak – fluorapatite system [122]. In nut-shell, despite being a potential system for developing fluoride-releasing bioactive glasses and glass-ceramics (for scaffold fabrication), diopside – fluorapatite system has not been thoroughly studied for its structural, thermal and physico-chemical properties that could lead to development of biomaterials for bone tissue engineering. Therefore, we focused on understanding the connection between composition, molecular structure, sintering behaviour and bioactivity of these glasses.

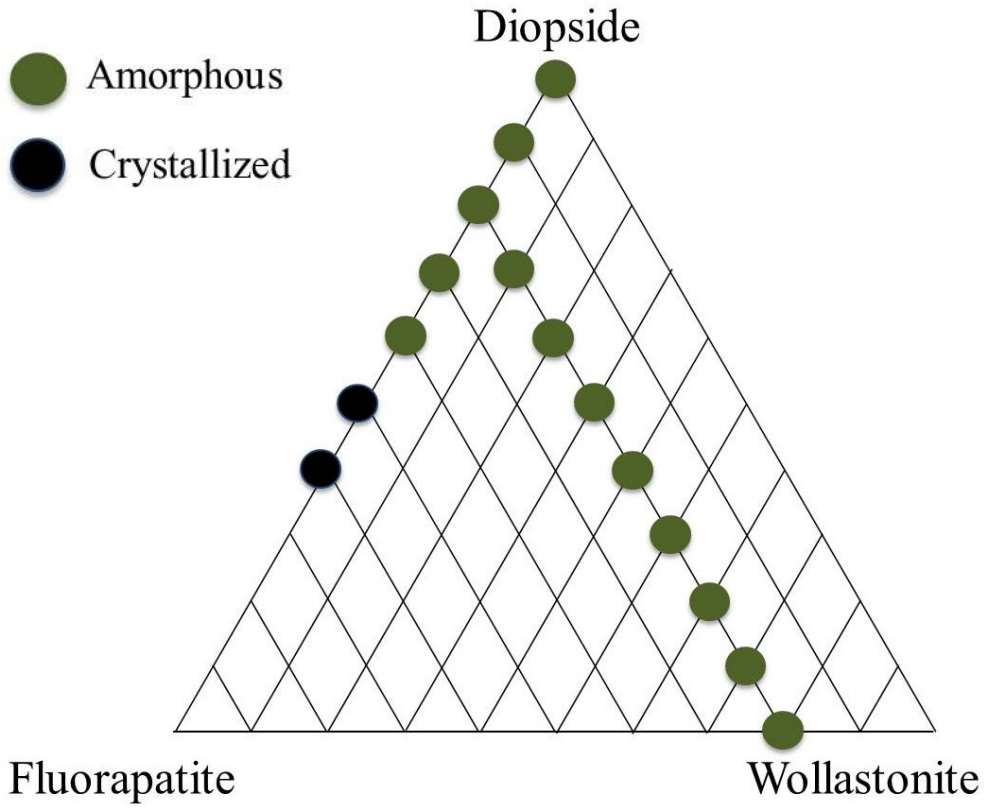

Figure 2.6 Glass compositions studied in CaO-MgO-P_2O_5-SiO_2-CaF_2 system. Glasses were synthesized by melting the batch in Pt-Rh crucibles and quenching the melt in water.

In the following set of glass compositions, we studied the influence of (i) Na_2O/MgO and (ii) CaO/MgO ratios on the structure and sintering ability of bioactive glasses designed in the glass forming regions of diopside – fluorapatite – wollastonite system, as demonstrated in Figure 2.6. Alkali oxides (mainly Na_2O and K_2O), though non-essential, have become integral component of bioactive glasses owing to their ability to lower the glass melting temperatures and tailor their

chemical dissolution behaviour [8, 9, 12]. However, as discussed in section 2.3, fast dissolution behaviour [40] and poor sintering ability [41] of glasses with high alkali-content, for example: 45S5 Bioglass®, renders them unfit for their aqueous processing and scaffold fabrication. Therefore, in order to design glasses with controlled dissolution behaviour, good sintering ability and minimal cytotoxicity *in vitro*, their alkali content needs to be well optimized. Thus, we focused on understanding the influence of alkali on chemical dissolution behaviour, thermal stability and bioactivity of these glasses.

Similarly as discussed in section 2.3, the influence of magnesium on structure and bioactivity of silicate/phosphosilicate glasses has been well discussed in literature. However, there is considerable dearth of literature on the influence of MgO on thermal properties of bioactive glasses. Therefore, a part of our work has been focused on elucidating the influence of CaO/MgO ratio on the sintering ability of bioactive glasses.

On the basis of results obtained in our previous studies, we designed a final set of glass compositions in the primary crystallization field of diopside – fluorapatite – wollastonite, containing optimized concentrations of Na_2O and MgO. The molecular structure and sintering ability of this series of glasses has been studied in the framework of this thesis while detailed bioactivity studies (*in vitro*, *in vivo* and human clinical trials) on a glass composition from our work have been reported elsewhere [123] and is out of scope of the present study.

References

[1] D. F. Williams, "Definitions in biomaterials:Proceedings of a consensus conference of the European Society for Biomaterials, Chester, England, March 3-5, 1986."

[2] L. L. Hench, "Bioceramics," *Journal of the American Ceramic Society,* vol. 81, pp. 1705-1728, 1998.

[3] G. Heness and B. Ben-Nissan, "Innovative Bioceramics," *Materials Forum,* vol. 27, pp. 104-114, 2004.

[4] S. F. Hulbert, "The use of alumina and zirconia in surgical implants," in *An introduction to bioceramics* L. L. Hench and J. Wilson, Eds., ed: World Scientific, UK, 1993, pp. 25-40.

[5] J.-M. Bouler, R. Z. LeGeros, and G. Daculsi, "Biphasic calcium phosphates: Influence of three synthesis parameters on the HA/β-TCP ratio," *Journal of Biomedical Materials Research,* vol. 51, pp. 680-684, 2000.

[6] J. C. Knowles, "Phosphate based glasses for biomedical applications," *Journal of Materials Chemistry,* vol. 13, pp. 2395-2401, 2003.

[7] L. Hench, "The story of Bioglass®," *Journal of Materials Science: Materials in Medicine,* vol. 17, pp. 967-978, 2006.

[8] L. L. Hench and H. A. Paschall, "Direct chemical bond of bioactive glass-ceramic materials to bone and muscle," *Journal of Biomedical Materials Research,* vol. 7, pp. 25-42, 1973.

[9] L. L. Hench, D. E. Day, W. Holand, and V. M. Rheinberger, "Glass and Medicine," *International Journal of Applied Glass Science,* vol. 1, pp. 104-117, 2010.

[10] T. Kokubo, H.-M. Kim, and M. Kawashita, "Novel bioactive materials with different mechanical properties," *Biomaterials,* vol. 24, pp. 2161-2175, 2003.

[11] M. Bohner and J. Lemaitre, "Can bioactivity be tested in vitro with SBF solution?," *Biomaterials,* vol. 30, pp. 2175-2179, 2009.

[12] L. L. Hench and J. M. Polak, "Third-Generation Biomedical Materials," *Science,* vol. 295, pp. 1014-1017, 2002.

[13] I. D. Xynos, A. J. Edgar, L. D. K. Buttery, L. L. Hench, and J. M. Polak, "Gene-expression profiling of human osteoblasts following treatment with the ionic products of Bioglass (R) 45S5 dissolution," *Journal of Biomedical Materials Research,* vol. 55, pp. 151-157, May 2001.

[14] A. Hoppe, N. S. Gueldal, and A. R. Boccaccini, "A review of the biological response to ionic dissolution products from bioactive glasses and glass-ceramics," *Biomaterials,* vol. 32, pp. 2757-2774, Apr 2011.

[15] T. Kokubo and H. Takadama, "How useful is SBF in predicting in vivo bone bioactivity?," *Biomaterials,* vol. 27, pp. 2907-2915, May 2006.

[16] L. L. Hench, "Bioceramics - from Concept to Clinic," *Journal of the American Ceramic Society,* vol. 74, pp. 1487-1510, Jul 1991.

[17] G. Kaur, O. P. Pandey, K. Singh, D. Homa, B. Scott, and G. Pickrell, "A review of bioactive glasses: Their structure, properties, fabrication, and apatite formation," *Journal of Biomedical Materials Research Part A,* vol. 102, pp. 254-274, 2014.

[18] A. R. Boccaccini, A. A. Gorustovich, and J. A. Roether, "Effect of Bioactive Glasses on Angiogenesis: A Review of In Vitro and In Vivo Evidences," *Tissue Engineering Part B-Reviews,* vol. 16, pp. 199-207, Apr 2010.

[19] L. L. Hench, N. Roki, and M. B. Fenn, "Bioactive glasses: Importance of structure and properties in bone regeneration," *Journal of Molecular Structure,* vol. 1073, pp. 24-30, 2014.

[20] J. R. Jones, "Review of bioactive glass: From Hench to hybrids," *Acta Biomaterialia,* vol. 9, pp. 4457-4486, 2013.

[21] A. M. Abdelghany, H. A. ElBatal, and F. M. EzzElDin, "Bone bonding ability behavior of some ternary borate glasses by immersion in sodium phosphate solution," *Ceramics International,* vol. 38, pp. 1105-1113, 2012.

[22] Manupriya, K. S. Thind, G. Sharma, K. Singh, V. Rajendran, and S. Aravindan, "Soluble borate glasses: In vitro analysis," *Journal of the American Ceramic Society,* vol. 90, pp. 467-471, 2007.

[23] P. P. Lopes, B. J. Ferreira, P. S. Gomes, R. N. Correia, M. H. Fernandes, M. H. V. Fernandes, "Silicate and borate glasses as composite fillers: a bioactivity and biocompatibility study," *Journal of Materials Science-Materials in Medicine,* vol. 22, pp. 1501-1510, 2011.

[24] L. Morejon Alonso, J. A. Delgado Garcia-Menocal, M. Tarrago Aymerich, J. A. Alvarez Guichard, M. Garcia-Valles, S. Martinez Manent*, et al.*, "Calcium phosphate glasses: Silanation process and effect on the bioactivity behavior of Glass-PMMA composites,"

Journal of Biomedical Materials Research Part B-Applied Biomaterials, vol. 102, pp. 205-213, 2014.

[25] A. Goel, S. Kapoor, R. R. Rajagopal, M. J. Pascual, H. W. Kim, and J. M. F. Ferreira, "Alkali-free bioactive glasses for bone tissue engineering: A preliminary investigation," *Acta Biomaterialia,* vol. 8, pp. 361-372, 2012.

[26] D. S. Brauer, N. Karpulthina, M. D. O'Donnell, R. V. Law, and R. G. Hill, "Fluoride-containing bioactive glasses: Effect of glass design and structure on degradation, pH and apatite formation in simulated body fluid," *Acta Biomaterialia,* vol. 6, pp. 3275-3282, 2010.

[27] I. Christodoulou, L. D. K. Buttery, P. Saravanapavan, G. P. Tai, L. L. Hench, and J. M. Polak, "Dose- and time-dependent effect of bioactive gel-glass ionic-dissolution products on human fetal osteoblast-specific gene expression," *Journal of Biomedical Materials Research Part B-Applied Biomaterials,* vol. 74B, pp. 529-537, 2005.

[28] M. Ogino, F. Ohuchi, and L. L. Hench, "Compositional dependence of the formation of calcium phosphate films on bioglass," *Journal of Biomedical Materials Research,* vol. 14, pp. 55-64, 1980.

[29] R. Li, A. E. Clark, and L. L. Hench, "An investigation of bioactive glass powders by sol-gel processing," *Journal of Applied Biomaterials,* vol. 2, pp. 231-239, 1991.

[30] A. Tilocca, "Structural models of bioactive glasses from molecular dynamics simulations," *Proceedings of the Royal Society a-Mathematical Physical and Engineering Sciences,* vol. 465, pp. 1003-1027, 2009.

[31] M. W. G. Lockyer, D. Holland, and R. Dupree, "Nmr Investigation of the Structure of Some Bioactive and Related Glasses," *Journal of Non-Crystalline Solids,* vol. 188, pp. 207-219, 1995.

[32] I. Kansal, D. U. Tulyaganov, A. Goel, M. J. Pascual, and J. M. F. Ferreira, "Structural analysis and thermal behavior of diopside-fluorapatite-wollastonite-based glasses and glass-ceramics," *Acta Biomaterialia,* vol. 6, pp. 4380-4388, 2010.

[33] A. Tilocca and A. N. Cormack, "Structural effects of phosphorus inclusion in bioactive silicate glasses," *Journal of Physical Chemistry B,* vol. 111, pp. 14256-14264, 2007.

[34] R. Mathew, B. Stevensson, A. Tilocca, and M. Eden, "Toward a Rational Design of Bioactive Glasses with Optimal Structural Features: Composition-Structure Correlations

Unveiled by Solid-State NMR and MD Simulations," *Journal of Physical Chemistry B,* vol. 118, pp. 833-844, 2014.

[35] R. G. Hill and D. S. Brauer, "Predicting the bioactivity of glasses using the network connectivity or split network models," *Journal of Non-Crystalline Solids,* vol. 357, pp. 3884-3887, 2011.

[36] H. Aguiar, E. L. Solla, J. Serra, P. Gonzalez, B. Leon, N. Almeida*, et al.*, "Orthophosphate nanostructures in SiO_2-P_2O_5-CaO-Na_2O-MgO bioactive glasses," *Journal of Non-Crystalline Solids,* vol. 354, pp. 4075-4080, 2008.

[37] T. Yamaguchi, N. Chattopadhyay, O. Kifor, R. R. Butters, T. Sugimoto, and E. M. Brown, "Mouse osteoblastic cell line (MC3T3-E1) expresses extracellular calcium (Ca2+o)-sensing receptor and its agonists stimulate chemotaxis and proliferation of MC3T3-E1 cells," *Journal of Bone and Mineral Research,* vol. 13, pp. 1530-1538, 1998.

[38] K. E. Wallace, R. G. Hill, J. T. Pembroke, C. J. Brown, and P. V. Hatton, "Influence of sodium oxide content on bioactive glass properties," *Journal of Materials Science: Materials in Medicine,* vol. 10, pp. 697-701, 1999.

[39] I. Kansal, A. Reddy, F. Munoz, S.-J. Choi, H.-W. Kim, D. U. Tulyaganov*, et al.*, "Structure, biodegradation behavior and cytotoxicity of alkali-containing alkaline-earth phosphosilicate glasses," *Materials science & engineering. C,* vol. 44, pp. 159-65, 2014.

[40] M. Vogel, C. Voigt, U. M. Gross, and C. M. Muller-Mai, "In vivo comparison of bioactive glass particles in rabbits," *Biomaterials,* vol. 22, pp. 357-362, 2001.

[41] A. R. Boccaccini, Q. Chen, L. Lefebvre, L. Gremillard, and J. Chevalier, "Sintering, crystallisation and biodegradation behaviour of Bioglass®-derived glass-ceramics," *Faraday Discussions,* vol. 136, pp. 27-44, 2007.

[42] M. P. Staiger, A. M. Pietak, J. Huadmai, and G. Dias, "Magnesium and its alloys as orthopedic biomaterials: A review," *Biomaterials,* vol. 27, pp. 1728-1734, 2006.

[43] H. Zreiqat, C. R. Howlett, A. Zannettino, P. Evans, G. Schulze-Tanzil, C. Knabe, and M. Shakibaei, "Mechanisms of magnesium-stimulated adhesion of osteoblastic cells to commonly used orthopaedic implants," *Journal of Biomedical Materials Research A,* vol. 62, pp. 175-184, 2002.

[44] R. K. Rude, H. E. Gruber, L. Y. Wei, A. Frausto, and B. G. Mills, "Magnesium deficiency: Effect on bone and mineral metabolism in the mouse," *Calcified Tissue International,* vol. 72, pp. 32-41, 2003.

[45] R. K. Rude, H. E. Gruber, H. J. Norton, L. Y. Wei, A. Frausto, and J. Kilburn, "Dietary magnesium reduction to 25% of nutrient requirement disrupts bone and mineral metabolism in the rat," *Bone,* vol. 37, pp. 211-219, 2005.

[46] N. E. L. Saris, E. Mervaala, H. Karppanen, J. A. Khawaja, and A. Lewenstam, "Magnesium - An update on physiological, clinical and analytical aspects," *Clinica Chimica Acta,* vol. 294, pp. 1-26, 2000.

[47] J. Vormann, "Magnesium: Nutrition and metabolism," *Molecular Aspects of Medicine,* vol. 24, pp. 27-37, 2003.

[48] A. Pedone, G. Malavasi, and M. C. Menziani, "Computational insight into the effect of CaO/MgO substitution on the structural properties of phospho-silicate bioactive glasses," *Journal of Physical Chemistry C,* vol. 113, pp. 15723-15730, 2009.

[49] A. Pedone, G. Malavasi, M. C. Menziani, U. Segre, and A. N. Cormack, "Role of magnesium in soda-lime glasses: insight into structural, transport, and mechanical properties through computer simulations," *Journal of Physical Chemistry C,* vol. 112, pp. 11034-11041, 2008.

[50] J. Ma, C. Z. Chen, D. G. Wang, Y. Jiao, and J. Z. Shi, "Effect of magnesia on the degradability and bioactivity of sol-gel derived SiO2-CaO-MgO-P2O5 system glasses," *Colloids and Surfaces B-Biointerfaces,* vol. 81, pp. 87-95, 2010.

[51] S. J. Watts, R. G. Hill, M. D. O'Donnell, and R. V. Law, "Influence of magnesia on the structure and properties of bioactive glasses," *Journal of Non-Crystalline Solids,* vol. 356, pp. 517-524, 2010.

[52] M. Vallet-Regi, A. J. Salinas, J. Roman, and M. Gil, "Effect of magnesium content on the in vitro bioactivity of CaO-MgO-SiO_2-P_2O_5 sol-gel glasses," *Journal of Materials Chemistry,* vol. 9, pp. 515-518, 1999.

[53] J. Perez-Pariente, F. Balas, and M. Vallet-Regi, "Surface and chemical study of SiO_2•P_2O_5•CaO•(MgO) bioactive glasses," *Chemistry of Materials,* vol. 12, pp. 750-755, 2000.

[54] J. M. Oliveira, R. N. Correia, M. H. Fernandez, and J. Rocha, "Influence of the CaO/MgO ratio on the structure of phase-separated glasses: a solid state ^{29}Si and ^{31}P MAS NMR study," *Journal of Non-Crystalline Solids,* vol. 265, pp. 221-229, 2000.

[55] A. Goel, S. Kapoor, A. Tilocca, R. R. Rajagopal, and J. M. F. Ferreira, "Structural role of zinc in biodegradation of alkali-free bioactive glasses," *Journal of Materials Chemistry B,* vol. 1, pp. 3073-3082, 2013.

[56] A. Al-Noaman, S. C. F. Rawlinson, and R. G. Hill, "The role of MgO on thermal properties, structure and bioactivity of bioactive glass coating for dental implants," *Journal of Non-Crystalline Solids,* vol. 358, pp. 3019-3027, 2012.

[57] M. Diba, F. Tapia, A. R. Boccaccini, and L. A. Strobel, "Magnesium-Containing Bioactive Glasses for Biomedical Applications," *International Journal of Applied Glass Science,* vol. 3, pp. 221-253, 2012.

[58] J. Massera, L. Hupa, and M. Hupa, "Influence of the partial substitution of CaO with MgO on the thermal properties and in vitro reactivity of the bioactive glass S53P4," *Journal of Non-Crystalline Solids,* vol. 358, pp. 2701-2707, 15 2012.

[59] E. Jallot, "Role of magnesium during spontaneous formation of a calcium phosphate layer at the periphery of a bioactive glass coating doped with MgO," *Applied Surface Science,* vol. 211, pp. 89-95, 30 2003.

[60] E. Dietrich, H. Oudadesse, A. Lucas-Girot, and M. Mami, "In vitro bioactivity of melt-derived glass 46S6 doped with magnesium," *Journal of Biomedical Materials Research Part A,* vol. 88A, pp. 1087-1096, 2009.

[61] J. M. Oliveira, R. N. Correia, and M. H. Fernandes, "Surface modifications of a glass and a glass-ceramic of the MgO-3CaO•P_2O_5-SiO_2 system in a simulated body fluid," *Biomaterials,* vol. 16, pp. 849-854, 1995.

[62] A. Goel, R. R. Rajagopal, and J. M. F. Ferreira, "Influence of strontium on structure, sintering and biodegradation behaviour of CaO-MgO-SrO-SiO_2-P_2O_5-CaF_2 glasses," *Acta Biomaterialia,* vol. 7, pp. 4071-4080, 2011.

[63] O. H. Andersson, J. Rosenqvist, and K. H. Karlsson, "Dissolution, leaching and Al_2O_3 enrichment at the surface of bioactive glasses studied by solution analysis," *Journal of Biomedical Materials Research,* vol. 27, pp. 941-948, 1993.

[64] C. Ohtsuki, T. Kokubo, and T. Yamauro, "Compositional dependence of bioactivity of glasses in the system CaO-SiO_2-Al_2O_3: itsin vitro evaluation," *Journal of Materials Science: Materials in Medicine,* vol. 3, pp. 119-125, 1992.

[65] S. K. Nandi, B. Kundu, S. Datta, D. K. De, and D. Basu, "The repair of segmental bone defects with porous bioglass: An experimental study in goat," *Research in Veterinary Science,* vol. 86, pp. 162-173, 2009.

[66] S. Haimi, G. Gorianc, L. Moimas, B. Lindroos, H. Huhtala, S. Raty*, et al.*, "Characterization of zinc-releasing three-dimensional bioactive glass scaffolds and their effect on human adipose stem cell proliferation and osteogenic differentiation," *Acta Biomaterialia,* vol. 5, pp. 3122-3131, 2009.

[67] R. D. Goodridge, D. J. Wood, C. Ohtsuki, and K. W. Dalgarno, "Biological evaluation of an apatite-mullite glass-ceramic produced via selective laser sintering," *Acta Biomaterialia,* vol. 3, pp. 221-231, 2007.

[68] A. S. Monem, H. A. ElBatal, E. M. A. Khalil, M. A. Azooz, and Y. M. Hamdy, "In vivo behavior of bioactive phosphate glass-ceramics from the system P_2O_5-Na_2O-CaO containing TiO_2," *Journal of Materials Science-Materials in Medicine,* vol. 19, pp. 1097-1108, 2008.

[69] D. M. Pickup, E. A. Abou Neel, R. M. Moss, K. M. Wetherall, P. Guerry, and M. E. Smith, "Ti K-edge XANES study of the local environment of titanium in bioresorbable TiO_2-CaO-Na_2O-P_2O_5 glasses," *Journal of Materials Science-Materials in Medicine,* vol. 19, pp. 1681-1685, 2008.

[70] M. Navarro, M. P. Ginebra, J. Clement, S. Martinez, G. Avila, and J. A. Planell, "Physicochemical degradation of titania-stabilized soluble phosphate glasses for medical applications," *Journal of the American Ceramic Society,* vol. 86, pp. 1345-1352, 2003.

[71] S. Pors Nielsen, "The biological role of strontium," *Bone,* vol. 35, pp. 583-8, 2004.

[72] J. Lao, E. Jallot, and J.-M. Nedelec, "Strontium-delivering glasses with enhanced bioactivity: A new biomaterial for antiosteoporotic applications?," *Chemistry of Materials,* vol. 20, pp. 4969-4973, 2008.

[73] J. Lao, J. M. Nedelec, and E. Jallot, "New strontium-based bioactive glasses: physicochemical reactivity and delivering capability of biologically active dissolution products," *Journal of Materials Chemistry,* vol. 19, pp. 2940-2949, 2009.

[74] Y. Xiang and J. C. Du, "Effect of Strontium Substitution on the Structure of 45S5 Bioglasses," *Chemistry of Materials,* vol. 23, pp. 2703-2717, 2011.

[75] K. Fujikura, N. Karpukhina, T. Kasuga, D. S. Brauer, R. G. Hill, and R. V. Law, "Influence of strontium substitution on structure and crystallisation of Bioglass® 45S5," *Journal of Materials Chemistry,* vol. 22, pp. 7395-7402, 2012.

[76] C. Bonhomme, C. Gervais, N. Folliet, F. Pourpoint, C. Coelho Diogo, J. Lao*, et al.*, "^{87}Sr Solid-State NMR as a Structurally Sensitive Tool for the Investigation of Materials: Antiosteoporotic Pharmaceuticals and Bioactive Glasses," *Journal of the American Chemical Society,* vol. 134, pp. 12611-12628, 2012.

[77] A. Wiegand, W. Buchalla, and T. Attin, "Review on fluoride-releasing restorative materials - Fluoride release and uptake characteristics, antibacterial activity and influence on caries formation," *Dental Materials,* vol. 23, pp. 343-362, 2007.

[78] P. Vestergaard, N. R. Jorgensen, P. Schwarz, and L. Mosekilde, "Effects of treatment with fluoride on bone mineral density and fracture risk - a meta-analysis," *Osteoporosis International,* vol. 19, pp. 257-268, 2008.

[79] G. Rølla and J. Ekstrand, *Fluoride in oral fluids and dental plaque*, 1996.

[80] L. G. Petersson, "The role of fluoride in the preventive management of dentin hypersensitivity and root caries," *Clinical Oral Investigations,* vol. 17, pp. S63-S71, 2013.

[81] D. S. Brauer, M. Mneimne, and R. G. Hill, "Fluoride-containing bioactive glasses: Fluoride loss during melting and ion release in tris buffer solution," *Journal of Non-Crystalline Solids,* vol. 357, pp. 3328-3333, 2011.

[82] T. M. Duncan, D. C. Douglass, R. Csencsits, and K. L. Walker, "Study of fluorine in silicate glass with [sup 19]F nuclear magnetic resonance spectroscopy," *Journal of Applied Physics,* vol. 60, pp. 130-136, 1986.

[83] R. E. Youngman and S. Sen, "Structural role of fluorine in amorphous silica," *Journal of Non-Crystalline Solids,* vol. 349, pp. 10-15, 2004.

[84] R. E. Youngman and S. Sen, "The nature of fluorine in amorphous silica," *Journal of Non-Crystalline Solids,* vol. 337, pp. 182-186, 2004.

[85] S. Hayakawa, C. Ohtsuki, S. Matsumoto, A. Osaka, and Y. Miura, "Molecular dynamic simulation of heterogeneity and chemical states of fluorine in amorphous alkaline earth silicate systems," *Computational Materials Science,* vol. 9, pp. 337-342, 1998.

[86] S. Kapoor, A. Goel, A. Tilocca, V. Dhuna, G. Bhatia, K. Dhuna*, et al.*, "Role of glass structure in defining the chemical dissolution behavior, bioactivity and antioxidant properties of zinc and strontium co-doped alkali-free phosphosilicate glasses," *Acta Biomaterialia,* vol. 10, pp. 3264-3278, 2014.

[87] G. Lusvardi, G. Malavasi, M. Cortada, L. Menabue, M. C. Menziani, A. Pedone*, et al.*, "Elucidation of the structural role of fluorine in potentially bioactive glasses by experimental and computational investigation," *Journal of Physical Chemistry B,* vol. 112, pp. 12730-12739, 2008.

[88] G. Lusvardi, G. Malavasi, L. Menabue, V. Aina, and C. Morterra, "Fluoride-containing bioactive glasses: Surface reactivity in simulated body fluids solutions," *Acta Biomaterialia,* vol. 5, pp. 3548-3562, 2009.

[89] D. S. Brauer, N. Karpukhina, R. V. Law, and R. G. Hill, "Structure of fluoride-containing bioactive glasses," *Journal of Materials Chemistry,* vol. 19, pp. 5629-5636, 2009.

[90] G. Lusvardi, G. Malavasi, F. Tarsitano, L. Menabue, M. C. Menziani, and A. Pedone, "Quantitative Structure-Property Relationships of Potentially Bioactive Fluoro Phospho-silicate Glasses," *Journal of Physical Chemistry B,* vol. 113, pp. 10331-10338, 2009.

[91] R. Langer and J. P. Vacanti, "Tissue Engineering," *Science,* vol. 260, pp. 920-926, 1993.

[92] S. J. Hollister, "Porous scaffold design for tissue engineering," *Nature Materials,* vol. 4, pp. 518-524, 2005.

[93] P. Li, Q. Yang, F. Zhang, and T. Kokubo, "The effect of residual glassy phase in a bioactive glass-ceramic on the formation of its surface apatite layerin vitro," *Journal of Materials Science: Materials in Medicine,* vol. 3, pp. 452-456, 1992.

[94] O. Bretcanu, X. Chatzistavrou, K. Paraskevopoulos, R. Conradt, I. Thompson, and A. R. Boccaccini, "Sintering and crystallisation of 45S5 Bioglass (R) powder," *Journal of the European Ceramic Society,* vol. 29, pp. 3299-3306, 2009.

[95] R. Huang, J. Pan, A. R. Boccaccini, and Q. Z. Chen, "A two-scale model for simultaneous sintering and crystallization of glass-ceramic scaffolds for tissue engineering," *Acta Biomaterialia,* vol. 4, pp. 1095-1103, Jul 2008.

[96] O. Guillon, S. Cao, J. Chang, L. Wondraczek, and A. R. Boccaccini, "Effect of uniaxial load on the sintering behaviour of 45S5 Bioglass® powder compacts," *Journal of the European Ceramic Society,* vol. 31, pp. 999-1007, 2011.

[97] S. Grasso, R. K. Chinnam, H. Porwal, A. R. Boccaccini, and M. J. Reece, "Low temperature spark plasma sintering of 45S5 Bioglass®," *Journal of Non-Crystalline Solids,* vol. 362, pp. 25-29, 2013.

[98] Q. Z. Chen, I. D. Thompson, and A. R. Boccaccini, "45S5 Bioglass®-derived glass–ceramic scaffolds for bone tissue engineering," *Biomaterials,* vol. 27, pp. 2414-2425, 2006.

[99] A. R. Boccaccini, Q. Chen, L. Lefebvre, L. Gremillard, and J. Chevalier, "Sintering, crystallisation and biodegradation behaviour of Bioglass (R)-derived glass-ceramics," *Faraday Discussions,* vol. 136, pp. 27-44, 2007.

[100] L. Lefebvre, L. Gremillard, J. Chevalier, R. Zenati, and D. Bernache-Assolant, "Sintering behaviour of 45S5 bioactive glass," *Acta Biomaterialia,* vol. 4, pp. 1894-1903, 2008.

[101] L. Lefebvre, J. Chevalier, L. Gremillard, R. Zenati, G. Thollet, D. Bernache-Assolant, and A. Govin, "Structural transformations of bioactive glass 45S5 with thermal treatments," *Acta Materialia,* vol. 55, pp. 3305-3313, 2007.

[102] D. C. Clupper and L. L. Hench, "Crystallization kinetics of tape cast bioactive glass 45S5," *Journal of Non-Crystalline Solids,* vol. 318, pp. 43-48, 2003.

[103] H. Zhang, X.-J. Ye, and J.-S. Li, "Preparation and biocompatibility evaluation of apatite/wollastonite-derived porous bioactive glass ceramic scaffolds," *Biomedical Materials,* vol. 4, pp. 045007, 2009.

[104] S. Eqtesadi, A. Motealleh, P. Miranda, A. Lemos, A. Rebelo, J.M.F. Ferreira, A simple recipe for direct writing complex 45S5 Bioglass® 3D scaffolds, *Materials Letters,* vol. 93, pp. 68-71, 2013.

[105] S. Eqtesadi, A. Motealleh, P. Miranda, A. Pajares, A. Lemos, J.M.F. Ferreira, Robocasting of 45S5 bioactive glass scaffolds for bone tissue engineering, *Journal of the European Ceramic Society,* vol. 34, pp. 107-117, 2014.

[106] T. Kokubo, M. Shigematsu, Y. Nagashima, M. Tashiro, T. Nakamura, T. Yamamuro, *et al.*, "Apatite and wollastonite containing glass-ceramics for prosthetic applications," *Bulletin of Institute of Chemical Research, Kyoto University,* vol. 60, pp. 260-268, 1982.

[107] W. Holand and G. Beall, "Applications of glass-ceramics," in *Glass-Ceramic Technology*, ed: The American Ceramic Society, 2002.

[108] V. Cannillo, F. Pierli, S. Sampath, and C. Siligardi, "Thermal and physical characterisation of apatite/wollastonite bioactive glass-ceramics," *Journal of the European Ceramic Society,* vol. 29, pp. 611-619, 2009.

[109] P. Sponer, K. Urban, and T. Kucera, "Comparison of apatite-wollastonite glass-ceramic and beta-tricalcium phosphate used as bone graft substitutes after curettage of bone cysts," in *Advances in Ceramics - Electric and Magnetic Ceramics, Bioceramics, Ceramics and Environment*, C. Sikalidis, Ed., ed: InTech Publishers, 2011.

[110] M. Neo, T. Nakamura, C. Ohtsuki, R. Kasai, T. Kokubo, and T. Yamamuro, "Ultrastructural study of the A-W GC- bone interface after long-term implantation in rat and human," *Journal of Biomedical Materials Research,* vol. 28, pp. 365-372, 1994.

[111] H. Fujita, H. Iida, K. Ido, Y. Matsuda, M. Oka, and T. Nakamura, "Porous apatite-wollastonite glass-ceramic as an intramedullary plug," *Journal of Bone and Joint Surgery-British Volume,* vol. 82B, pp. 614-618, 2000.

[112] A. Karamanov and M. Pelino, "Induced crystallization porosity and properties of sintereds diopside and wollastonite glass-ceramics," *Journal of the European Ceramic Society,* vol. 28, pp. 555-562, 2008.

[113] N. Y. Iwata, G. H. Lee, Y. Tokuoka, and N. Kawashima, "Sintering behavior and apatite formation of diopside prepared by coprecipitation process," *Colloids and Surfaces B-Biointerfaces,* vol. 34, pp. 239-245, 2004.

[114] C. Wu, Y. Ramaswamy, and H. Zreiqat, "Porous diopside ($CaMgSi_2O_6$) scaffold: A promising bioactive material for bone tissue engineering," *Acta Biomaterialia,* vol. 6, pp. 2237-45, 2010.

[115] C. Wu and H. Zreiqat, "Porous bioactive diopside ($CaMgSi_2O_6$) ceramic microspheres for drug delivery," *Acta Biomaterialia,* vol. 6, pp. 820-9, Mar 2010.

[116] M. Razavi, M. Fathi, O. Savabi, S. M. Razavi, F. Heidari, M. Manshaei, D. Vashaee, L. Tayebi, "In vivo study of nanostructured diopside ($CaMgSi_2O_6$) coating on magnesium alloy as biodegradable orthopedic implants," *Applied Surface Science,* vol. 313, pp. 60-66, 2014.

[117] P. N. De Aza, Z. B. Luklinska, and M. Anseau, “Bioactivity of diopside ceramic in human parotid saliva,” *Journal of Biomedical Materials Research Part B-Applied Biomaterials,* vol. 73B, pp. 54-60, 2005.

[118] T. Nonami, “In Vivo and In Vitro Testing of Diopside for Biomaterial,” *Journal of Society of Materials Engineering for Resources of Japan,* vol. 8, pp. 12-18, 1995.

[119] D. U. Tulyaganov, “Phase Equilibrium in the Fluorapatite–Anorthite–Diopside System,” *Journal of the American Ceramic Society,* vol. 83, pp. 3141-3146, 2000.

[120] D. U. Tulyaganov and R. Y. Khodakovskaya, “Glass-ceramic biomaterials based on the fluorapatite-anorthite and fluorapatitie-diopside systems,” *Glass and Ceramics,* vol. 48, pp. 221-222, 1991.

[121] D. U. Tulyaganov, S. Agathopoulos, H. R. Fernandes, J. M. Ventura, and J. M. F. Ferreira, “Preparation and crystallization of glasses in the system tetrasilicic mica-fluorapatite-diopside,” *Journal of the European Ceramic Society,* vol. 24, pp. 3521-3528, 2004.

[122] S. N. Salama, H. Darwish, and H. A. Abo-Mosallam, “Crystallization and properties of glasses based on diopside-Ca-Tschermak's-fluorapatite system,” *Journal of the European Ceramic Society,* vol. 25, pp. 1133-1142, 2005.

[123] D. U. Tulyaganov, M. E. Makhkamov, A. Urazbaev, A. Goel, and J. M. F. Ferreira, “Synthesis, processing and characterization of a bioactive glass composition for bone regeneration,” *Ceramics International,* vol. 39, pp. 2519-2526, 2013.

…….

Chapter 3. Experimental

3.1 Synthesis of glasses

High purity powders of SiO_2 (Alfa Aesar; 99%), $CaCO_3$ (Alf Aesar, 99%), $MgCO_3$ (Sigma Aldrich, purum p.a.), $NH_4H_2PO_4$ (Alfa Aesar, 99%), Na_2CO_3 (Sigma Aldrich; 99%) and CaF_2 (99%, Alfa Aesar) were used. Homogeneous mixtures of batches (~100 g), in accordance with the designed compositions, obtained by ball milling, were calcined at 900 ºC for 1 h and then melted in Pt-Rh crucibles in temperature range 1500 – 1600 ºC for 1 h, in air. Glasses in bulk form were produced by pouring the melts on preheated bronze moulds following by annealing in temperature range 500 – 550 ºC for 1 h, depending on glass composition. The glasses in frit form were obtained by quenching of glass melts in cold water. The frits were dried and then milled in a high-speed agate mill resulting in glass powders with different particle sizes varying between 10 – 225 μm (determined by light scattering technique; Coulter LS 230, UK; Fraunhofer optical model). The amorphous nature of glasses was confirmed by X-ray diffraction (XRD) analysis (Rigaku Geigerflex D/Max, Tokyo, Japan; C Series; Cu K_α radiation; 2θ angle range 10–80º; step 0.02º s^{-1}).

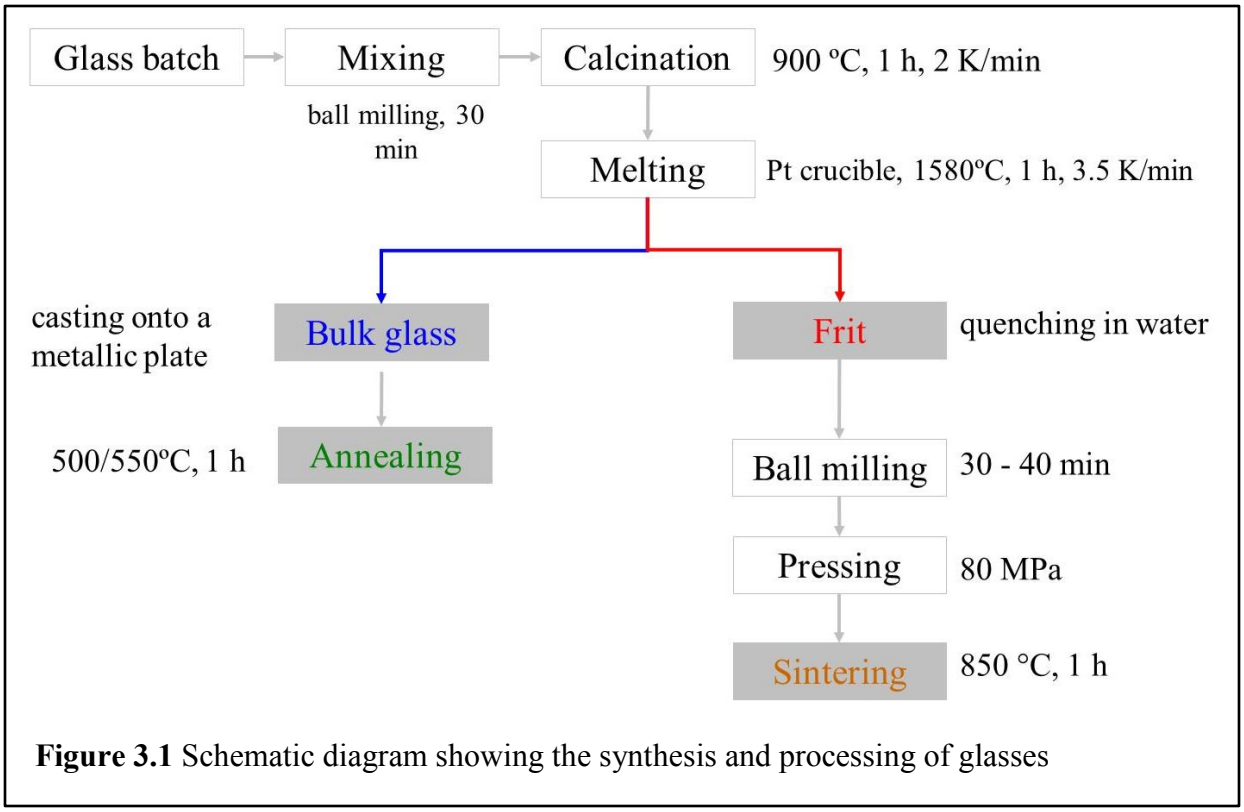

Figure 3.1 Schematic diagram showing the synthesis and processing of glasses

3.2 Structural characterization of glasses

3.2.1 Infrared spectroscopy

Infrared spectra of glass powders were obtained using a Fourier Transform Infrared Spectrometer (FT-IR, model Mattson Galaxy S-7000, USA). For this purpose each sample was mixed with KBr in the proportion of 1/150 (by weight) for 15 min and pressed into a pellet using a hand press.

3.2.2 Magic angle spinning - Nuclear magnetic resonance (MAS-NMR)

The ^{29}Si MAS NMR spectra were recorded on a Bruker ASX 400 spectrometer operating at 79.52 MHz (9.4 T) using a 7 mm probe at a spinning rate of 5 kHz. The pulse length was 2 μs and 60 seconds delay time was used. Kaolinite was used as the chemical shift reference. The ^{31}P MAS NMR spectra of glasses were recorded on a Bruker ASX 400 spectrometer operating at 161.97 MHz with 45º pulses, spinning rates of 12 kHz, a 60 s recycle delay and the chemical shift was quoted in ppm from phosphoric acid (85%).

3.3 Density measurements

Archimedes' method (i.e. immersion in diethyl phthalate) was employed to measure the apparent density of the bulk annealed glasses. Molar Volume (V_m), and excess volume (V_e) were calculated using the density data for the bulk glasses using following relations:

$$V_m = \frac{M}{\rho} \qquad (3.1),$$

where M is the molar mass of the glass and ρ is the apparent density of the bulk glasses. Similarly, excess volume of the glasses can be expressed as:

$$V_e = V_m - \sum_i x_i V_m(i) \qquad (3.2),$$

Here, x_i is the molar concentration of every oxide and $V_m(i)$ is the molar volume of every oxide.

3.4 Thermal analysis

3.4.1 Dilatometry

Dilatometry measurements were done with prismatic samples with cross section of 4x5 mm^2 (Bahr Thermo Analyse DIL 801 L, Hüllhorst, Germany GmbH; heating rate 5 ºC min^{-1}).

The mean values and standard deviations (SD) presented for coefficient of thermal expansion (CTE), dilatometric glass transition temperature (T_{dg}), and softening temperature (T_s) have been obtained from (at least) three different samples.

3.4.2 Differential thermal analysis (DTA)

The crystallization kinetics of glass powders was studied using DTA (Labsys, Setaram, Caluire, France). 50 mg of glass powders were heated in ambient environment from room temperature up to 1000 ºC in alumina pans at heating rates (β) varying between 5 – 20 ºC min^{-1}. α-alumina was used as a reference material. Glass transition temperature (T_g), temperature for onset of crystallization (T_c) and peak temperature of crystallization (T_p) were obtained from DTA thermographs.

3.2.4.3 Hot-stage microscopy

A side-view hot-stage microscope (HSM) EM 201 equipped with image analysis system and electrical furnace 1750/15 Leica was used. The microscope projects the image of the sample through a quartz window and onto the recording device. The computerized image analysis system automatically records and analyses the geometry changes of the sample during heating. The image analyser takes into account the thermal expansion of the alumina substrate while measuring the height of the sample during firing, with the base as a reference. The HSM software calculates the percentage of decrease in height, width and area of the sample images. The measurements were conducted in air with a heating rate of 5 ºC min^{-1}. The cylindrical shaped samples with height and diameter of ≈3 mm were prepared by cold-pressing the glass powders. The cylindrical samples were placed on a 10×15×1 mm alumina (>99.5 wt.% Al_2O_3) support. The temperature was measured with a Pt/Rh (6/30) thermocouple contacted under the alumina support. The temperatures corresponding to the characteristic viscosity points (first shrinkage, maximum shrinkage, softening, half ball and flow) were obtained from the photographs taken during the hot-stage microscopy experiment following Scholze's definition [1].

3.5 Synthesis of sintered glass-ceramics

Round shaped pellets with 20 mm diameter and ~3 mm thickness were prepared from glass powder by uniaxial pressing (80 MPa). The samples were sintered under non-isothermal conditions (β = 5 ºC min^{-1}) at 825 ºC or 850 ºC for 1 h in a box furnace in air.

3.6 Characterization of glass-ceramics

3.6.1 Crystalline phase analysis and microstructure

The qualitative and quantitative analysis of crystalline phases in the glass–ceramics (crushed to particle size <63 μm) was made by XRD analysis using a conventional Bragg-Brentano diffractometer (Philips PW 3710, Eindhoven, The Netherlands) with Ni-filtered Cu-K_α radiation. The quantitative phase analysis of the glass–ceramics was made by combined Rietveld-R.I.R (reference intensity ratio) method. A 10 wt.% of corundum (NIST SRM 676a) was added to all the glass–ceramic samples as an internal standard. The mixtures, ground in an agate mortar, were side loaded in aluminium flat holder in order to minimize the preferred orientation problems. Data were recorded in 2θ range = 5–115º (step size 0.02° and 50 s of counting time for each step). The phase fractions were extracted by Rietveld-R.I.R refinements using the software GSAS–EXPGUI and were rescaled on the basis of the absolute weight of corundum originally added to their mixtures as an internal standard, and therefore, internally renormalized.

Microstructural observations were done on polished (mirror finishing) and chemically etched (by immersion in 2 vol.% HF solution for a duration of 2 min and washing with distilled water in order to stop the etching process and avoid the fluorides formation) glass–ceramics. The etched glass–ceramic samples were observed by scanning electron microscopy (SEM; SU-70, Hitachi) combined with energy dispersive spectroscopy (EDS; Bruker Quantax, Germany) to study the distribution of elements in the crystals.

3.6.2 Linear shrinkage, density and mechanical strength

Parallelopiped bars with dimensions of 4 mm × 5 mm × 50 mm were prepared from glass powders by uniaxial pressing (80 MPa). The samples were sintered under non-isothermal conditions (β = 5 ºC min^{-1}) at 850 ºC for 1 h in a box furnace in air. The mechanical properties were evaluated by measuring the three-point bending strength of rectified parallelepiped bars of

sintered glass-ceramics (Shimadzu Autograph AG 25 TA; 0.5 mm min^{-1} displacement). The linear shrinkage during sintering was calculated from the difference of the dimensions between the green and the sintered bars. The mean values and the standard deviations (SD) presented for linear shrinkage, and bending strength have been obtained from (at least) 10 different samples.

The mechanical reliability was tested by applying the well-known Weibull statistics to the bending strength data. According to Weibull statistics, the increasing probability of failure (F) for a brittle material can be expressed by $F = 1 - \exp(-\sigma/\sigma_0)^m$, where F is the failure probability for an applied stress (σ), σ_0 is a normalizing parameter known as Weibull characteristic strength, and m is the Weibull modulus. Here, the Weibull modulus m is a measure of the degree of strength data dispersion.

3.7 Chemical degradation and apatite forming ability

The biodegradation and apatite forming ability of glasses and glass-ceramics in SBF was investigated by immersion of glass powders or sintered glass-ceramic circular discs (green diameter: 10 mm) in 50 ml SBF solution at 37 ºC. SBF had an ionic concentration (Na^+ 142.0, K^+ 5.0, Ca^{2+} 2.5, Mg^{2+} 1.5, Cl^- 148.8, HPO_4^- 1.0, HCO_3^{2-} 4.2, SO_4^{2-} 0.5 mmol l^{-1}) nearly equivalent to human plasma, as discussed by Tas [2]. The sample – SBF mixtures were immediately sealed into sterilized plastic flasks and were placed in an oven at 37 ºC (± 0.5 ºC) which was agitating in a circular motion at 120 rpm. The sampling took place at different times varying between 1 h and 28 days depending on the nature of samples (will be discussed in Chapter 4). Some experiments were performed in static mode (SBF was not replaced/refreshed) while SBF was completely replaced after every 48 h in other experiments. The experiments were performed in triplicate in order to ensure the accuracy of results. After each experiment, the solids and liquids were separated and pH along with their ionic concentrations [Ca^{2+}, Mg^{2+}, P^{5+}, Si^{4+}; inductively coupled plasma-optical emission spectroscopy (ICP-OES), Jobin Yvon, JY 70 plus, France] were measured. The apatite forming ability on glass powders and glass-ceramics was followed by XRD, FTIR and SEM-EDS analysis.

The degradation tests were performed according to the standard ISO 10993-14 "Biological evaluation of medical devices – Part 14: Identification and quantification of degradation products from ceramics". The test simulates the more frequently encountered *in vivo* pH (7.4 ± 0.1) and therefore investigates the degradation of glasses/ceramics in freshly

prepared Tris–HCl buffered solution. The glass powder with particle size varying between 300 μm and 425 μm was added to the Tris–HCl solution in the powder/solution ratio of 0.05 g ml^{-1} (5 g glass powder in 100 ml Tris–HCl solution). The tests were performed without solution replacement at 37 ºC and with a mixing speed of 120 rpm. The sampling was done after duration of 120 h where the solid and liquid phases were separated by filtering (0.22 μm, Millex GP, Millipore Corporation, U.S.A). The solid samples were then washed in deionised water and dried in an oven to constant weight. The pH along with elemental concentration, as measured by ICP-OES or by atomic absorption spectroscopy (AAS), of the soaking solutions was measured. A relative weight loss percentage (W_L) of glass samples after 120 h of immersion in solutions was calculated from the following equation:

$$W_L = \left(\frac{W_0 - W_t}{W_0} \right) \times 100 ,$$

where W_0 refers to the weight of glasses before immersion and W_t refers to the weight of glasses after immersion. The dried glass samples (after immersion) were analysed by XRD for possible occurrence of crystalline phases (if any).

3.8 In vitro study on cell growth and osteogenic differentiation

The biological performance of glasses and glass-ceramics was studied by the *in vitro* cellular responses, including cell proliferation and osteoblastic differentiation. Results were compared with the tissue culture plastic used as a control. For the cellular study, mesenchymal stem cells (MSCs) derived from rat bone marrow were used. MSCs have been a potential source for the regenerative therapy of tissues including bone, because of their multipotent and self-renewal capacity without the concern of ethical issues. The experimental procedures were based on our previous work [3] and followed by the guidelines approved by the Animal Ethics Committee of Dankook University. MSCs gathered from the bone marrow of rats were maintained in a normal culture medium containing α-minimal essential medium (MEM) supplemented with 10% foetal bovine serum (FBS), 100 U ml^{-1} penicillin and 100 mg ml^{-1} streptomycin in a humidified atmosphere of 5% CO_2 in air at 37 ºC.

MSCs maintained up to 3–4 passages were used for cellular study. The glass-ceramics were sterilized with 70% ethanol for 1 h prior to seeding cells. For the cell growth study, MSCs were seeded on each sample (15 mm x 2 mm disc type) and then cultured in the normal culture

medium condition as described above. After culture for 3, 7 and 14 days, the cell growth level was analyzed by the (3-(4,5-dimethylthiazol-2-yl)-5(3-carboxymethonyphenol)-2-(4-sulfophenyl)-2H-tetrazolium) (MTS) assay. At each culture time, the culture medium was decanted and the CellTitero 96 AQueous One Solution Reagent (Promega) was added to each sample and then reacted at 37 ºC for 3 h. The absorbance at 490 nm was read using an Elisa Plate Reader (Lab systems Inc.). The cell growth morphology was observed by SEM (Hitachi) after fixation the cells with 2.5% glutaraldehyde, dehydration with a graded series of ethanol (50, 70, 90 and 100%) and coating with gold.

The osteoblast differentiation of the MSCs on the glass-ceramics was determined by measuring the alkaline phosphatise (ALP) activity. Cells were seeded on each sample (20 mm x 2 mm disc type), and cultured in the osteogenic medium containing 50 μg ml^{-1} sodium ascorbate, 10 mM β-glycerol phosphate, and 10 nM dexamethasone. After culture for 7 and 14 days, cellular samples were gathered and added to the ALP reaction media to allow an enzymatic reaction according to the manufacturer's instruction (Sigma). The quantity of samples used for the reaction was determined based on the total protein content which was determined by using a commercial DC protein assay kit (BioRad).

The MTS and ALP assays were performed on three replicate samples ($n = 3$). Data were represented as means ± standard deviations. Statistical analysis was carried out by analysis of variance (ANOVA) and significance level was considered at $p < 0.05$.

References

[1] M. J. Pascual, A. Duran, and M. O. prado, “A new method for determining fixed viscosity points of glasses,” *Physics and Chemistry of Glasses,* vol. 46, pp. 512-520, 2005.

[2] A. Cüneyt Tas, “Synthesis of biomimetic Ca-hydroxyapatite powders at 37°C in synthetic body fluids,” *Biomaterials,* vol. 21, pp. 1429-1438, 2000.

[3] S.-A. Oh, S.-H. Kim, J.-E. Won, J.-J. Kim, U. S. Shin, and H.-W. Kim, “Effects on growth and osteogenic differentiation of mesenchymal stem cells by the zinc-added sol-gel bioactive glass granules,” *Journal of tissue engineering,* vol. 2010, pp. 475260-475260, 2011.

…….

Chapter 4. Results and Discussion

Section 4.1

Understanding the molecular structure, sintering ability and bioactivity of glasses along diopside – fluorapatite join

1. Glass forming ability

A series of glass compositions in the system $(CaMgSi_2O_6)_{(100-x)}$ - $[Ca_5(PO_4)_3F]_x$ (x = 0 – 50 wt%) have been prepared in Pt-Rh crucibles at 1590 ºC by melt-quenching technique. The glass compositions have been labelled in accordance with their fluorapatite (hereafter referred as FA) content. For example, FA-0 corresponds to x = 0, FA-10 corresponds to x = 10, etc. Table 4.1 presents the detailed compositions of glasses investigated in the present study.

Table 4.1 Chemical composition of glasses

Glass		MgO	CaO	SiO_2	P_2O_5	CaF_2
FA-0	mol%	25.00	25.00	50.00	-	-
	wt%	18.61	25.90	55.49	-	-
FA-10	mol%	23.20	28.19	46.40	1.66	0.55
	wt.	16.75	28.31	49.94	4.22	0.77
FA-20	mol%	21.29	31.58	42.57	3.43	1.14
	wt%	14.89	30.73	44.39	8.44	1.55
FA-25	mol%	20.28	33.34	40.56	4.36	1.46
	wt%	13.96	31.93	41.62	10.56	1.94
FA-30	mol%	19.25	35.18	38.48	5.31	1.77
	wt%	13.03	33.14	38.84	12.67	2.32
FA-35	mol%	18.17	37.08	36.34	6.30	2.10
	wt%	12.10	34.34	36.07	14.78	2.71
FA-40	mol%	17.07	39.04	34.12	7.33	2.45
	wt%	11.17	35.55	33.29	16.89	3.10
FA-50	mol%	14.73	43.18	29.45	9.48	3.16
	wt%	9.31	37.97	27.75	21.11	3.87

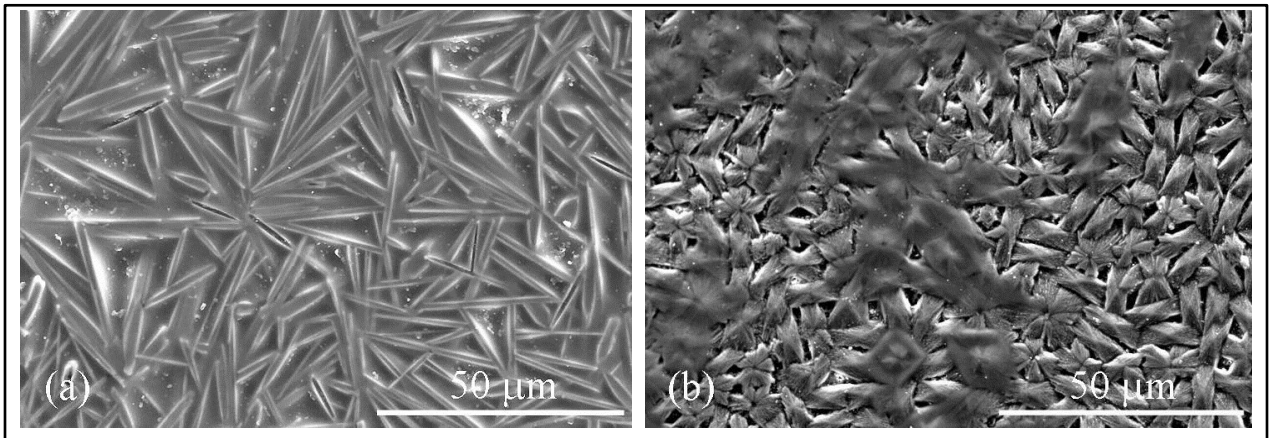

Figure 4.1 SEM images of crystallized glass surface: (a) FA-35, and (b) FA-40. Fluorapatite phase crystallized on the surface of both the glasses immediately after pouring the glass melt on metallic mould.

Among all the investigated compositions, we could obtain amorphous monolithic glasses (by pouring glass melt on metallic mould) only for compositions with x = 10 - 30 wt% while glasses in frit form (by quenching glass melt in cold water) were obtained for compositions with $x \leq 40$ wt%. The monolithic glass rods as obtained for compositions FA-0, FA-35 and FA-40 exhibited severe tendency towards surface devitrification, thus, resulting in the formation of diopside crystals in composition FA-0 and FA crystals for FA-35 (needle-like) and FA-40 (rosette morphology) as depicted in Figure 4.1. The difference in morphology of fluorapatite crystals observed on the surface of these glasses may be attributed to the liquid-liquid phase separation commonly observed in SiO_2 and P_2O_5-containing glasses [1, 2]. Phase separation processes have been shown to have a major impact on the structure and chemistry of parent glasses which in turn determine the fluorapatite morphology observed [1]. Similar observations regarding morphology of fluorapatite crystals in glass-ceramics (needle vs. spherical) have been reported by Hoche et al. [1] in glass system SiO_2-Al_2O_3-CaO-P_2O_5-K_2O-F.

The melting of compositions with x > 40 wt% at 1590 ºC for 2 h resulted in highly viscous liquid which was prone to spontaneous crystallization even after quenching in cold water resulting in white, opaque material with FA as the only crystalline phase, as revealed by XRD analysis. This was expected considering almost equal concentrations of SiO_2 and P_2O_5 leading to immiscibility between silicate and phosphate-rich phases. Further, increasing FA content in glasses will shift the liquidus temperature of the overall system towards higher side (liquidus temperature of stoichiometric fluorapatite is 1630 ºC while that for stoichiometric diopside is

1392 ºC) [3]. Therefore, higher melting temperatures and faster quenching rates are required to obtain glasses from compositions with $x > 40$ wt%. Thus, the present study is dedicated towards the understanding the molecular structure, sintering and crystallization kinetics, and bioactivity of glasses along diopside- fluorapatite system where FA content varies between 0 – 40 wt%.

2. Structure of glasses

The broad ^{29}Si MAS-NMR spectra for all the investigated glasses (Figure 4.2a) implies towards a wider distribution of Q^n (Si) species in the glass structure with dominance of Q^2 (Si) structural units. [4]. No significant shifts were observed in the peak position of ^{29}Si NMR spectra of glasses with varying diopside/fluorapatite ratio. Although it is difficult to provide a concrete explanation for this observation owing to the complex chemistry of the glass system, the possible reason may be attributed to the significant increase in CaO concentration in glasses (25 mol% for FA-0 and ~39 mol% for FA-40) in comparison to P_2O_5 (varies between 0 – 7 mol%). The higher concentration of network modifying cations and decrease in SiO_2 content (50 mol% for FA-0 and ~34 mol% for FA-40) in glasses possibly negated the re-polymerization effect induced by P_2O_5. It has been reported that in a stoichiometric diopside glass (FA-0 in the present case), the distribution of Q^n (Si) is: 28% Q^1, 43% Q^2, 25% Q^3 and 4% Q^4 [5]. This distribution of Q^n (Si) species in FA-0 glass is quite close to the Q^n (Si) distribution of the 45S5 glass (15% Q^1, 67% Q^2, 18% Q^3) calculated by Linati et al. [6], since a mixture of (Q^1 + Q^2) units predominate in both cases, thus giving an indication of good bioactivity. These results are in good agreement with recently published studies by Goel et al. [7] and Kapoor et al. [8] on similar glass compositions where the

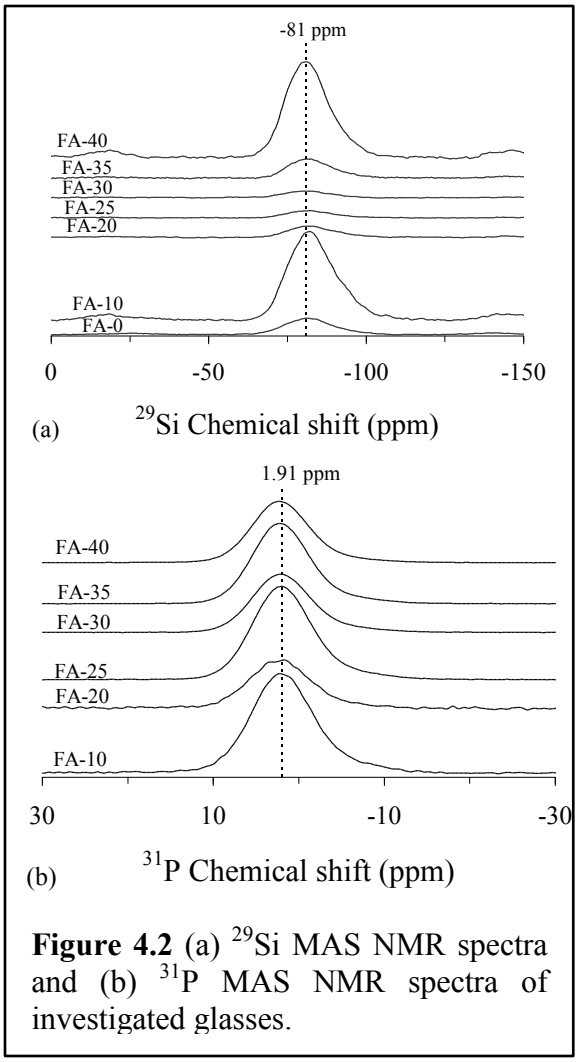

Figure 4.2 (a) ^{29}Si MAS NMR spectra and (b) ^{31}P MAS NMR spectra of investigated glasses.

NC values for these glasses, as calculated using MD simulations, have been obtained to be varying between 1.95 – 2.0.

The ^{31}P MAS-NMR spectra of all the glasses show a predominance of an orthophosphate-type environment (Figure 4.2b). In fact, the observed chemical shifts, 1–3 ppm, are close to that of the calcium orthophosphate (3.1 ppm) and that of the amorphous magnesium orthophosphate (*ca.* 0.5 ppm) [9]. These results are in good co-relation with those reported by Lusvardi et al. [10] and Linati et al. [6] for the 45S5 glass where it has been deduced a fraction of orthophosphate units of ~82% while the rest might be comprised of meta- or pyrophosphates. Furthermore, the introduction of fluoride ion in the phospho-silicate glass network is known to induce significant changes in the local oxygen environment. As has been discussed in Chapter 2, the possibility of Si–F bond formation in bioactive glasses is unlikely. In bioactive glasses, fluoride remains predominantly in ionic state and prefers to form ionic bonds with alkali/alkaline-earth cations (preferably with calcium [7, 8]), thus avoiding the de-polymerization of silicate glass network and forcing phosphate groups to link with silicate groups, leading to higher glass connectivity [10]. However, considering the small concentration of fluoride incorporated in the glass batch (0 – 2.45 mol%) and possibility of significant fluoride volatilization during glass melting [11], the feasibility of the formation of Si–O–P bonds is low if not negligible (as depicted by insignificant shift in ^{29}Si and ^{31}P NMR spectra). In fact, according to the NMR results, phosphate groups are not part of the actual glass network backbone. Similar results have also been obtained by Brauer et al. [4] on a series of SiO_2-P_2O_5-CaO-Na_2O-CaF_2 glasses where it was found that addition of CaF_2 did not disrupt the network connectivity by forming Si–F bonds, instead, formed mixed calcium sodium fluoride species.

3. Glass transition and thermal expansion behaviour

As is evident from Figure 4.3, T_g of the glasses decreased while CTE increased with increase in FA content. It should be noted that since monolithic glass of composition FA-0 was prone to surface crystallization, we could not obtain experimental CTE value for this composition. Therefore, CTE value for glass FA-0 has been obtained from literature to be 8×10^{-6} K^{-1} [12]. The decrease in T_g can be explained by the decreasing concentration of silica, increasing network modifier content (CaO), and the low fraction of Si-O-P linkages as has been explained above. Additionally, with addition of CaF_2 in glasses, fluoride is complexing with

calcium or magnesium, thus, hypothetical CaF^+ and MgF^+ species are added to the silicate ions which reduce the electrostatic forces between NBOs considerably [7], thus decreasing the T_g and increasing CTE of glasses.

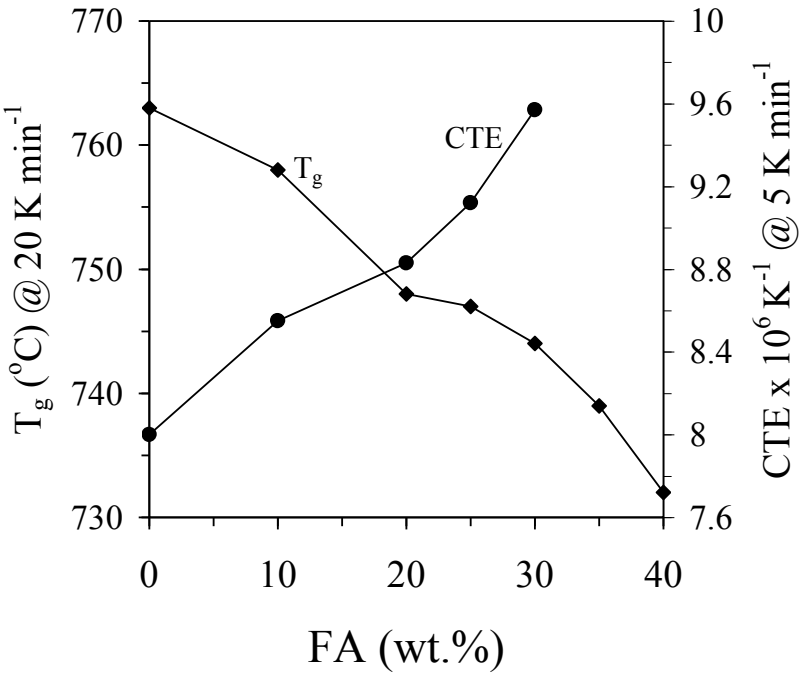

Figure 4.3 Plot depicting variation in glass transition temperature (T_g) and coefficient of thermal expansion (CTE) with respect to fluorapatite content in glasses.

4. Sintering behaviour of glass powders

Figure 4.4 presents the data as obtained from DTA and HSM (β =5 K min^{-1}) pertaining to sintering and devitrification behaviour of glass powders (particle size varying between 10 – 15 μm) that allows observing the following trends:

i) Figure 4.4(a-c) presents the variation in the relative area obtained from the HSM measurement and heat flow with respect to temperature for glass FA-0 (Figure 4.4a), FA-20 (Figure 4.4b) and FA-35 (Figure 4.4c), respectively. The DTA thermographs of glasses with FA content varying between 0-30 wt% exhibited a single crystallization exothermic curve as presented in Figure 4.4a and Figure 4.4b. This signifies that the glass-ceramic is formed either as a result of single phase crystallization or of an almost simultaneous precipitation of two or more crystalline phases. Further, two well defined crystallization exotherms could be observed from DTA thermographs for glasses FA-35 (Figure 4.4c) and FA-40 (not shown) implying towards the precipitation of at least two different crystalline phases. Similar trends were observed for respective glasses at different heating rates.

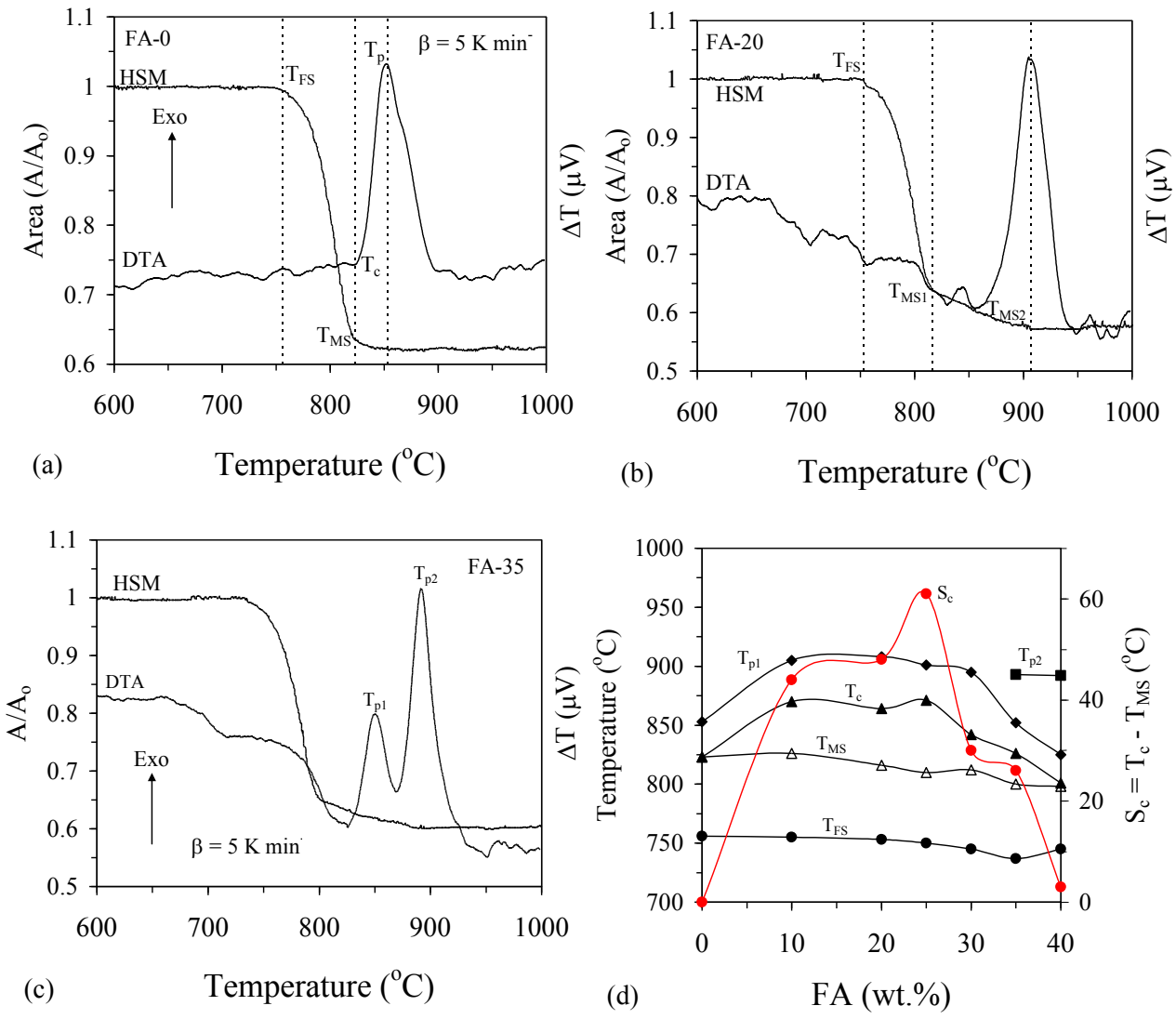

Figure 4.4 Comparison of DTA and HSM curves on the same temperature scale for glasses (a) FA-0, (b) FA-20, (c) FA-35 at heating rate of 5 K min^{-1}. Figure 4.4(d) presents the variation in different thermal parameters for glasses obtained from DTA and HSM, respectively with respect to fluorapatite content in glasses.

ii) The temperature of first shrinkage (T_{FS}; $\log\eta = 9.1 \pm 0.1$, η is viscosity; dPa s) (Figure 4.4a) showed a slight decrease with increasing FA content in glasses (Figure 4.4d).

iii) A single stage shrinkage behaviour was observed for glass FA-0 with its temperature of maximum shrinkage (T_{MS}; $\log\eta = 7.8 \pm 0.1$) coinciding with its onset of crystallization (T_c) (Figure 4.4a), thus leading to value of sintering ability, S_c ($T_c - T_{MS}$) = 0 as has been shown in Figure 4.4d. The low value of sintering ability (S_c) implies towards poor

densification [13]. However, since, maximum densification was achieved exactly at the onset of crystallization (i.e. crystallization did not start before maximum densification could be achieved), therefore, well sintered glass powder compact but with high amount of crystallinity (as will be shown in next section) was obtained after heat treatment at 850 ^{o}C for 1 h.

iv) The introduction of FA in glasses (FA-10) enhanced the sintering ability of glass system considerably by inducing a two-stage shrinkage as has been shown in Figure 4.4b (for glass FA-20), thus leading to a significant difference between T_c and T_{MS} (T_{MS1} for glass FA-10), resulting in a higher value of S_c (Figure 4.4d). Similar two-stage shrinkage behaviour was observed for all the FA containing glasses and can be attributed to the presence of glass-in-glass phase separation in the parent glasses due to the presence of silicate and phosphate rich phases.

v) As is evident from Figure 4.4d, the value of sintering ability parameter (S_c) increased with increase in FA content until glass FA-25 while further increase in FA content in glasses led to degradation of sintering ability. In agreement with the HSM and DTA results, well sintered and dense glass powder compacts were obtained for compositions with $10 \leq FA \leq 25$ wt% while glass-ceramic from composition FA-40 was highly porous and mechanically weak.

5. Crystalline phase evolution in sintered glass-ceramics

Figure 4.5a presents the X-ray diffractograms of glass powder compacts depicting their crystalline phase assemblage after sintering at 850 ºC for 1 h. Diopside ($CaMgSi_2O_6$; ICDD card: 01-078-1390) crystallized as the only phase in compositions FA-0 and FA-10 while further increase in FA/Di ratio led to the precipitation of both diopside as well as fluorapatite. The quantitative crystalline phase analysis of investigated glass-ceramics as presented in Figure 4.5b exhibits that glass FA-0 showed an extensive crystallization with ~2 wt% of residual glassy phase. This result is in good agreement with the microstructure of glass-ceramic FA-0 as presented in Figure 4.6a, where it is difficult to observe any amorphous phase in the sintered glass powder compact. Under such circumstances, we cannot possibly expect good bioactivity from this composition. However, introduction of fluorapatite in diopside glass system significantly influenced its crystallization tendency with the residual glassy phase increasing

from ~2 wt% (for glass FA-0) to ~72 wt% for glass FA-10 (Figure 4.5b and Figure 4.6b). At this juncture, we would like to mention that it was not possible to calculate the amount of crystalline and amorphous phase in GC FA-20 from Rietveld-refinement technique, possibly due to very high amount of residual amorphous phase as can be judged from very low peak intensity of X-ray diffractograms presented in Figure 4.5a.

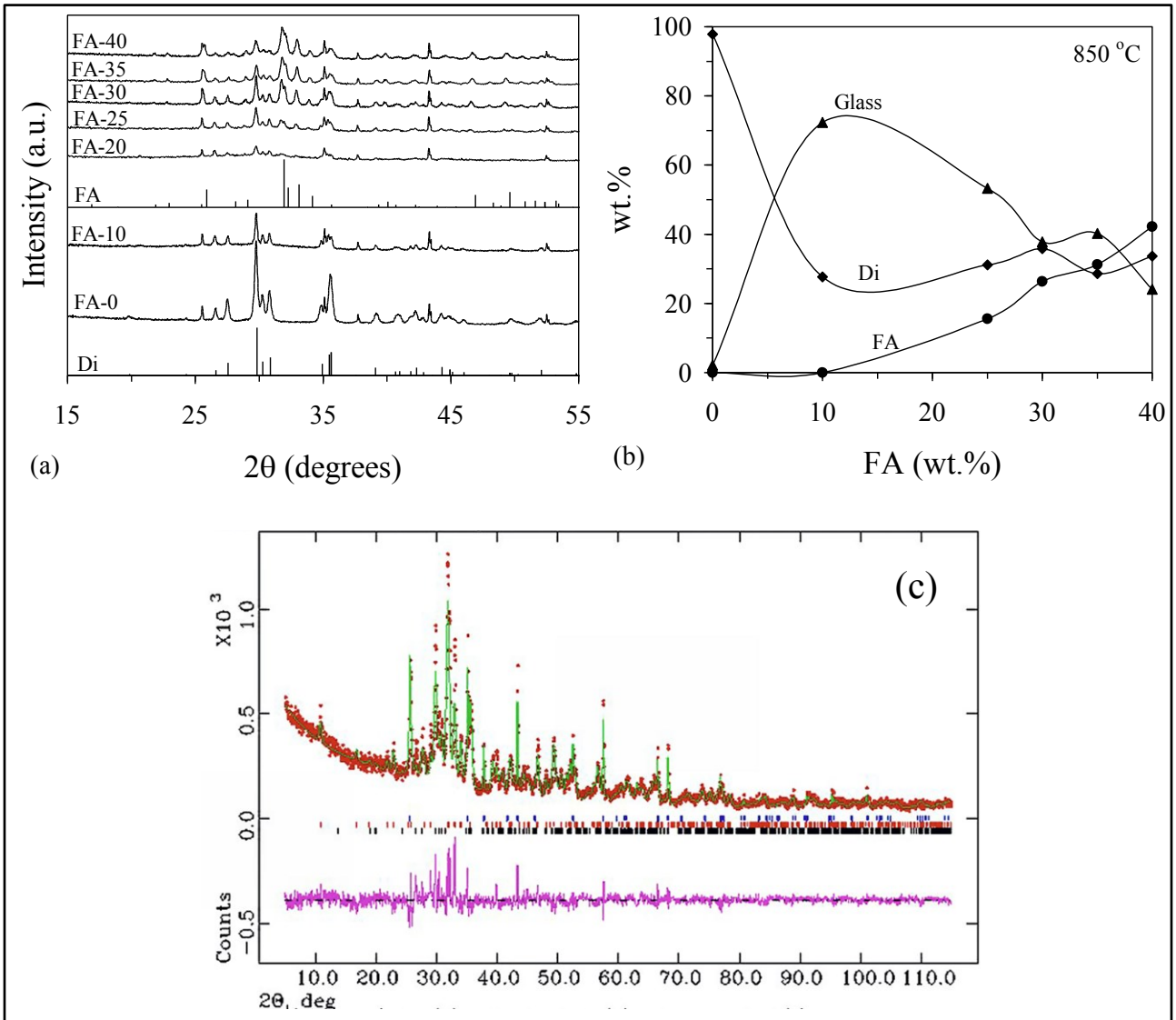

Figure 4.5 (a) X-ray diffractograms of glass-powder compacts sintered at 850 °C for 1 h, (b) quantitative crystalline phase analysis of glass-ceramics with respect to fluorapatite content in glasses as obtained from Rietveld-R.I.R. technique. (c) Observed (crosses), calculated (continuous line), and difference curve from the Rietveld refinement of the glass-ceramic FA-35. Markers representing the phase reflections correspond to corundum, fluorapatite, and diopside (from top to bottom).

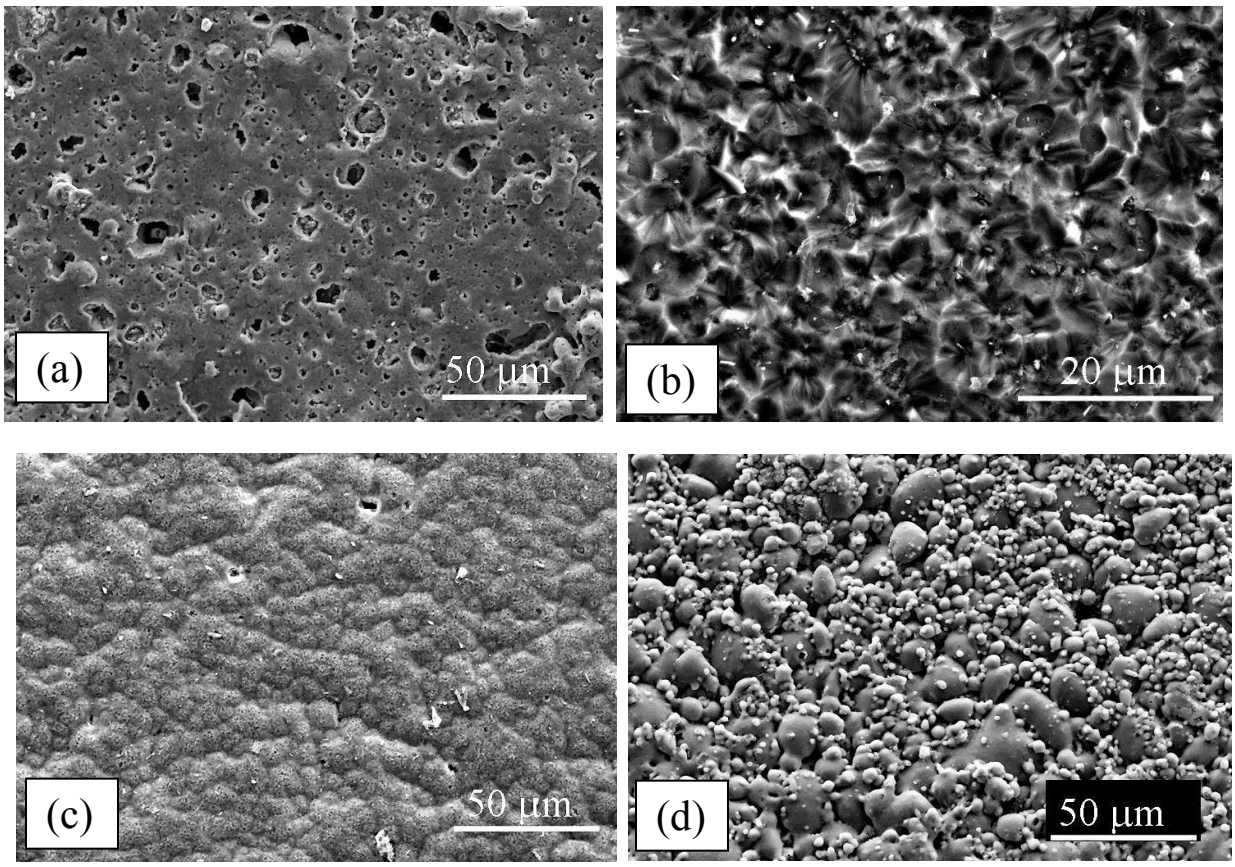

Figure 4.6 SEM images of glass-ceramics (a) FA-0, (b) FA-10, (c) FA-25, and (d) FA-40 after sintering of glass powder compacts at 850 ^{o}C for 1 h.

Therefore, we expect that the amorphous phase in composition FA-20 is higher (> 72 wt%) in comparison to FA-10. Further increase in fluorapatite content (> 20 wt%) increased the crystalline/amorphous ratio in glass-ceramics (as is also evident from the SEM images presented in Figure 4.6c and 4.6d) with fluorapatite (ICDD card: 04-008-0676) emerging as dominant crystalline phase in composition FA-40. Figure 4.5c shows the fit of a measured XRD pattern of glass-ceramic FA-35 by using the GSAS-EXPGUI software. The difference plot does not show any significant misfits. The differences under the main peaks of diopside, fluorapatite, and corundum (internal standard) are caused by adjustment difficulties based on crystallinity of phases.

6. Biodegradation of glasses in simulated body fluid (SBF)

The surface reactivity of glasses was investigated by immersion of glass powders in SBF (0.25 g glass powder in 50 ml SBF solution) at 37 ºC. 45S5 Bioglass® was used as a reference material.

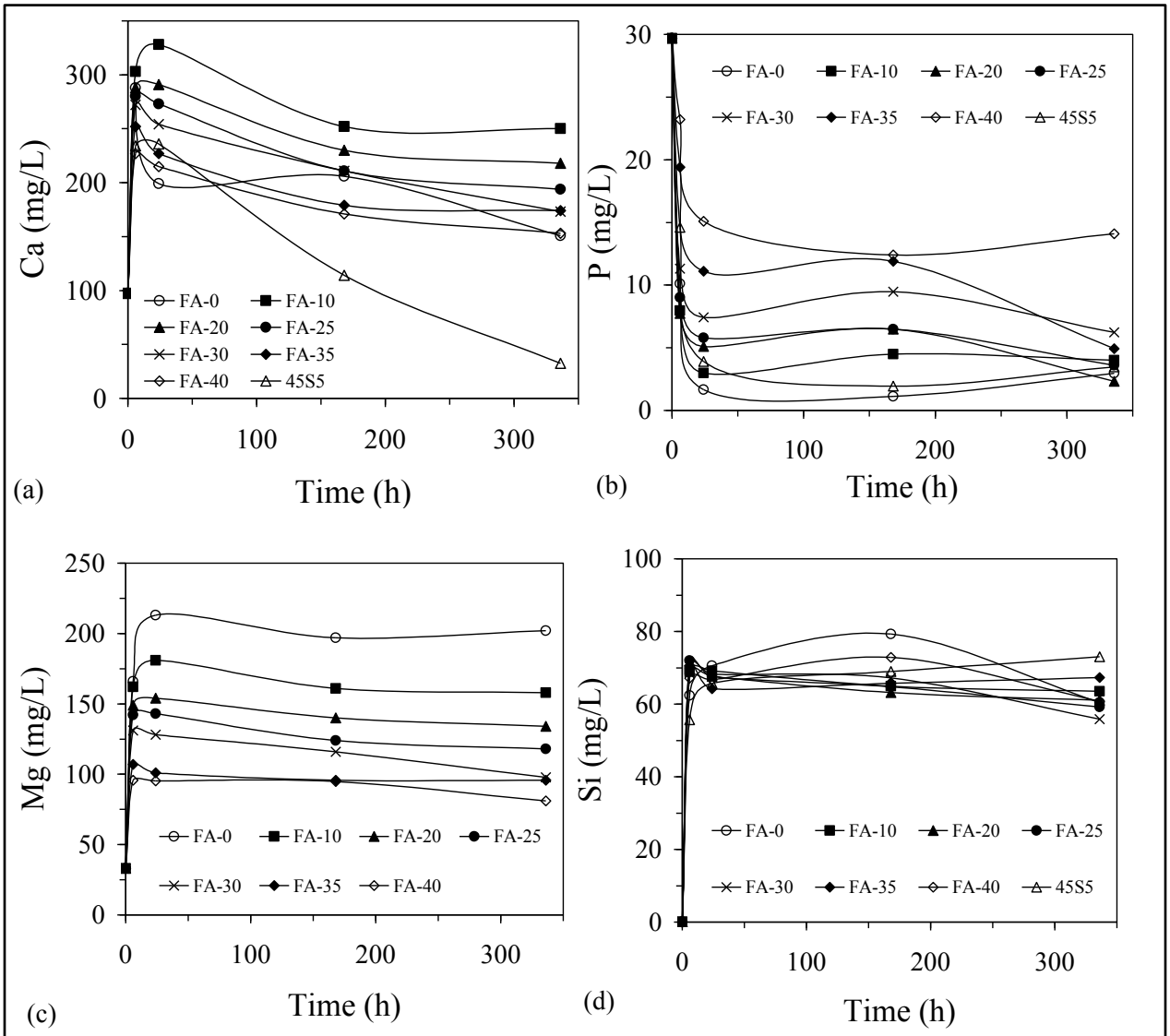

Figure 4.7 ICP plots of elemental concentration of (a) Ca, (b) P, (c) Mg, (d) Si, in SBF solution versus immersion time for the investigated glasses.

6.1 Elemental release profile of glasses in SBF

Figure 4.7 presents the trends observed for elemental release profile of glasses in SBF solution. The following observations have been made:

i) The trend of calcium concentration after 6 h of immersion corresponds to an increase for all glasses which reaches its maximum within 1-24 h of immersion (Figure 4.7a). The increasing Ca concentration in SBF during 1-24 h of immersion for all glasses corresponds to the forward dissolution rate of glasses and imply towards the initiation of bio-mineralization process, where modifier cations in the glass exchange with hydronium ions in the external solution [14]. A decrease in calcium concentration in SBF with increasing immersion time is due to the solution feedback effect that will lead to the formation of calcium-containing compounds on the glass surface, for example: carbonated-hydroxyapatite (HA) or calcite ($CaCO_3$). After ~100 h of immersion time in SBF, calcium concentration reached a plateau exhibiting equilibrium between glass and contact solution.

ii) The trend of overall phosphate concentration demonstrates a slowly decreasing value as a function of soaking time (Figure 4.7b) which is due to migration of phosphorus ions to glass surface to form calcium phosphate rich layer [15]. Increasing FA content in glasses led to increasing concentration of phosphorus-ions in SBF as is evident from Figure 4.7b which may be attributed to either the release of additional soluble phosphate species or fast hydrolysis of small amounts of labile P-O-Si bridges from the glasses in fluid which might lead to local super-saturation and accelerate the calcium phosphate precipitation from solution.

iii) The Mg concentration exhibited behaviour similar to that of Ca in SBF solution and was detected to be highest after 24 h of immersion time for all the glass compositions while no significant variations were observed after prolonged SBF immersions (Figure 4.7c) possibly due to attainment of equilibrium between the Mg^{2+} concentration in glass and SBF, respectively. In general, the amount of Mg detected in SBF solution after any particular immersion time was highest for glass FA-0 and it decreased with decreasing Di/FA ratio. This behaviour can be attributed to the decreasing Mg concentration in the glasses due to increasing FA/Di ratio.

iv) Among all the investigated glasses, the Si ion concentration in SBF was highest after 7 days for glasses FA-0 and FA-40 (Figure 4.7d). However after 14 days (336 h), glasses FA-10 and FA-20 presented higher Si leaching rates, thus indicating a higher ability to form apatite. The loss of silica species from glass indirectly enhances the

bioactive behaviour through the surface Si–OH groups generated in the Si–O–Si hydrolysis process which in turn decrease the interface energy between apatite and glasses [16]. It has been shown that silica gel induces apatite formation on its surface in simulated body environment while silica glass and quartz do not induce it in the same environment [16].

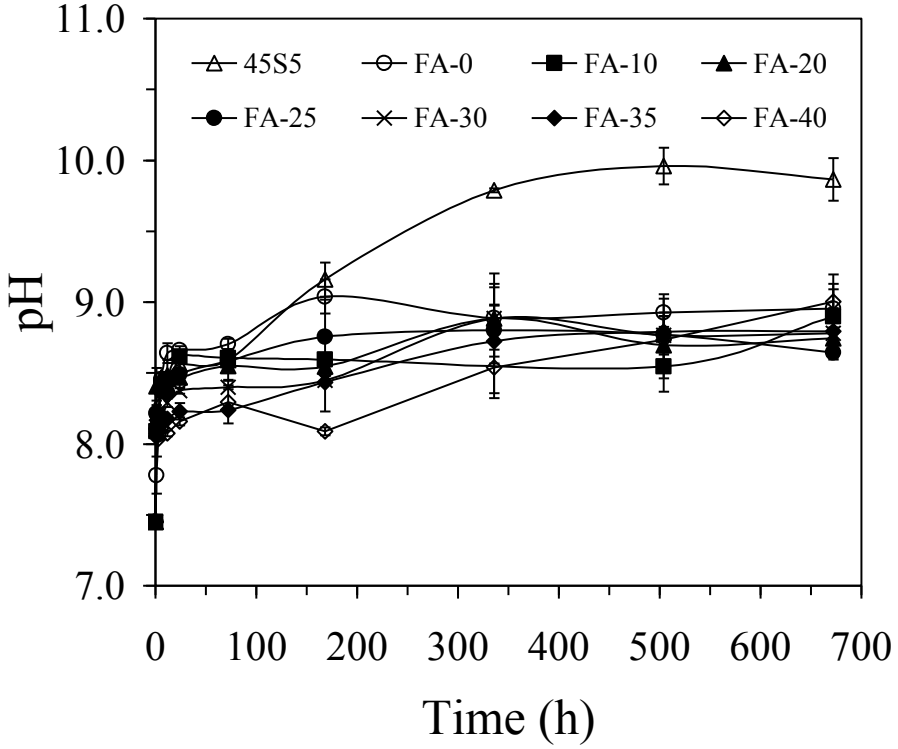

Figure 4.8 The plots depicting pH of SBF solution as a function of immersion time duration for the investigated glasses.

6.2 pH evolution in SBF

The trend of pH evolution after dissolution of investigated glasses in SBF solution for time duration varying between 1 h – 28 days is presented in Figure 4.8 and described below:

i) The pH values observed during dissolution of the 45S5 glass in SBF correspond to a gradual increase from 7.45 to 9.96 during the first 21 days of immersion time, reaching a plateau for ~ 500 h of immersion time. The pH maximum reached by the whole series of Di-FA glasses is definitely lower than the one obtained for the 45S5 glass.

ii) In the case of glass FA-0, the pH values increased until 7 days of glass immersion in SBF, reaching a pH maximum of 9.04, which remained almost constant for higher immersion times.

iii) The pH values of SBF solutions with FA containing glasses were higher during the initial 3 h of immersion, in comparison to glass FA-0. However, with further increase in immersion time, the pH value of the SBF solution containing glass FA-0 surpassed the values of SBF solutions with FA containing glasses. This increase in pH during initial hours of dissolution may be attributed to the excess leaching of alkaline earth cations from phosphate and fluoride component of glasses in SBF solution, as has also been confirmed by ICP-OES results (Fig. 4.7).

In general, pH > 8 was achieved for all the glasses after immersion in SBF for 3 h and the pH of all solutions remained higher than 8.5 for the longest exposure times. It has been reported that, in case of 45S5 glass, the total reconstruction of glass occurs at pH = 8. At pH > 8, calcium phosphate precipitation occurs immediately after immersion, thus preventing any further large ion release and favouring the formation of $CaCO_3$ in comparison to HA [17]. Similar results have been obtained, in the present study, which will be discussed in the following sections. It is noteworthy that antibacterial properties of bioactive glasses are based on their potential to raise the pH in aqueous suspensions [18], resulting from the exchange of modifier cations from glass matrix with hydronium ions from aqueous environment. Bioactive glasses, however not only dissolve or release calcium; they can also release silica, phosphate and sodium. This ion release promotes an additional indirect pH-related antibacterial effect [19].

6.3 FTIR and XRD analysis

The XRD patterns observed for all as-quenched parent glasses (not shown) are in good agreement with their FTIR spectra (Figure 4.9a), exhibiting a broad amorphous halo. The FTIR spectra of 45S5 Bioglass® has been taken as a reference in order to make its structural comparison with the glasses under investigation. As evident from Figure 4.9a, despite significant differences in the chemical composition of the investigated glasses in comparison to the composition of 45S5 Bioglass®, the structure of all the glasses is almost similar to that of 45S5 glass. The infra-red spectra of all the investigated glasses exhibit three broad transmittance bands in the region of 300–1300 cm^{-1}. This lack of sharp features is indicative of the general disorder in the silicate and phosphate network mainly due to a wide distribution of Q^n units occurring in

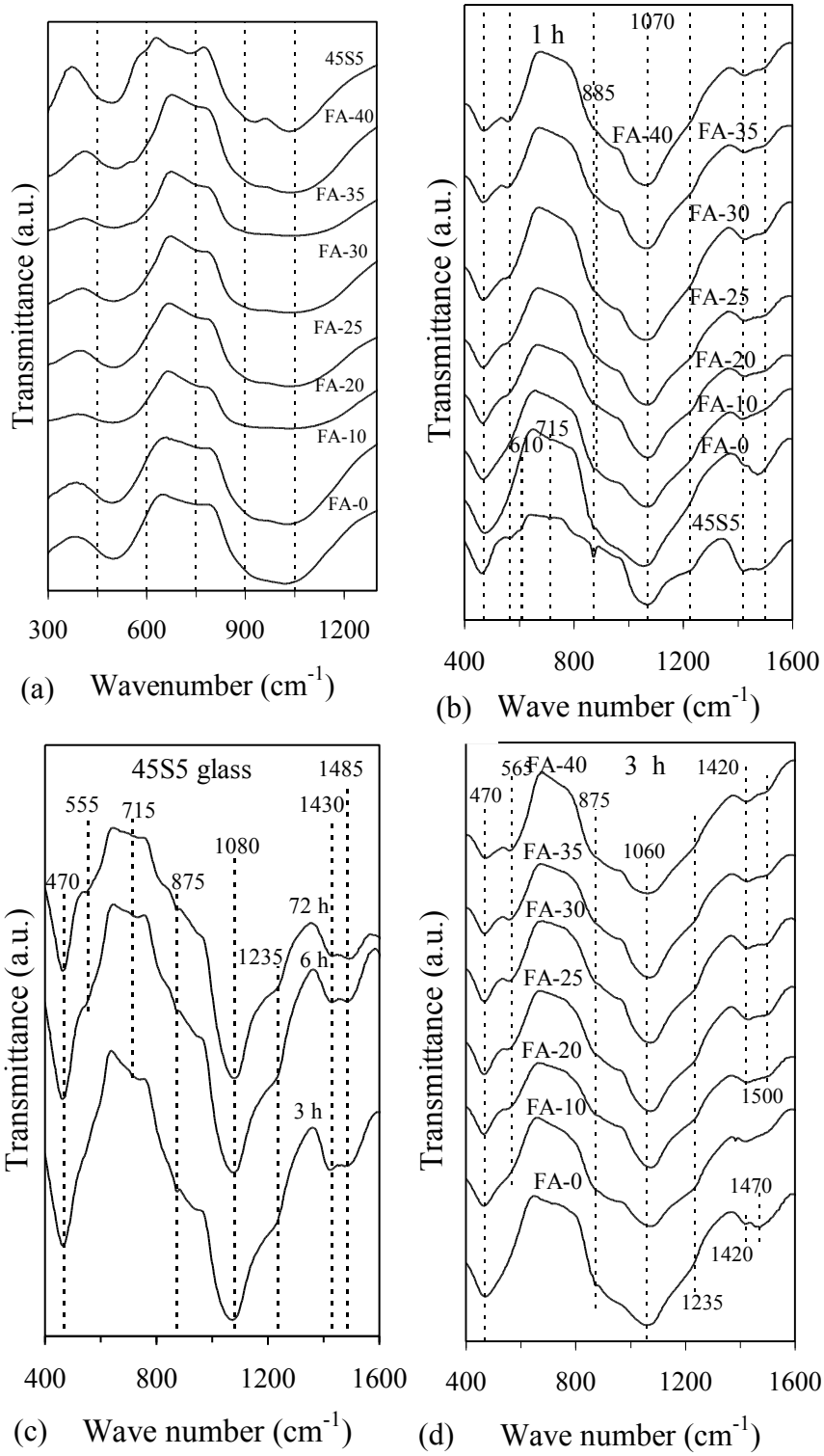

Figure 4.9 FTIR spectra of: (a) glasses before immersion in SBF, (b) glasses after immersion in SBF for 1 h, (c) 45S5 Bioglass after immersion in SBF for different time durations, (d) glasses after immersion in SBF for 3 h

these glasses. The most intense bands in the 800–1300 cm^{-1} region correspond to the stretching vibrations of the SiO_4 tetrahedron with a different number of bridging oxygen atoms [20]. In case of glass FA-0, this region (i.e. 800–1300 cm^{-1}) is further split in two transmittance bands centred at ~1022 cm^{-1} and ~940 cm^{-1}. The high frequency band can be assigned to the Si-O asymmetric stretching mode of BOs, whereas the ~940 cm^{-1} may be attributed to the Si-O asymmetric stretching mode of the non-bridging oxygens (NBOs) [21, 22]. Further, the 498 cm^{-1} band can be attributed to Si-O-Si bending modes [22], while the weak 750 cm^{-1} shoulder may be due to Si–O–Si symmetric stretching with simultaneous Si cation motions [23]. The systematic substitution of diopside by fluorapatite led to a gradual shift of the 1022 cm^{-1} and 498 cm^{-1} bands (in glass FA-0) to 1039 cm^{-1} and 505 cm^{-1} (in glass FA-40), respectively, while the bands at ~940 cm^{-1} and the ~750 cm^{-1} remain unchanged. In glasses with higher FA content (i.e. FA-35 and FA-40), a shoulder was observed at ~560 cm^{-1}, which is due to the bending modes of the PO_4 unit [24]. It is noteworthy that the high frequency band at 1039 cm^{-1} may also be assigned to the asymmetric stretching of PO_4 units which has been reported to appear in crystalline FA at 1038 cm^{-1} [24].

After immersion in SBF for 1 h, FTIR spectra of all the glasses (including the 45S5 glass) showed considerable differences in comparison to the spectra of their respective parent glasses as shown in Figure 4.9b. A strong low frequency band centred at ~470 cm^{-1}, ascribed to the deformation mode of silica layer that develops on the dissolving glass particles [25] could be seen in all the glasses. The main IR band now occurs at 1070 cm^{-1} and a nearby shoulder, centred at ~1225 cm^{-1} and attributed to Si-O-Si vibration [17], can be observed in all the glasses, due to the interfacial formation of high-area silica gel layer, as postulated in Hench's inorganic reaction set [26]. Further, twin peaks at ~ 1420 cm^{-1} and ~ 1500 cm^{-1}, corresponding to the formation of complex carbonate species connected with the presence of Ca^{2+} ions in the surface [25], appear in all the glasses. Also, two sharp peaks at ~715 cm^{-1} and 875 cm^{-1}, indicative of the interfacial precipitation of a crystalline carbonate species, i.e. calcite ($CaCO_3$) (as confirmed by XRD, Figure 4.10a), could be observed in glasses 45S5 and FA-0, respectively. These two peaks were absent in all the FA containing glasses signifying a lower tendency of FA containing glasses towards calcite formation, as confirmed by XRD (Fig. 4.10a). These results are in good agreement with the ICP-OES results, where it has been depicted that Ca ion concentration in SBF solution decreased with increasing FA content. Therefore, lower amount of Ca is available for precipitation of carbonate species. Furthermore, two small sharp peaks were observed in the

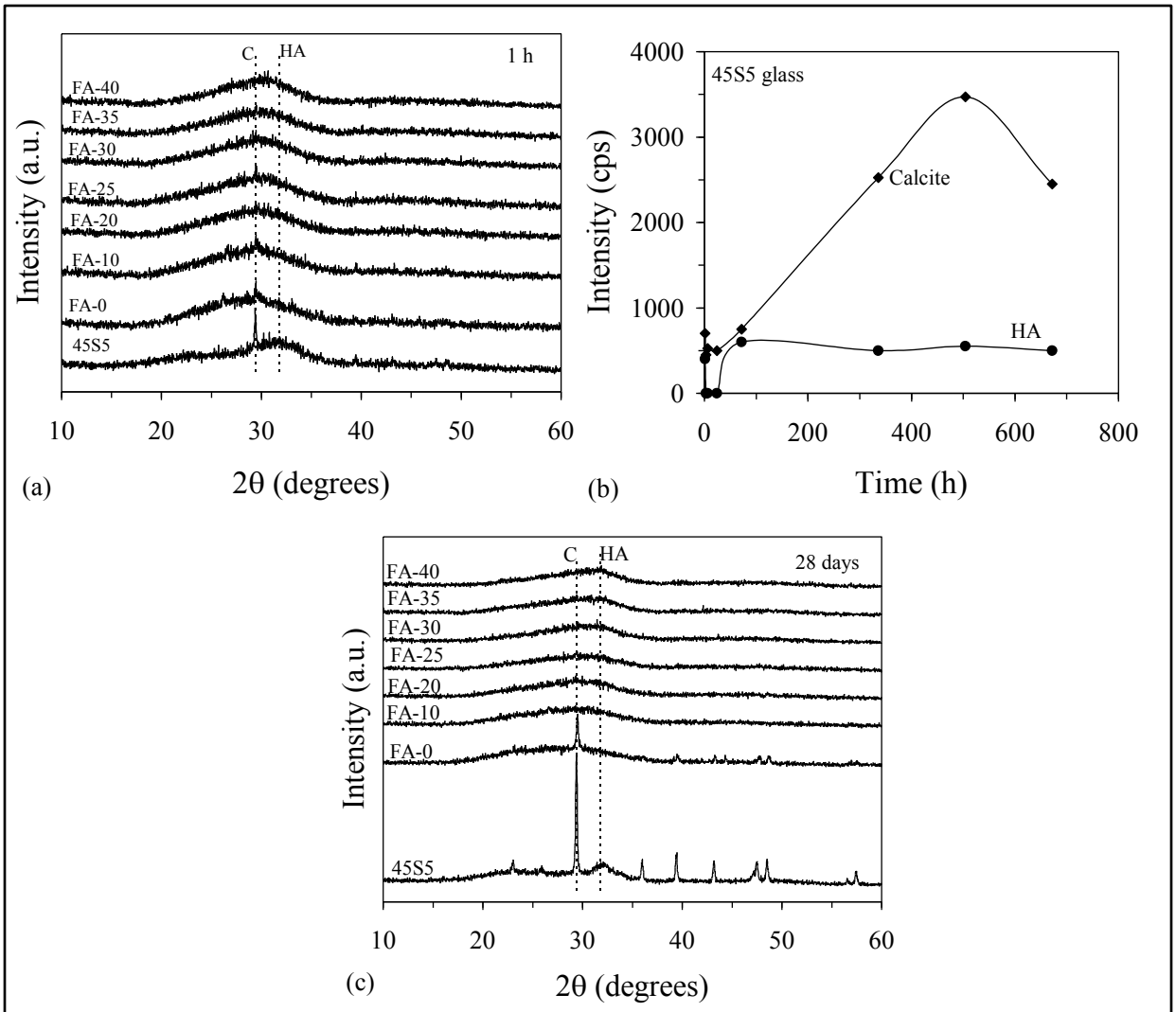

Figure 4.10 (a) XRD patterns of glasses after immersion in SBF solution for 1 h; (b) Plot depicting the change in peak intensities of XRD phase reflections of calcite (C) and hydroxyapatite (HA) for 45S5 Bioglass as a function of immersion time in SBF solution; (c) XRD pattern of glasses after immersion in SBF for 28 days.

45S5 glass at ~565 cm^{-1} and 610 cm^{-1}. This is the most characteristic region for apatite and other phosphates as it corresponds to P-O bending vibrations in a PO_4^{3-} tetrahedron and indicates the presence of crystalline calcium phosphates including HA. A single peak in this region suggests the presence of non-apatitic or amorphous calcium phosphate, which is usually taken as an indication of presence of precursors to HA. Apatitic PO_4^{3-} groups have characteristic split bands at ~560 and 600 cm^{-1}, with a third signal at ~575 cm^{-1} observed for crystallites of small size [25, 27]. No such bands could be observed in glasses FA-0 and FA-10, thus exhibiting no Ca-

phosphate formation. These results are in complete agreement with XRD data of glasses as presented in Figure 4.10a. However, with increment in FA content (≥20 wt%) in glasses, a band at 565 cm^{-1} could be observed which increased in intensity with increasing FA content, thus indicating towards rapid formation of amorphous Ca-phosphate layer on glass [25]. The increasing tendency towards development of amorphous Ca-phosphate rich layer with increasing FA content in glasses may be explained on the basis of increasing phosphate concentration and decreasing Mg concentration in glasses. It has been reported in literature that Mg tends to associate preferentially with phosphorus at glass surface, which consequently leads to the decrease in concentration of apatite like-calcium phosphate domains on the glass surface that are supposed to act as nucleation centres for apatite formation [28]. Also, glass compositions containing phosphate are known to be more soluble and exhibit faster release of silica in solution. Further, isolated orthophosphate groups can be directly released without breaking any chemical bond; thus high rate of formation of amorphous calcium phosphate rich layer in FA containing glasses is likely related to the high availability of this species [15]. An increase in immersion time of glasses in SBF solution for 3 h led to disappearance of the bands at ~565 cm^{-1} and 610 cm^{-1} bands, in the 45S5 glass IR spectrum (Figure 4.9c) implying towards dissolution of crystalline Ca-phosphate while the bands pertaining to the formation of complex carbonates (~1430, 1485 cm^{-1}), crystalline carbonates (~875 cm^{-1}) and high- silica gel layer (~1225 cm^{-1}) became more evident. FTIR data is supported by XRD results presented in Table 4.2, where it is clear that calcite formation masked the precipitation of crystalline apatite in all the glasses including 45S5 glass (Figure 4.10b). However, as revealed by the intensity of XRD phase reflections corresponding to calcite (Figure 4.10a and 4.10c), it is evident that increasing fluoride content in glasses decreased the tendency of calcite formation in glasses. With SBF immersion time of 7 days, the twin peaks at ~565 cm^{-1} and 610 cm^{-1} appeared again for the 45S5 glass, while all the investigated glasses including glass FA-0 exhibited only the formation of amorphous calcium phosphate layer as observed in Figure 4.9d. According to XRD results, precipitation of calcite was favoured in comparison to HA, in all the glasses, as the intensities of peak reflections corresponding to HA be considerably lower than the calcite peak intensities, as presented in Figure 4.10. HA formation was favoured mainly in the FA-40 glass after 28 days of immersion time in SBF (Table 4.2, Figure 4.10c). It is noteworthy that Ca-carbonate phases present a higher solubility product ($K_{ps\ calcite} = 1.7 \times 10^{-8}$) with respect to HA

Table 4.2 Crystalline phase evolution on glass surface after immersion of glasses in SBF solution for varying time durations. (C: Calcite; A: Aragonite; HA: Hydroxyapatite)

	Glass labels							
	45S5	FA-0	FA-10	FA-20	FA-25	FA-30	FA-35	FA-40
1 h	C; HA	C; A	C; A	C	C	C	C	Amorphous
3 h	C	C	C; A	Amorphous	Amorphous	Amorphous	Amorphous	Amorphous
6 h	C	C	A	Amorphous	Amorphous	Amorphous	Amorphous	Amorphous
12 h	C	Amorphous	C; A	Amorphous	Amorphous	HA	Amorphous	Amorphous
1 day	C	C	Amorphous	Amorphous	Amorphous	HA	Amorphous	Amorphous
3 days	C; HA	C	A	Amorphous	Amorphous	Amorphous	Amorphous	Amorphous
7 days	C; HA	C	A	Amorphous	Amorphous	Amorphous	Amorphous	Amorphous
14 days	C; HA	C	A	C	Amorphous	Amorphous	Amorphous	C
21 days	C; HA	C	C; HA	A	Amorphous	Amorphous	Amorphous	C; HA
28 days	C; HA	C	Amorphous	C	Amorphous	Amorphous	Amorphous	HA

($K_{ps\ HA} = 1.6 \times 10^{-58}$) at pH 7.4 [25], and this should favour the precipitation of latter, but Ca-carbonate phases are likely to present a higher rate of crystallization because of the presence of basic surface species (for instance: O^{2-} ions, OH^- ions or coordinatively unsaturated cation-anion pairs), which can coordinate with CO_2, thus giving rise to many possible types of carbonate like species. According to Cerruti and Morterra [17], the carbonate formation in silica-based bioactive glasses occur only if both CO_2 and an excess of water are present at the same time as it is believed that the gas-phase admission of both CO_2 and an excess of water mimics the long-lasting process of carbonate formation. According to Jones et al. [14], the crystallization mechanism of calcite at the expense of HA during *in vitro* bioactivity analysis of glasses in SBF is dose dependant and in case of 45S5 glass, calcite formation is favoured at the expense of HA when the concentration of glass to SBF solution exceeds 0.002 g ml^{-1} (0.005 g ml^{-1} in present study) due to an increase in the ratio of Ca/P ions, in solution. At high concentrations, when there are excessive Ca ions in solution causing an increase in pH of the solution, $CaCO_3$ forms at the expense of HA formation.

7. Physico-chemical degradation of glasses in Tris-HCl buffer

One of the relevant parameters in the study of glass dissolution is the kind of medium used. The pH and ionic strength of the medium play an important role in the rate at which the glasses dissolve. The variation in pH of Tris–HCl with respect to FA content in glasses is presented in Figure 4.11a. A slight increase in pH from 7.4 to 8.41 was observed with increasing FA content in glasses while highest pH value of 9.68 was observed for the 45S5 glass, which exhibited higher dissolution rate than the investigated glasses. This steep pH increase for 45S5 Bioglass may be attributed to the preferential release of sodium over calcium from this glass as has been computationally predicted by Tilocca [29] and experimentally reported by us [30]. It is due to this reason that glass 45S5 exhibited the highest weight loss in Tris-HCl among all the investigated glasses (Figure 4.11c). The increasing pH of buffer solution with increasing FA content in glasses may be attributed to the increasing dissolution of Ca and Mg ions from glasses due to dissolution of charged ion pairs $(Ca\text{-}F)^+$ or $(Mg\text{-}F)^+$ along with the partial disruption of silicate glass network as depicted by the ICP-OES results presented in Figure 4.11b. According to recent studies by Goel et al. [7] and Kapoor et al. [8], fluoride as well as phosphate component in alkali-free bioactive glasses tends to associate preferentially with calcium in comparison to

magnesium. Therefore, higher release of calcium is expected from glass compositions comprising equimolar concentration of two cations. The weight loss increased with increasing FA content in glasses (Figure 4.11c), the highest weight loss of ~1 wt% was observed for glass FA-40. The FTIR spectra of the glasses after immersion in Tris-HCl (not shown) are almost similar to the spectra of their corresponding parent glasses (Figure 4.9a).

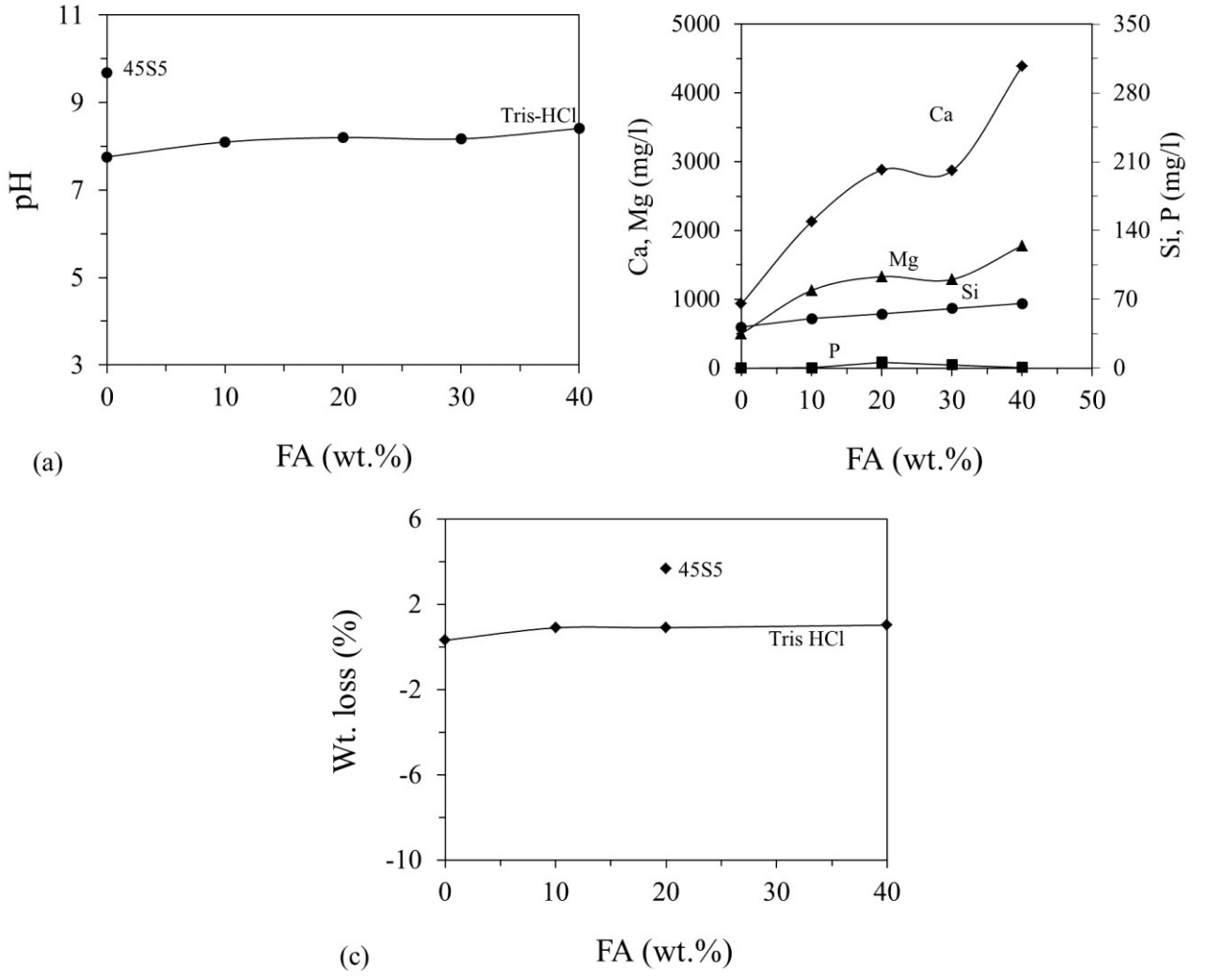

Figure 4.11 (a) The graphs depicting change in pH; (b) ICP plots of elemental concentration of Ca, Mg, P, and Si; (c) weight loss of glasses in Tris-HCl a function of FA content in glasses.

8. Biodegradation of glass-ceramics in simulated body fluid (SBF) and Tris-HCl

The elemental release profile of glass-ceramics (sintered at 850 ^{o}C for 1 h) in SBF as measured by ICP-OES has been presented in Figure 4.12. The following observations can be made:

i) The concentrations of Ca and Mg show similar increasing trends along the soaking time for all glass-ceramics corresponding to forward dissolution rate. The maximum Ca and Mg concentrations in SBF were obtained for glass-ceramic FA-20 with glass-ceramic FA-10 exhibiting the second highest leaching behaviour. In the cases of glass-ceramics FA-0, FA-30 and FA-40, a saturation plateau for Ca and Mg species are attained after the first 24 h. These results are in good co-relation with amorphous/crystalline ratio in glass-ceramics. The compositions with highest amorphous/crystalline ratio exhibited highest leaching ability while increasing crystallinity in glass-ceramics decreased their surface reactivity. The increasing Ca concentration in SBF with increasing immersion time imply towards the initiation of the bio-mineralization process, where modifier cations in the glass exchange with hydronium ions in the external solution [14].

ii) The trend of phosphorus concentration after soaking corresponds to an overall increase for all glass-ceramics. In case of compositions FA-10 and FA-20, phosphorus concentrations reached maximums after 7 days of their immersion in SBF and then decreased considerably. The phosphorus concentration in SBF after 7 days of immersion was highest for glass-ceramic FA-20 and second highest for glass-ceramic FA-10. The increase in phosphorus concentration until 7 days of immersion time may be attributed to either the release of additional soluble phosphate species or to a fast hydrolysis of small amounts of labile P-O-Si bridges from the residual glassy phase in the fluid, which might lead to local super-saturation and accelerate the HA precipitation from solution [14]. This rise in phosphorus concentration apparently coincides with initial stage of the reactivity mechanism features, the formation of Si–OH groups on the glass surface. Further, the decrease in phosphate concentration after 7 days of immersion in SBF is due to migration of phosphorus ions to glass surface to form calcium phosphate rich layers [14].

iii) Among all the investigated glass-ceramics, the Si ion concentration in SBF was highest after 7 days for composition FA-20 and second highest for glass-ceramic FA-10. The lowest Si leaching ability was exhibited by GC FA-0 and FA-40. The loss of silica

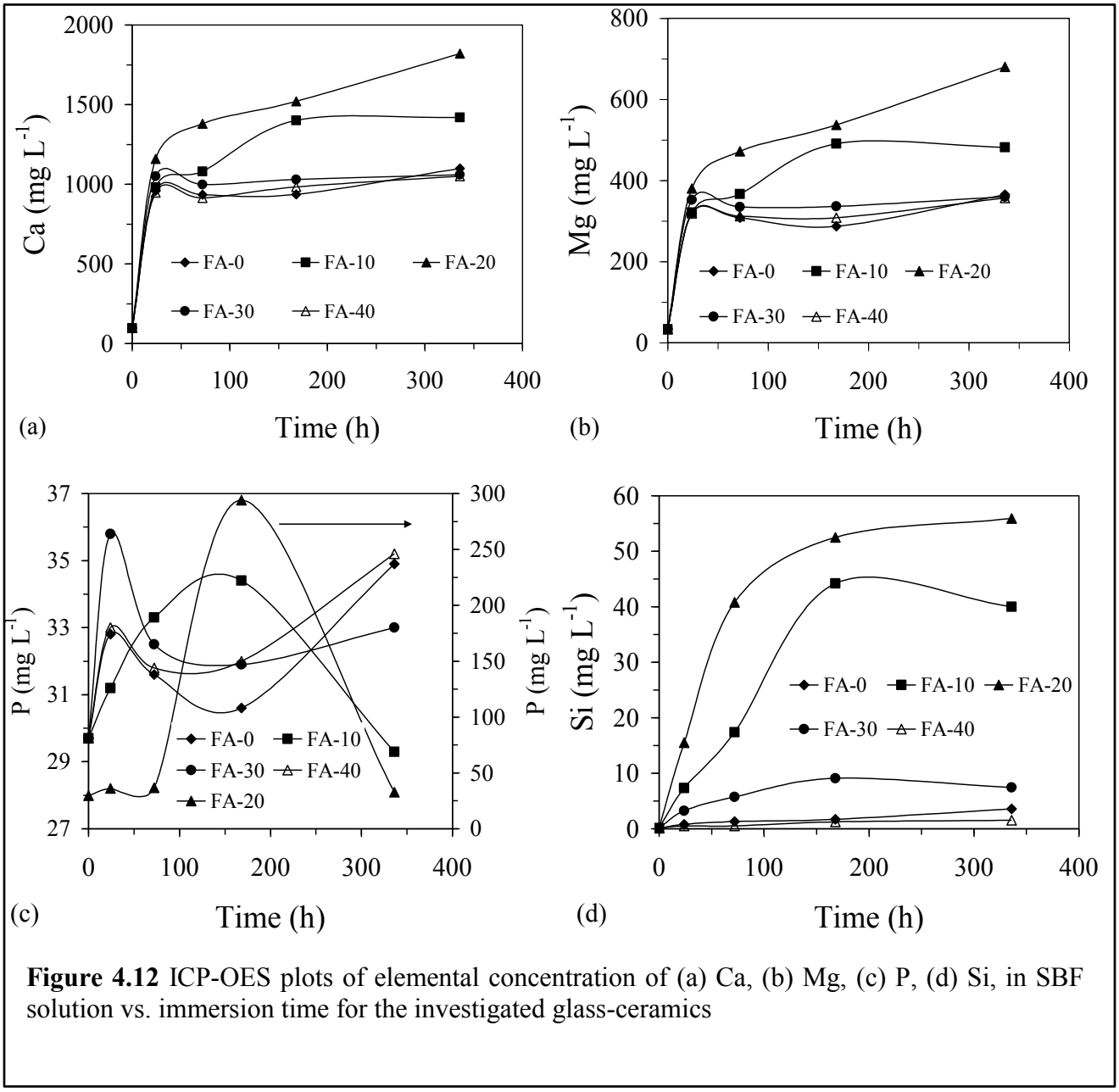

Figure 4.12 ICP-OES plots of elemental concentration of (a) Ca, (b) Mg, (c) P, (d) Si, in SBF solution vs. immersion time for the investigated glass-ceramics

species from glass-ceramic indirectly enhances the bioactive behaviour, through the surface Si-OH groups generated in the Si-O-Si hydrolysis process, which in turn decrease the interface energy between hydroxyapatite and glass-ceramic [31]. The soluble silica species are also thought to play a direct role as nucleation centres for precipitation of calcium phosphate; new applications of bioactive glass-ceramics as scaffolds for *in vitro* tissue engineering require the direct action of released silica and calcium in activating genes, which induce osteoblast proliferation [32].

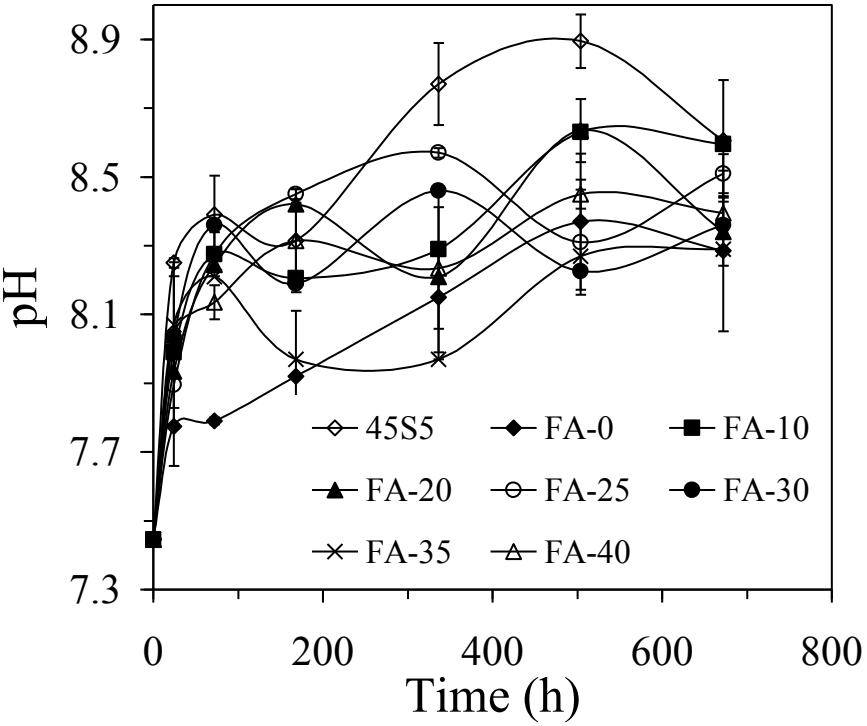

Figure 4.13 The graphs of pH of SBF solution as a function of immersion time duration for the investigated glass-ceramics.

In general, a pH > 8 was achieved for all the glass-ceramics after immersion in SBF for 3 days except glass-ceramic FA-0 (Figure 4.13). As has been reported in *section 6.2*, at pH > 8 (weak base), carbonate formation is preferred instead of HA [17]. The SEM images of glass-ceramic samples after immersion in SBF solution for different time periods are presented in Figure 4.14. As is evident from 4.14a, no apatite-layer formation occurred on glass-ceramic FA-0 after 14 days of immersion in SBF. This may be attributed to its low residual glassy phase content i.e. ~2 wt% as calculated from XRD data. It is worth mentioning that glass-ceramic FA-0 corresponds to stoichiometric diopside ($CaMgSi_2O_6$) composition which is a proven biomaterial for bone regeneration, tissue engineering [33] as well as drug delivery [34]. However, in the present case, this material proved out to be non-bioactive after sintering its precursor glass at 850 ºC for 1 h. This difference in surface active behaviour of diopside based ceramics may be attributed to different synthesis routes and amorphous/crystalline ratio. For example, diopside based bioactive glass-ceramics as synthesized by Yoganand et al. [35] contained a high amount of residual glassy phase as was clear from their XRD data. Nevertheless, *in vivo* tests will be

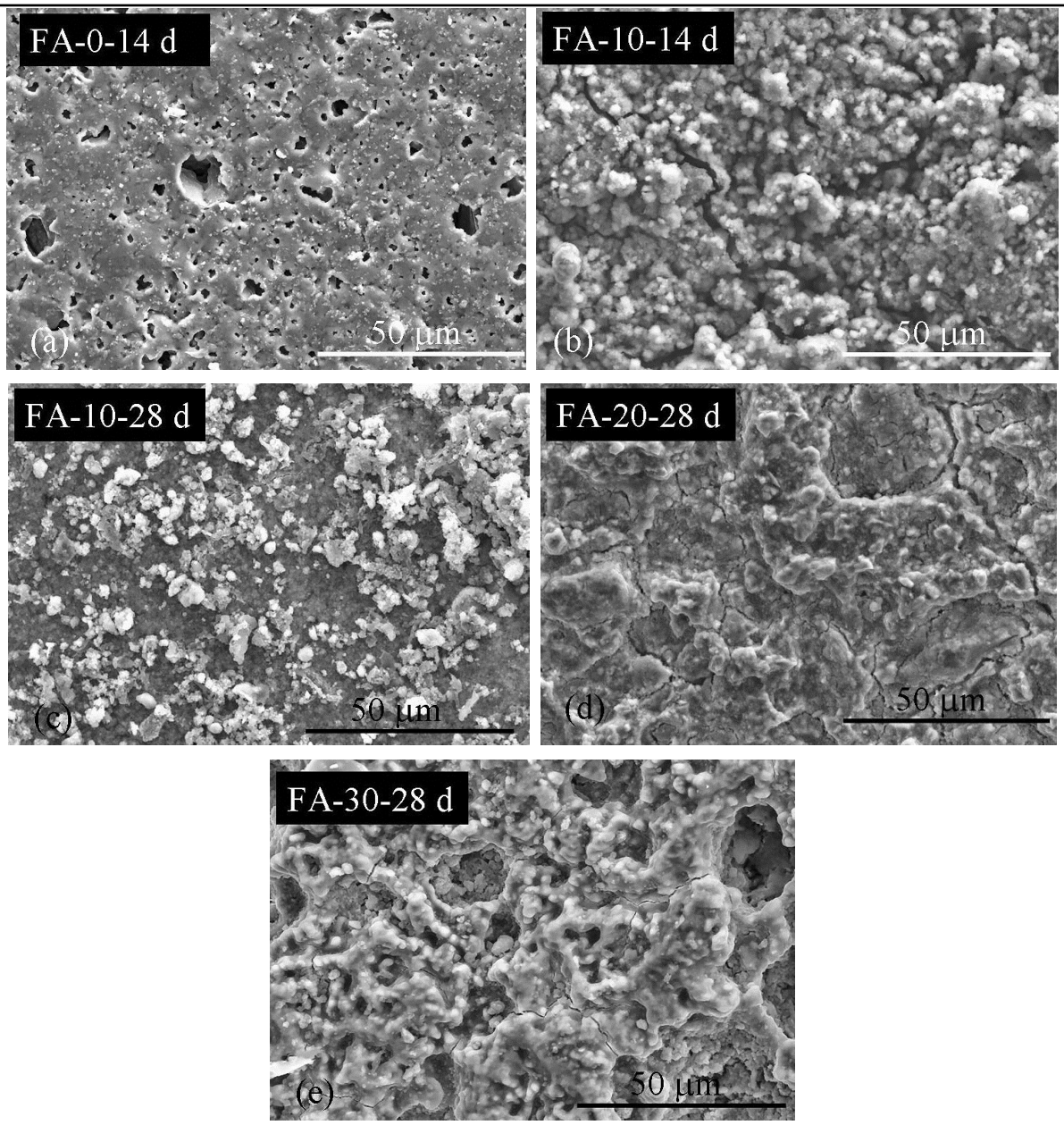

Figure 4.14 SEM images of glass-ceramics after immersion in SBF (a) FA-0 for 14 days, (b) FA-10 for 14 days, (c) FA-10 for 28 days, (d) FA-20 for 28 days, (d) FA-30 for 28 days, respectively.

crucial in order to determine the actual bone bonding ability of glass-ceramic FA-0. Further, FA containing compositions FA-10 and FA-20 exhibited formation of apatite like layer on their surfaces after immersion in SBF after 14 days as has been presented in Figure 4.14b. The Ca/P ratio as calculated from EDS analysis on these samples varied between 1.6-1.7 indicating

towards the precipitation of calcium phosphate layer on their respective surfaces. The intensity of apatite formation on glass-ceramics FA-10 and FA-20 increased significantly with increase in immersion time from 14 to 28 days (Figure 4.14c and Figure 4.14d). The apatite-like layer was also observed on the surface of glass-ceramic compositions FA-25 and FA-30, respectively but only after 21 days of immersion in SBF (Figure. 4.14e) while low apatite forming tendency was observed for glass-ceramic FA-40 in accordance with ICP-OES results.

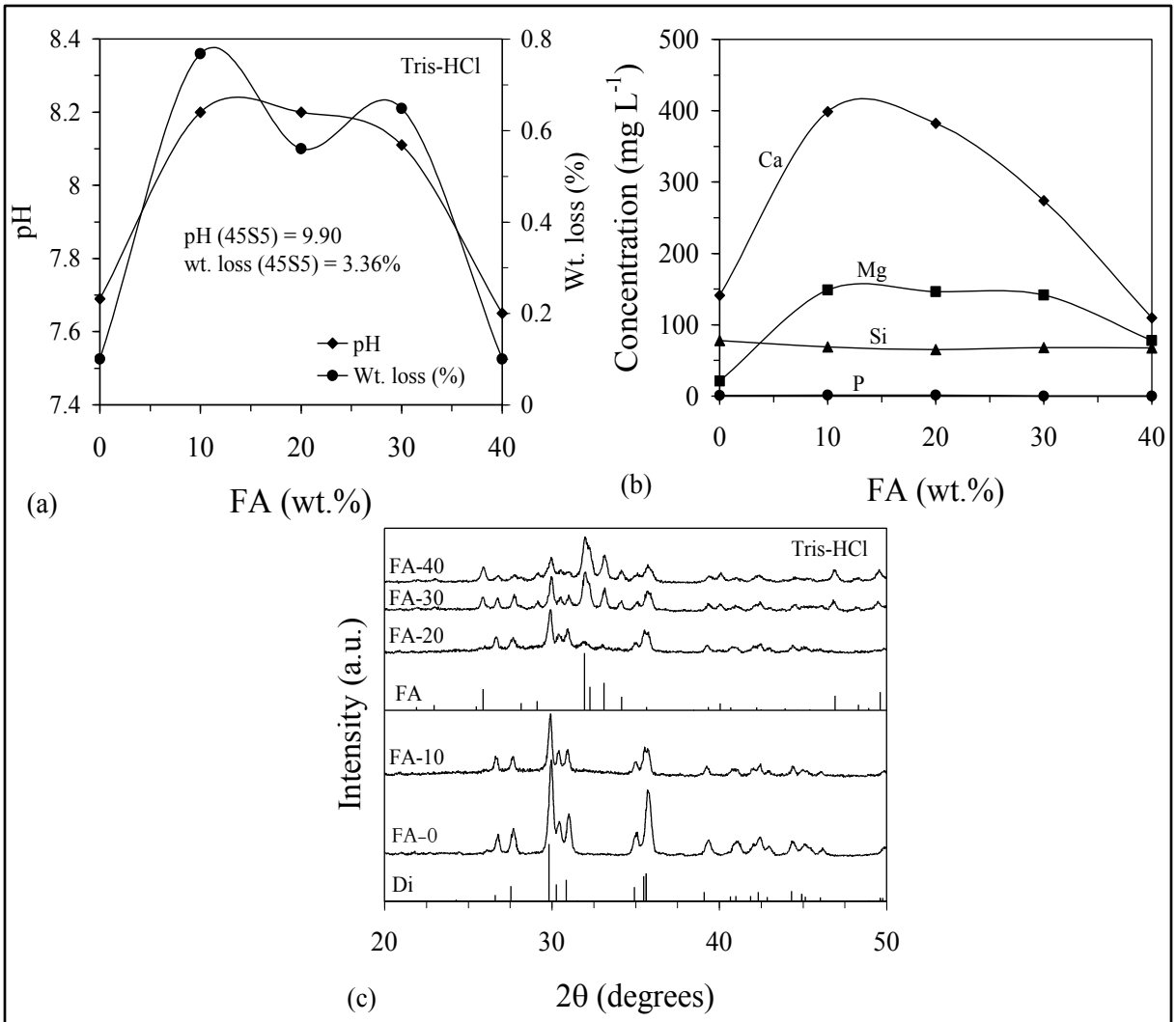

Figure 4.15 (a) Plots for variation in pH of Tris-HCl and weight loss of glass-ceramics (%), and (b) elemental release profile of glass-ceramics in Tris-HCl with respect to fluorapatite content; (c) XRD patterns of glass-ceramics, after immersion in Tris-HCl for 5 days.

The variation in pH and weight loss of glass-ceramics with respect to FA content after soaking in Tris–HCl is presented in Figure 4.15a. The pH in case of glass-ceramic FA-0 is almost equivalent to the pH of the freshly prepared Tris-HCl solution indicating towards its negligible degradation and weight loss in solution owing to its low amorphous content. ICP-OES results, as presented in Figure 4.15b, are in good agreement with pH and weight loss results as glass-ceramic FA-0 exhibits lowest leaching of Ca and Mg ions in the solution among all the investigated glass-ceramic compositions. The introduction of FA enhanced the dissolution behaviour of the investigated glass-ceramics due to their higher residual glassy phase, thus leading to an increase in pH as well as weight loss. The highest weight loss among all the investigated compositions was observed for glass-ceramic FA-10 owing to highest leaching of Ca and Mg ions from this sample in Tris-HCl solution (Figure 4.15b) due to dissolution of charged ion pairs $(Ca–F)^+$ or $(Mg–F)^+$. Further increase in FA content (≥ 30 wt%) led to decrease in leaching ability of glass-ceramics, thus resulting in decreases in pH and weight loss. Among all the investigated glass-ceramic compositions, 45S5 Bioglass® exhibited highest weight loss of >3 wt%, thus proving its high dissolution rate. The XRD data of glass-ceramics after immersion in Tris-HCl did not reveal any significant changes in their crystalline phase assemblage in comparison to their parent glass-ceramics (Figure 4.15c).

With respect to the elemental release profile of glass-ceramics in Tris-HCl, previous studies have shown that Si release levels in the range 0.1 to 100 ppm [36, 37] from bioactive glasses and other biomaterials show stimulatory effects on osteoblasts and the expression of TGF-β mRNA in human osteoblast-like cells. Additionally, Si administration has been known to prevent trabecular bone loss and a silicon-deficient diet results in impaired collagen synthesis and defective skeletal structure [38]. Furthermore, gradual release of soluble silica over time may not only increase cytocompatibility but may also enhance bone bonding due to the increased formation of Si–OH (silanol) groups, which are known to play an active role in the precipitation of calcium phosphate. In the present study, the concentration of Si species in Tris-HCl varied between 65 – 78 ppm (1 ppm = 1 mg l^{-1}) which is in the range of attributing beneficial properties towards various biological processes.

Further, Ca^{2+} ion release from glass-ceramics in Tris-HCl solution varied between 109 – 348 ppm. Although, the significance of Ca in the process of bone mineralization is well established, the ability of extracellular Ca to regulate cell specific responses has been

demonstrated few years back [39]. Increased levels of extracellular Ca (13.1 to 90 ppm) have been shown to induce osteoblast proliferation and chemotaxis through binding to a G-protein coupled extracellular calcium sensing receptor and its gradual release over time may enhance therapeutic efficacy [37, 38].

Furthermore, increasing FA/Di ratio in glass-ceramics affected the elemental release profile of phosphorus as its concentration decreased from 1.6 ppm (FA-10) to 0.1 ppm (FA-40) in Tris HCl. Phosphorus release from biomaterials in controlled amounts (< 30 ppm) has been shown to favour biomineralization and induce expression of osteogenic messenger RNA transcripts while an increase in concentration of phosphorus beyond 30 ppm results in decrease in cell viability [40]. Meleti et al. [40] showed that treatment of human osteoblast like cells with 31 ppm – 217 ppm phosphorus exhibited a dose- and time dependent decrease in cell viability as

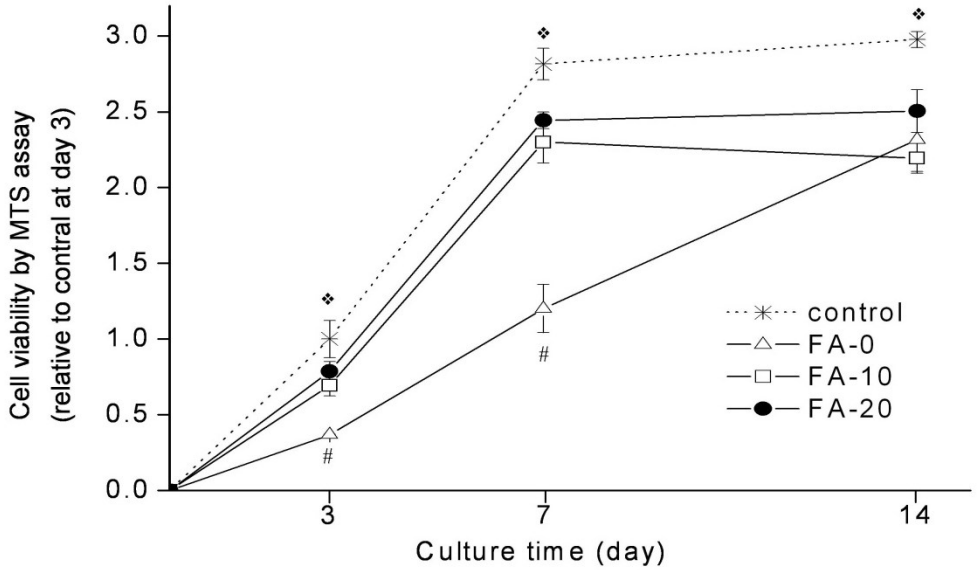

Figure 4.16 MTS cell viability showing the cell growth kinetics on the GC groups (FA-0, FA-10 and FA-20) and tissue culture plastic used as a positive control during culture for 3, 7 and 14 days. Mesenchymal stem cells (MSCs) from rat bone marrow were used for the assay. Statistically significance difference was noticed between groups; control vs. FA-0, FA-10 or FA-20 ($^{*}p < 0.05$) and FA-0 vs. FA-10 or FA-20 ($^{\#}p < 0.05$). ANOVA for n = 3.

a dose of 217 ppm of phosphorus caused an almost complete loss of osteoblast viability in 96 h. In the present study, the ionic concentration of phosphorus released from diopside – fluorapatite glass-ceramics lies within the dose limit in order to promote favourable biological activity.

The level of magnesium in the extracellular fluid ranges between 17 ppm and 25.5 ppm, where homeostasis is maintained by the kidneys and intestine [41, 42]. In the present study, the concentration of magnesium released from experimental glass-ceramics in Tris-HCl varied between 20 ppm (FA-0) and 149 ppm (FA-10) which is significantly higher than the dose required for favourable biological activity. However, it is noteworthy that although serum magnesium levels exceeding 25.5 ppm can lead to muscular paralysis, hypotension and respiratory distress [42], and cardiac arrest occurs for severely high serum levels of 145–170 ppm, the incidence of hyper-magnesium is rare due to the efficient excretion of the element in the urine [42, 43].

9. Cell culture studies on glass-ceramics

Figure 4.16 shows the cell viability on the glass-ceramic groups and control during culture for up to 14 days, as assessed by an MTS method. Apparently, the growth kinetics of the FA-0 group was substantially reduced with respect to that of tissue culture

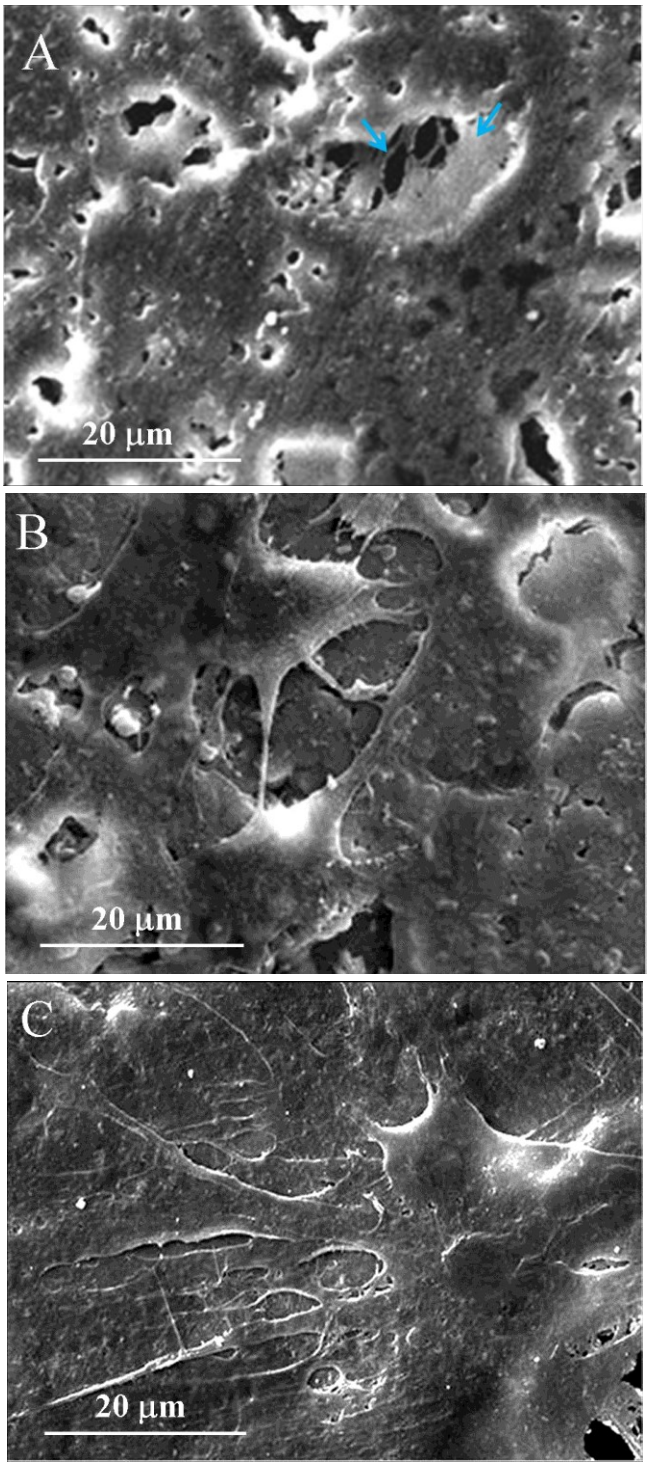

Figure 4.17 SEM morphologies of MSCs grown on the glass-ceramic samples during culture for 7 days; (A) FA-0, (B) FA-10 and (C) FA-20.

plastic control as well as to that of other glass-ceramic groups with significantly lower cell viability particularly at 3 and 7 days owing to its almost negligible residual glassy phase. However, the cell growth on FA-10 continued to increase further to 14 days, reaching the levels of other glass-ceramic groups. FA-10 and FA-20 samples appeared to show similar growth pattern to the culture dish control during the culture period although the cell viability on the glass-ceramic groups was also significantly lower than that of the culture dish control. The

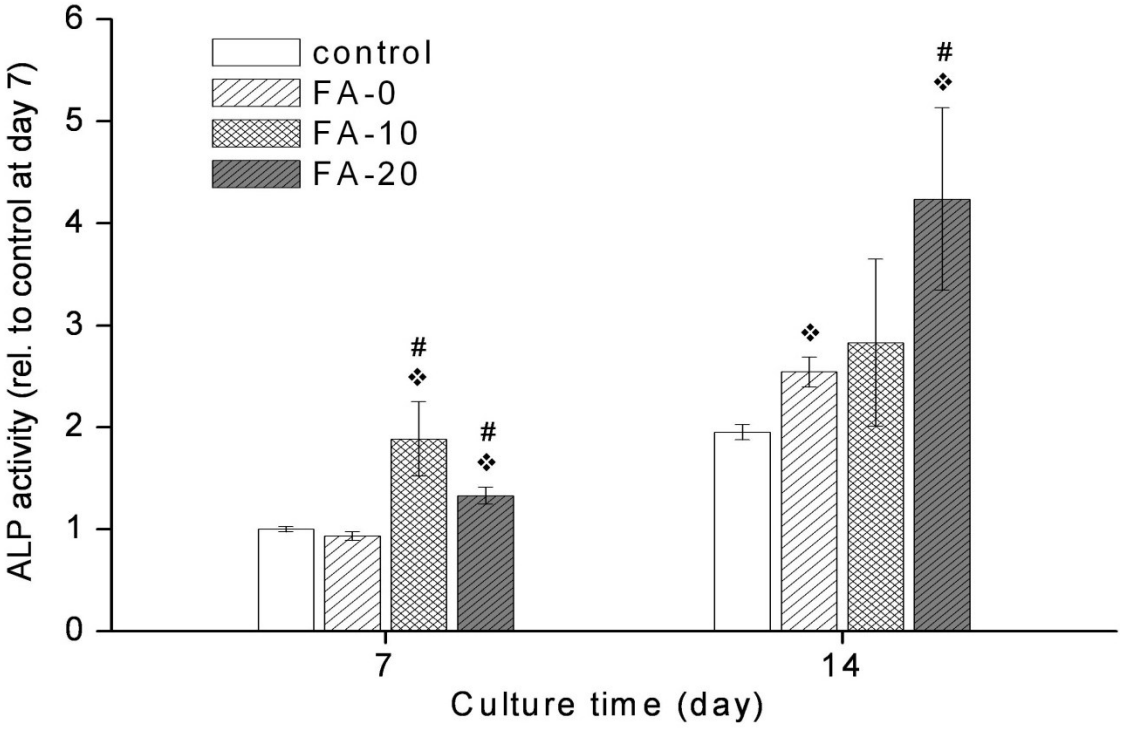

Figure 4.18 ALP activity of MSCs determined after culture for 7 and 14 days on the GCs (FA-0, FA-10 and FA-20) and tissue culture plastic control. Statistically significance difference was noticed between groups; control vs. FA-0, FA-10 or FA-20 ($^{*}p < 0.05$) and FA-0 vs. FA-10 or FA-20 ($^{\#}p < 0.05$). ANOVA for n = 3.

representative cell growth images at day 7 on glass-ceramic samples are presented in Figure 4.17. The cells were not readily noticed on the FA-0 sample (Figure 4.17a). Many pores were developed on the sample and some cellular processes were observed bridging the pores (arrowed). It is deduced that the large amount of pores produced in the FA-0 sample might restrict the proliferative potential of cells. On the other hand, when grown on FA-10 (Figure 4.17b) and FA-20 (Figure 4.17c), the cells were readily observed covering the surface almost

completely with active cytoskeletal processes, and the result suggests the developed FA-10 and FA-20 groups provide MSCs favourable conditions to adhere, spread and proliferate.

The osteogenic differentiation of the MSCs cultured on the glass-ceramic samples was investigated in terms of ALP activity (Figure 4.18). Under the osteogenic medium used herein, rat bone marrow MSCs have been shown to switch to the lineage of osteoblastic cells [44]. When cultured on the control dish, MSCs showed an increased ALP level from days 7 to 14. On the FA-0, the cells showed significantly higher ALP level particularly at day 14. The ALP activity was even further enhanced on FA-10 or FA-20 samples with respect to the cells on the FA-0. Based on the ALP activity assay, the MSCs demonstrated to be better stimulated to an osteogenic lineage when supported on the substrates of glass-ceramics, particularly in the groups containing FA composition (FA-10 and FA-20). This enhanced differentiation was possibly due in part to the change in the surface chemistry associated with the apatite deposition on the glass-ceramics as noticed in the acellular SBF tests. Moreover, the ionic releases from the samples should also affect the MSCs differentiation into osteoblasts in a positive manner. Although the optimal concentrations of the ions to be released from the samples that are effective in the cellular functions cannot be decisive in this study, it is considered that the effects should be more pronounced in the FA-10 and FA-20 with respect to FA-0 based on the much higher ionic releases in the FA-containing groups. Although more in-depth biocompatibility assessments are required in the future, the favourable responses of MSCs including growth behaviour and up-regulated ALP expression support the potential usefulness of the developed Di-FA glass-ceramic systems in bone regeneration field.

10. Summary

We have studied the structure, sintering behaviour and bioactivity of glasses and resultant glass-ceramics in the system $(100\text{-}x)(CaO{\bullet}MgO{\bullet}2SiO_2) - x(9CaO{\bullet}3P_2O_5{\bullet}CaF_2)$, where x varies between 10 – 40 wt%. The following points summarize the results obtained in this study:

1. With respect to the glass forming ability, monolithic glasses (by casting the melt on a metallic mould) could be obtained for compositions with x = 10 – 30 wt% while glass frits (by quenching the melt in cold water) could be obtained for x = 0 – 40 wt%.

2. The silicate glass network in all the glasses is dominated by Q^2 and Q^3 while the phosphate component is predominantly coordinated in orthophosphate environment. These structural features are expected from a glass with good bioactivity [45].
3. The glass transition temperature decreases with increasing fluorapatite content in glasses, due to a gradual decrease in silica content, increase in CaO content and addition of CaF^+ species to the glass structure.
4. The stoichiometric diopside glass (FA-0) exhibits single stage sintering behaviour with its temperature for maximum shrinkage coinciding with onset of crystallization, thus, rendering sintered glass-ceramics with very high crystallinity.
5. Diopside featured as the only crystalline phase in glass-ceramics with $x = 0 - 10$ wt%. Fluorapatite emerged as a secondary phase in glass-ceramics with $x \geq 20$ wt% and its concentration increased progressively with further increase in fluorapatite content. .
6. An extensive calcite precipitation was observed for all the glasses after immersion in SBF solution for 1 h which masked the formation of hydroxyapatite. The tendency towards formation of calcite decreased with increasing fluorapatite content in glasses.
7. The pH of Tris-HCl solution increased slightly with increasing fluorapatite content in glasses due to increasing dissolution of Ca and Mg ions owing to partial disruption of silicate glass network and the dissolution of charged ion pairs $(Ca–F)^+$ or $(Mg–F)^+$. It is due to this reason that highest weight loss (~1 wt%) in Tris-HCl was calculated for glass FA-40.
8. The stoichiometric diopside glass-ceramic did not exhibit any apatite forming ability owing to its negligible amorphous content. The glass-ceramics FA-10 and FA-20 exhibited appreciable densification level with highest amount of amorphous content which in turn led to high rate of apatite-forming ability on their surfaces with good biodegradation properties.
9. *In vitro* responses of MSCs to the glass-ceramics with different compositions showed favourable growth behaviours on FA-10 and FA-20 whilst substantially slowed-down growth kinetics on FA-0.
10. MSCs were supported to differentiate into an osteogenic lineage when cultured on all the glass-ceramics with respect to culture dish control, particularly with more significant stimulation on the FA-10 and FA-20.

Section 4.2

Understanding the structure and sintering ability of glasses in the diopside – fluorapatite – wollastonite system

1. Glass forming ability

A series of glasses with varying CaO/MgO ratio have been synthesized in the system $CaO-MgO-SiO_2-P_2O_5-CaF_2$ with parent composition corresponding to 80 wt% ($CaO•MgO•2SiO_2$) – 20 wt% ($9CaO•3P_2O_5•CaF_2$). The glasses were prepared in Pt-Rh crucibles at 1590 ºC by melt-quenching technique. Table 4.3 presents the composition of glasses investigated in this study. All the glasses exhibited good glass forming ability and resulted in amorphous glass frit upon quenching of glass melt in cold water.

Table 4.3 Chemical composition of glasses

		CaO	MgO	SiO_2	P_2O_5	CaF_2	CaO/MgO
W-10	mol%	34.12	18.76	42.52	3.45	1.15	1.82
	wt%	32.97	13.03	44.02	8.44	1.55	
W-20	mol%	36.70	16.20	42.46	3.48	1.16	2.26
	wt%	35.20	11.17	43.64	8.45	1.55	
W-30	mol%	39.32	13.60	42.41	3.50	1.17	2.89
	wt%	37.44	9.31	43.27	8.43	1.55	
W-40	mol%	41.98	10.96	42.35	3.53	1.18	3.83
	wt%	39.67	7.45	42.89	8.44	1.55	
W-50	mol%	44.68	8.28	42.29	3.56	1.19	5.40
	wt%	41.91	5.58	42.50	8.45	1.55	
W-60	mol%	47.42	5.56	42.24	3.58	1.19	8.52
	wt%	44.15	3.72	42.14	8.44	1.54	
W-70	mol%	50.21	2.80	42.18	3.61	1.20	17.93
	wt%	46.39	1.86	41.76	8.44	1.54	
W-80	mol%	53.03	0.00	42.12	3.64	1.21	-
	wt%	48.62	-	41.38	8.45	1.54	

2. Structure of glasses

In the present study, the room temperature FTIR transmittance spectra of all the investigated glasses (Figure 4.19) exhibit three broad transmittance bands in the region of 300-1500 cm^{-1}. This lack of sharp features is indicative of the general disorder in the silicate and phosphate network mainly due to a wide distribution of Q^n units occurring in these glasses. The most intense bands in the 800-1300 cm^{-1} region correspond to the stretching vibrations of the SiO_4 tetrahedron with a different number of bridging oxygen atoms [20]. This region (i.e. 800-1300 cm^{-1}) is split in two transmittance bands centred at ~1040 cm^{-1} and ~920 cm^{-1}. The high frequency band can be assigned to the Si-O asymmetric stretching mode of BOs, whereas the ~920 cm^{-1} may be attributed to the Si-O asymmetric stretching mode of the NBOs [21, 22]. The 510 cm^{-1} band can be attributed to Si-O-Si bending modes [21], while the weak 740 cm^{-1} shoulder may be due to Si–O–Si symmetric stretching with simultaneous Si cation motions [23]. It is noteworthy that the high frequency band at 1040 cm^{-1} may also be assigned to the asymmetric stretching of PO_4 units which has been reported to appear in crystalline fluorapatite at 1038 cm^{-1} [24]. No significant differences in the infrared spectra of the investigated glasses could be observed thus depicting that varying CaO/MgO ratio in glasses did not affect the structure of glasses substantially.

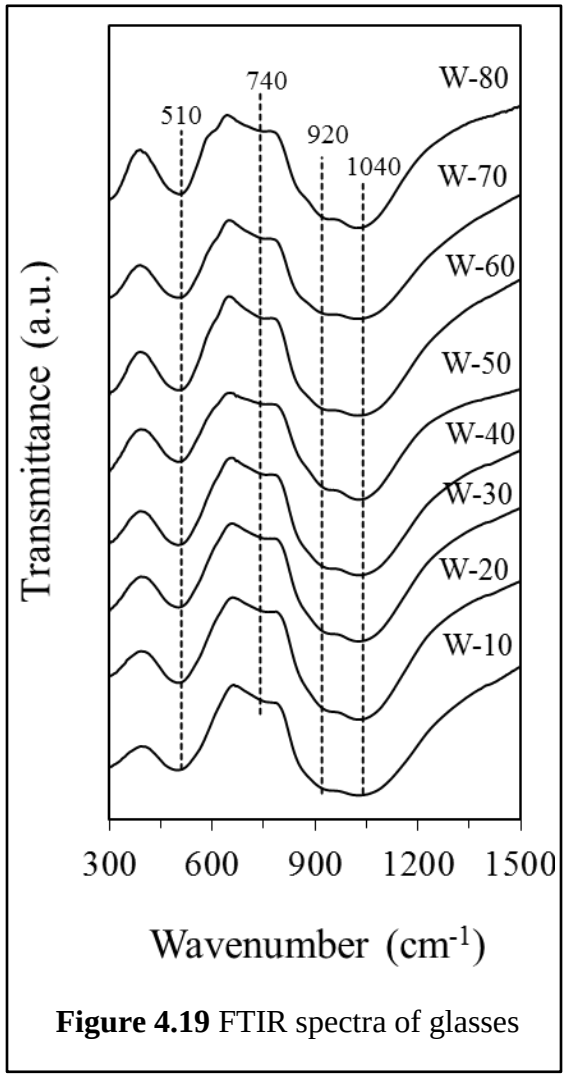

Figure 4.19 FTIR spectra of glasses

In agreement with FTIR studies, the ^{29}Si MAS-NMR spectra for all the investigated glasses (Figure 4.20a) depict the dominance of Q^2 (Si) structural units in the glasses [4]. Further, only slight shift in the peak positions of spectra could be observed and all the spectra are centred between –82.2 ppm and –82.9 ppm, thus depicting no significant changes in the silicon

coordination in glass structure. Similar results have been reported by Galliano et al. [46] where it has been shown that the type and distribution of silicate units in an alkaline-earth phosphosilicate glass does not depend on the nature of the alkaline-earth cations present in the system. Recent stuides by Pedone et al. [47, 48] and Goel et al. [7] have indicated that varying CaO/MgO or MgO/ZnO content in glasses does not affect the overall network connectivity of the glass and the number of NBOs remain unchanged.

The ^{31}P MAS-NMR spectra of all the glasses show a predominance of an orthophosphate-type environment (Figure 4.20b). The observed chemical shifts, ~2 ppm, are close to that of the calcium orthophosphate (3.1 ppm) implying towards preferential coordination of calcium instead of magnesium with orthophosphate groups (^{31}P chemical shift: 0.5 ppm for amorphous magnesium orthophosphate). These observations are consistent with literature as magnesium is known to exhibit least affinity towards associating with phosphate groups in comparison to calcium or sodium [7, 49]. [4]. These results are in good co-relation with those reported by Lusvardi et al. [10] and Linati et al. [6] for 45S5 glass where fraction of orthophosphate units has been calculated to be ~82% while the rest might be comprised of meta- or pyrophosphates.

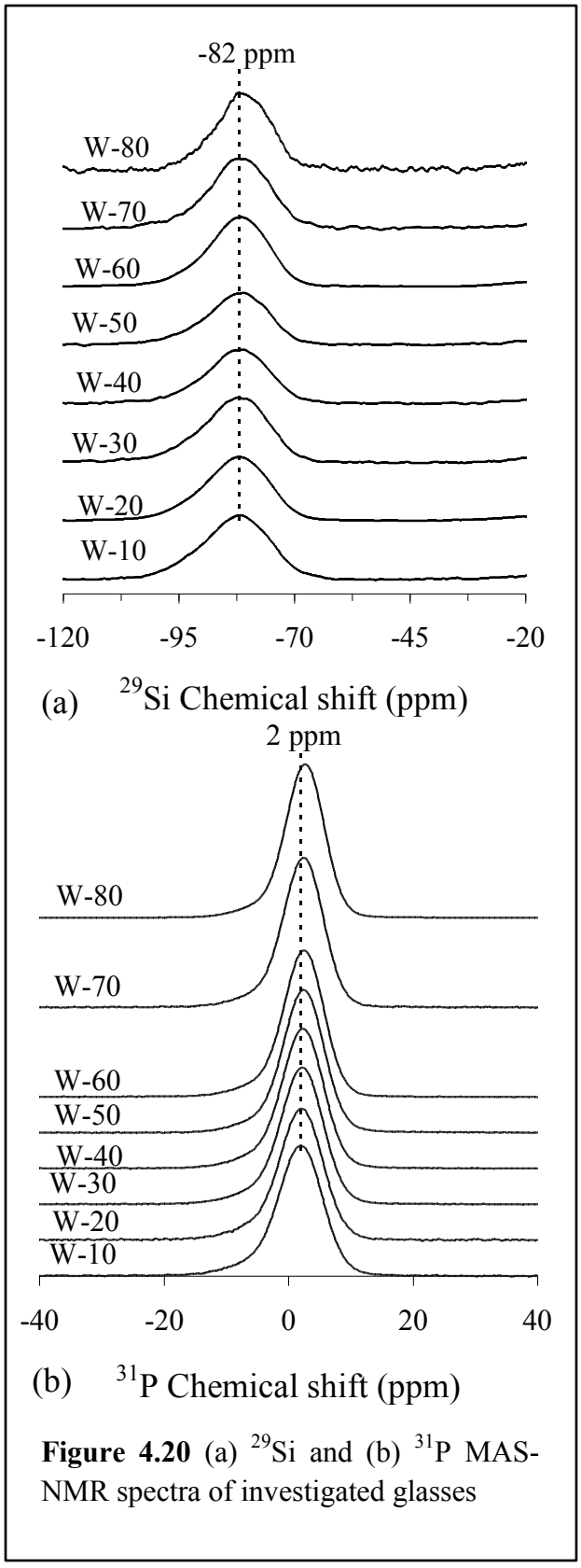

Figure 4.20 (a) ^{29}Si and (b) ^{31}P MAS-NMR spectra of investigated glasses

Therefore, it can be considered that majority of the phosphate component in glass is not part of the actual glass network backbone. Recent studies have shown that for bioactive glasses with P_2O_5 <10 mol%, the fractional population of the orthophosphate groups remains independent of their P_2O_5 concentration at a fixed NC value, but is slightly reduced as NC increases [50, 51]. While the bioactivity generally displays a non-monotonic dependence of P_2O_5 concentration, literature suggests that it is merely the net orthophosphate content that directly links to the bioactivity [50-52].

3. Thermal behaviour of glasses

The DTA plots of glass powders, shown in Figure 4.21, feature an endothermic dip corresponding to glass transition temperature (T_g) before the ons et of crystallization (T_c) and a

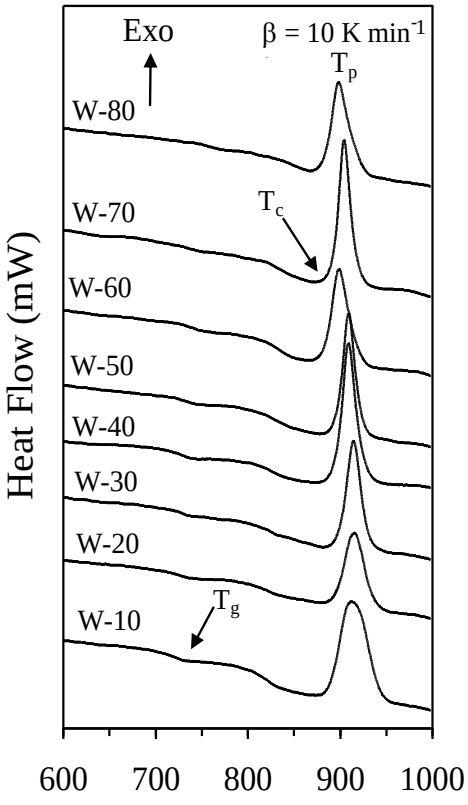

Figure 4.21 DTA thermographs of investigated glasses at heating rate of 10 K min^{-1}.

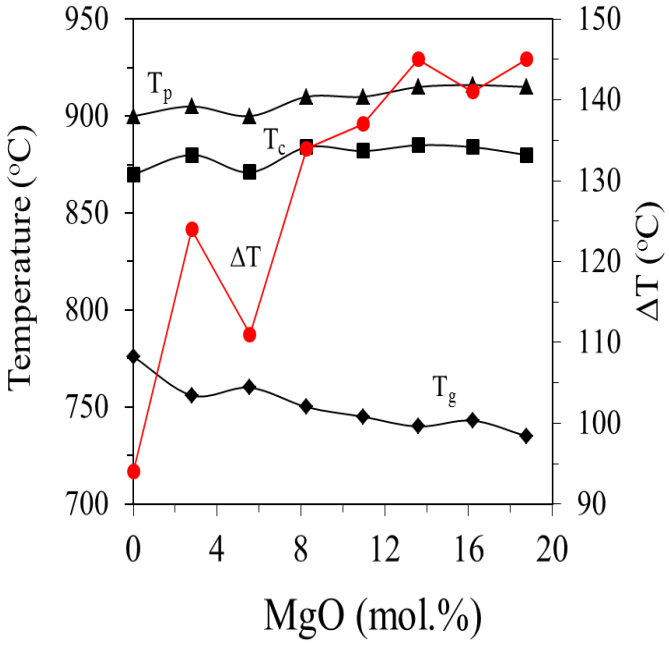

Figure 4.22 Influence of MgO on different thermal parameters of glasses as obtained by DTA.

well-defined single exothermic crystallization curve. The presence of single crystallization exotherm anticipates that the glass-ceramic is formed either as a result of single phase crystallization or of an almost simultaneous precipitation of different crystalline phases. Figure 4.22 present the variation in T_g, T_c and peak temperature of crystallization (T_p) with increasing MgO content in glasses. As is evident from Figure 4.22, T_g shifted towards lower temperature values with increasing MgO content in glasses. This may be attributed to magnesium entering the silicate glass network as tetrahedral MgO_4 units [53]. According to Watts et al. [49], Si–O–Mg bonds have, on average, a significantly lower bond strength with respect to Si–O–Si bonds in the silicate chain, and therefore, resulting in the observed reduction in T_g. This is also a key feature for lowering melt viscosities of Mg-containing silicate glasses [54]. No significant variations in the values of T_c (880 ± 6 °C) and T_p (809 ± 6 °C) were observed with varying CaO/MgO ratio in glasses (Figure 4.22).

With respect to the sintering ability of glasses, Figure 4.22 presents the variation in thermal stability parameter ΔT (= $T_c - T_g$) for all the investigated glasses. The higher values of ΔT correspond to delay in nucleation and thus, provide wider processing window for a glass composition to attain maximum densification. In the present study, increasing calcium content in glasses decreases the value of ΔT, thus implying towards degradation in sintering behaviour of glasses. However, still the values of ΔT obtained for all the investigated glasses are high enough to help glass powders attain good densification during sintering. These observations are in good agreement with the results of Karamanov et al. [55] where it has been reported that wollastonite ($CaO•SiO_2$) based glass-ceramics possess lower mechanical strength in comparison to diopside ($CaO•MgO•2SiO_2$) based glass-ceramics.

In accordance with DTA results, well sintered glass-ceramics were obtained after sintering of glass powders at 850 ºC for 1 h. As is evident from Figure 4.23, the XRD results reveal the presence of diopside ($CaMgSi_2O_6$; ICDD card: 01-078-1390), fluorapatite [$Ca_5(PO_4)_3F$; ICSD: 01-071-3848], and wollastonite ($CaSiO_3$; ICSD: 20589) in the crystalline phase assemblage of all the glass-ceramics except composition W-80 which is MgO-free. As is evident from the intensity of XRD phase reflections, the starting glass composition (W-10) comprised mainly of residual amorphous glassy phase which decreased with increasing CaO/MgO ratio in glasses until composition W-50. Wollastonite dominated the crystalline phase assemblage of glass-ceramics W-50, W-60 and W-70. Further increase in CaO/MgO ratio in

glasses led to decrease in crystallinity in glass-ceramics. The residual glassy phase in glass-ceramics is of crucial importance as it controls the apatite forming ability of glass-ceramics [56, 57] and the glass-ceramic may turn bio-inert if residual glassy phase is in low amount (< 5 wt%). Thus, the design of glass-ceramic compositions needs to be such that equilibrium is achieved in the midst of biological and mechanical properties of the final material. In the present investigation, the amount of residual glassy phase is high enough to render good bioactivity to resultant glass-ceramic material.

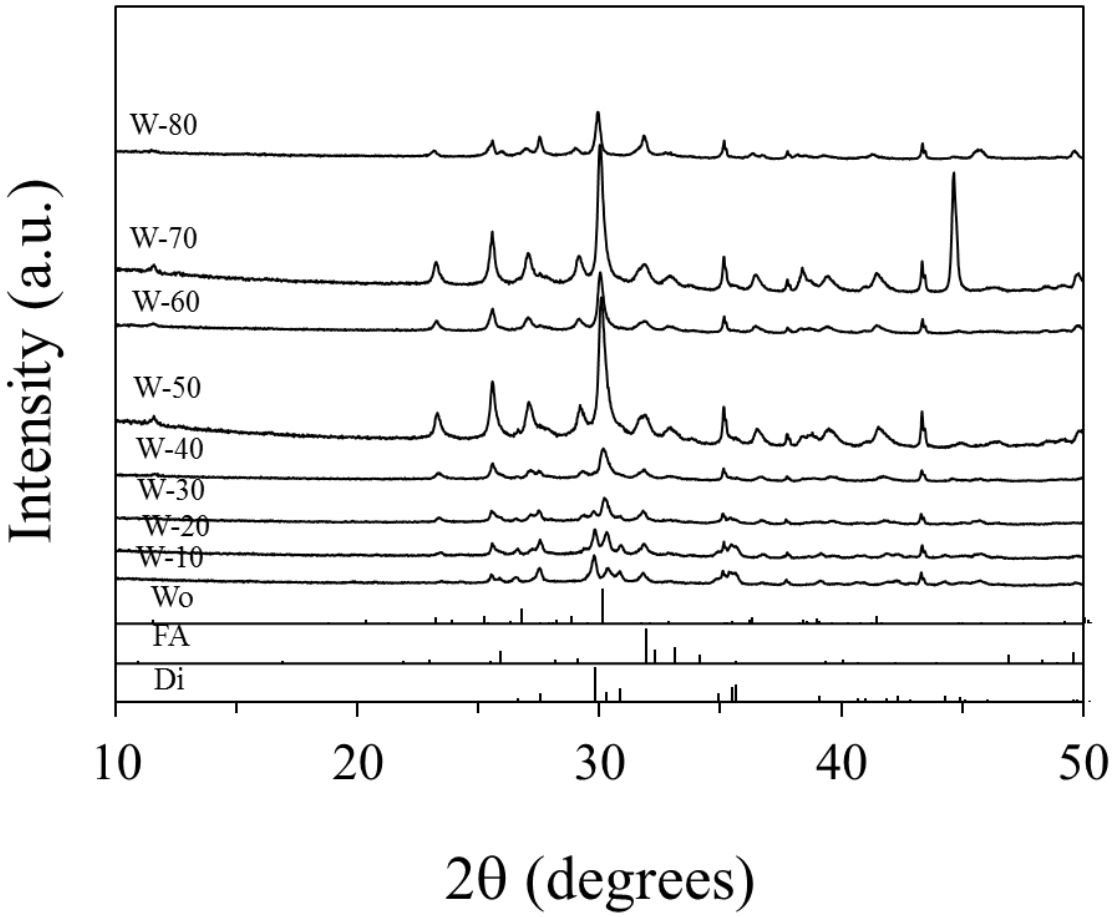

Figure 4.23 X-ray diffractograms of glass powder compacts sintered at 850 °C for 1 h

The microstructure of glass-ceramics as observed by SEM (Figure 4.24) is in good agreement with XRD results. The SEM images of glass-ceramics W-10 (Figure 4.24a) and W-20 (Figure 4.24b) exhibit highly dense microstructure implying towards good sintering behaviour of glass-ceramics. Although, the glass-ceramic compositions W-70 and W-80 possess almost similar or

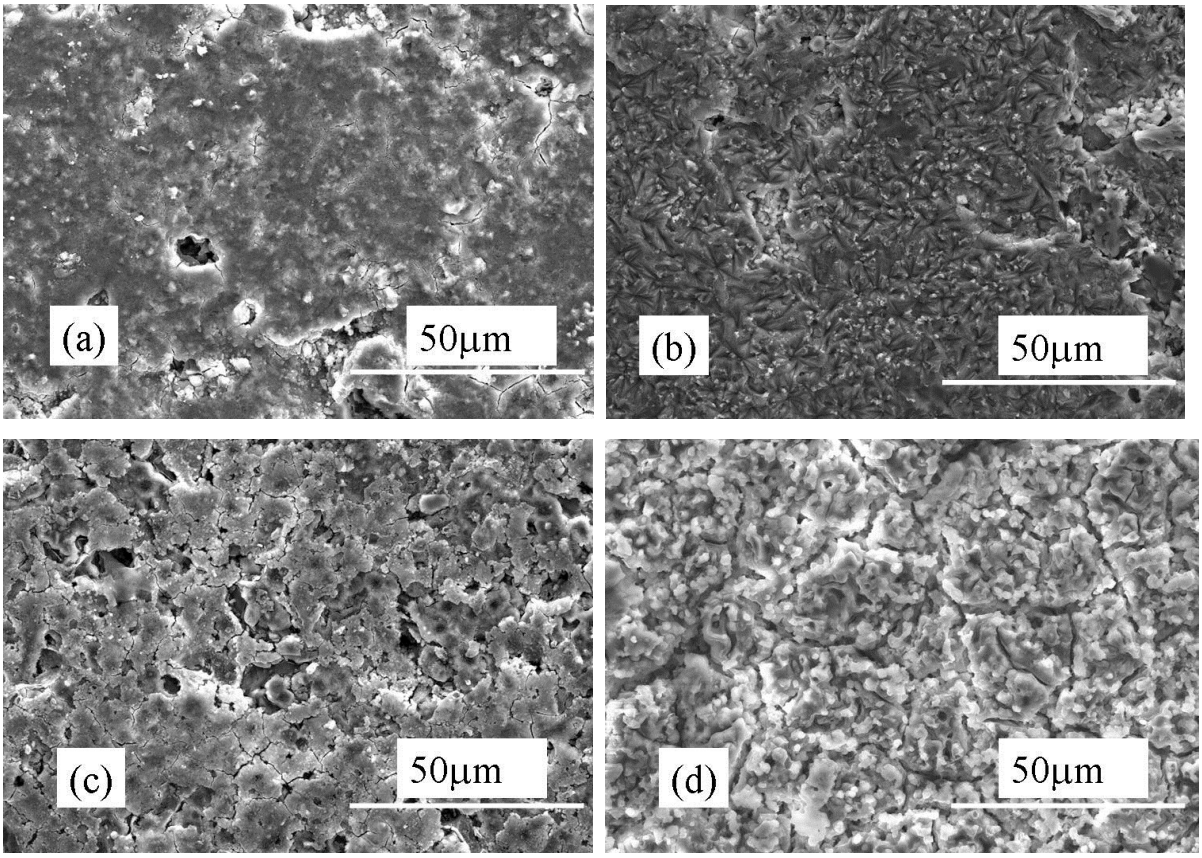

Figure 4.24 SEM images of glass-ceramics (a) W-10, (b) W-20, (c) W-70 and (d) W-80 after sintering at 850 ^{o}C for 1 h.

higher amount of residual glassy phase than W-10, still the degradation in sintering ability of these glass compositions may be attributed to the variation in the amount of porosity in these glass-ceramics owing to their different nature and amount of crystalline content. According to Karamanov et al. [38], both diopside as well as wollastonite based glass-ceramics possess good sintering ability. However, due to crystallization volume fraction of diopside and wollastonite, intragranular crystallization induced porosity is formed in these glass-ceramics which affects the sintering ability of these glass-ceramics, thus resulting in poor mechanical strength of wollastonite based compositions. This explanation is concurrent with the microstructure of glass-ceramics W-70 (Fig. 4.24c) and W-80 (Fig. 4.24d), respectively.

4. Summary

The influence of varying CaO/MgO ratio on the structure, sintering and crystallization behaviour of diopside-fluorapatite based glasses and glass-ceramics has been investigated. The variation in CaO/MgO ratio on glasses did not exhibit any significant effect on the structure of glasses with Si predominantly present in Q^2 units while phosphate is coordinated in orthophosphate environment. With respect to thermal behaviour of glasses, heat treatment of glass powders at 850 ºC for 1 h resulted in well sintered glass-ceramics with diopside, fluorapatite and wollastonite as the crystalline phases. Increasing CaO/MgO ratio in glasses degraded their sintering behaviour and resulted in different amorphous/crystalline ratio in resultant glass-ceramics. Considering the sintering ability of glasses (ΔT) along with amorphous/crystalline phase assemblage in resultant glass-ceramics (from the intensity of XRD phase reflections), composition W-30 appears to be a good candidate for further experimentation as potential material for scaffold fabrication.

Section 4.3

Understanding the influence of Na_2O on the structure, bioactivity and sintering ability of glasses in diopside – fluorapatite – wollastonite system

1. Glass forming ability

A series of glasses with compositions expressed as (16.20–*x*)MgO–*x*Na_2O–37.14CaO–3.62P_2O_5–42.46SiO_2–0.58CaF_2 (in mol%), where *x* varies between 0 – 10 has been prepared by melt-quenching technique. The glasses have been labelled in accordance with their respective Na_2O content, i.e. Na–0, Na–2, Na–4, Na–6, Na–8 and Na–10. The alkali-free parent glass composition (Na-0) has been designed in the glass forming region of diopside (CaO•MgO•2SiO_2) – fluorapatite (9CaO•3P_2O_5•CaF_2) – wollastonite (CaO•SiO_2) system. The glasses were prepared in Pt-Rh crucibles at 1550 ºC by melt-quenching technique. We could obtain homogeneous, transparent and amorphous monolithic annealed glasses (annealing at 500 ºC) as well as frit (by quenching in cold water).

2. Structure of glasses

Table 4.4 Density and molar volume of glasses

Glass	Density (g cm^{-3})	Molar volume (cm^3 mol^{-1})	Excess volume (cm^3 mol^{-1})
Na-0	2.92±0.004	20.03±0.027	0.062±0.027
Na-2	2.90±0.006	20.71±0.040	1.635±0.040
Na-4	2.88±0.007	20.56±0.050	– 0.053±0.013
Na-6	2.87±0.004	20.78±0.028	– 0.147±0.028
Na-8	2.86±0.004	21.05±0.026	– 0.205±0.026
Na-10	2.85±0.003	21.30±0.025	– 0.27±0.025

The experimental results showed that increasing Na_2O/MgO ratio in glasses resulted in lowering their density (ρ) (Table 4.4). Since density of a glass is an additive property and density of Na_2O (2.27 g cm^{-3}) is lower than that of MgO (3.58 g cm^{-3}), therefore, decrease in density with increasing Na_2O content is logical. As is usually observed in most oxide glass systems, decrease in density results in increase in their molar volume as is evident from Table 4.4. Since the addition of Na_2O at the expense of MgO results in the formation of less directed bonds, the structural skeleton collapses into a closer packing, thus, leading to decrease in excess molar volume (Table 4.4). In coherence with the excess volume data, a decreasing trend was observed

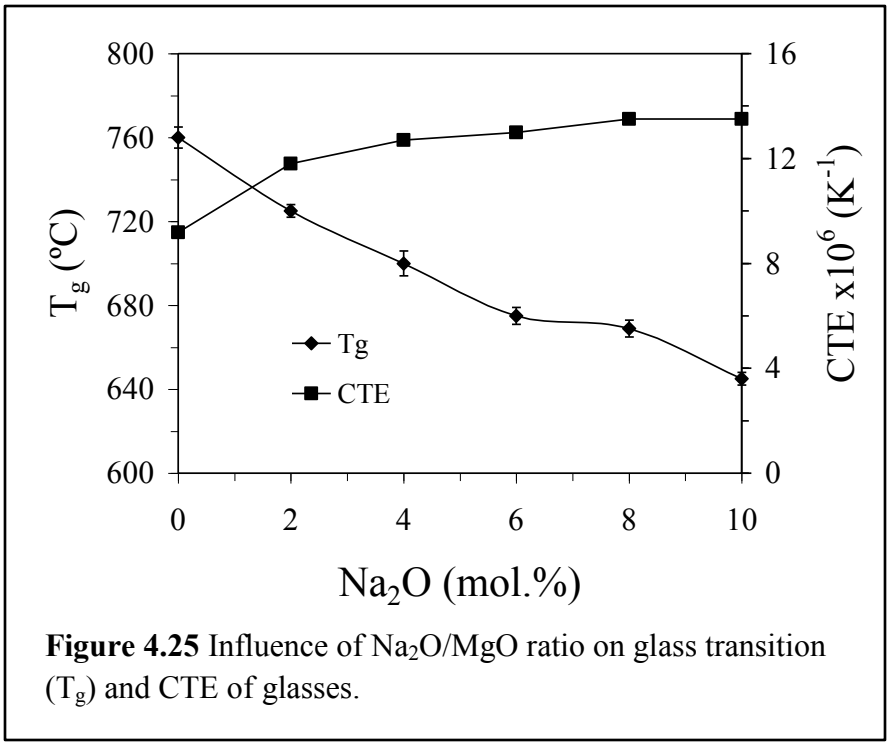

Figure 4.25 Influence of Na_2O/MgO ratio on glass transition (T_g) and CTE of glasses.

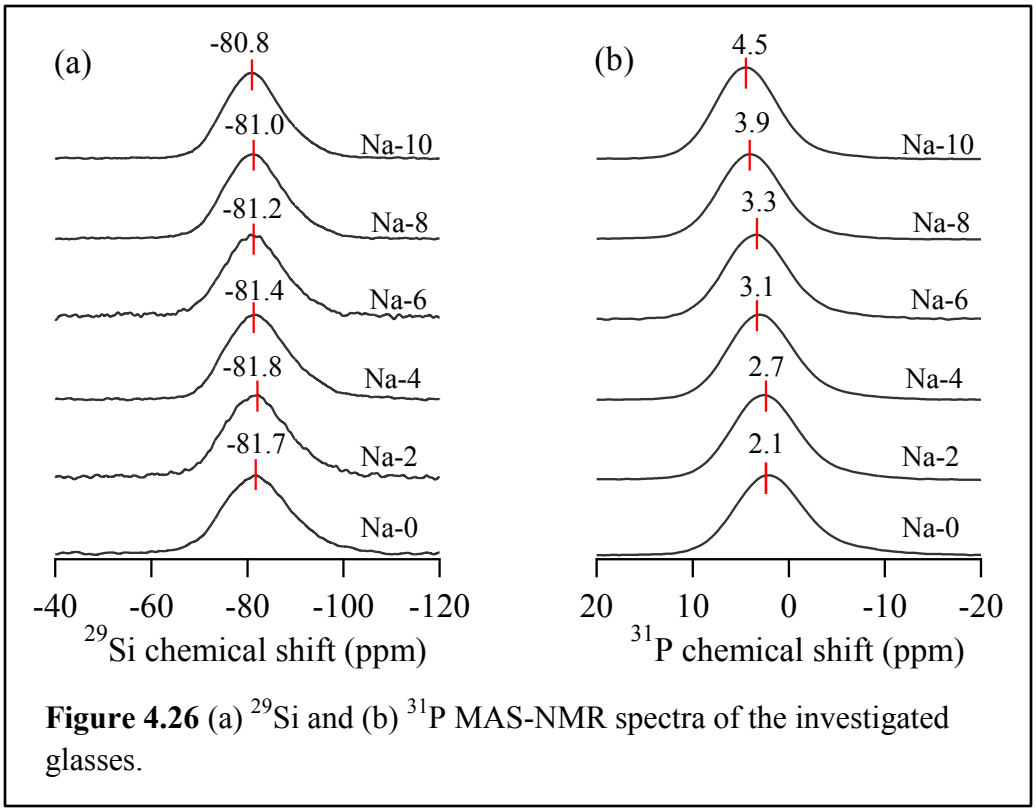

Figure 4.26 (a) ^{29}Si and (b) ^{31}P MAS-NMR spectra of the investigated glasses.

for T_g due to the gradual decrease of degree of cross-linking in the silicate network (Figure 4.25). An increase in the polarizability arises from the negatively charged non-bridging atoms. Consequently, both anharmonicity of thermal vibrations [58] and CTE (200–500 ºC) increase (Figure 4.25).

Figure 4.26a presents the ^{29}Si MASNMR spectra for all the investigated glasses depicting the dominance of Q^2(Si) structural units in the glasses. The maximum of the ^{29}Si NMR resonance slightly shifted from –81.8 ppm, for glass Na–0, to –80.8 ppm for glass Na–10, which could be interpreted as a slight depolymerisation of the silicate glass network with the increase of the sodium content at the expense of MgO. The change in the chemical shift to lower field may be attributed to the difference in ionic field strength of sodium and magnesium modifiers. The higher ionic field strength of MgO makes the chemical shift to move towards higher field while the incorporation of Na_2O (with lower ionic field strength) at the expense of MgO shifts the resonance to a lower field [49].

The ^{31}P MAS NMR spectra of all glasses (Figure 4.26b) exhibit the predominance of an orthophosphate-type environment *(Q^0)*. The maximum of ^{31}P NMR spectra varied between 2 ppm – 4 ppm for the studied glasses implying towards preferential association of calcium with amorphous orthophosphate species (chemical shift for $Ca_3(PO_4)_2$ is at 3 ppm). The positive shift in ^{31}P NMR spectra with increasing Na_2O content indicates increasing association of sodium with orthophosphate groups (the chemical shift for $Na_3(PO_4)$ species is at 14 ppm). However, calcium is still preferentially associated with phosphate groups due to its significantly higher concentration in comparison to sodium. As has been discussed in section 4.2, magnesium exhibits poor affinity towards association with phosphate groups. Therefore, in concurrence with ^{31}P NMR results, we do not expect significant amount of amorphous magnesium orthophosphate species in these glasses.

3. In vitro biodegradation of glasses

The XRD patterns observed for all as-quenched glasses (i.e. before soaking in SBF solution; not shown) exhibit a broad amorphous halo depicting the absence of crystallinity in glasses. The room temperature FTIR transmittance spectra of all the investigated glasses are shown in Figure 4.27. In general, FTIR spectra of all the investigated glasses exhibit three broad transmittance bands in the region of 300–1300 cm^{-1}. This lack of sharp features is indicative of the general disorder in the silicate and phosphate network mainly due to a wide distribution of Q^n

units occurring in these glasses. The most intense bands in the 800–1300 cm^{-1} region correspond to the stretching vibrations of the SiO_4 tetrahedron with a different number of bridging oxygen atoms [20]. Further, in all the glasses, this region (i.e. 800–1300 cm^{-1}) is split in two transmittance bands centred at ~1045 cm^{-1} and ~920 cm^{-1}. The high frequency band can be assigned to the Si–O asymmetric stretching mode of BOs, whereas the ~920 cm^{-1} may be attributed to the Si–O asymmetric stretching mode of the non-bridging oxygens (NBOs) [20, 21]. Furthermore, the 500 cm^{-1} band can be attributed to Si–O–Si bending modes [25], while the weak 740 cm^{-1} shoulder may be due to Si–O–Si symmetric stretching with simultaneous Si cation motions [22]. It is noteworthy that the high frequency band at 1045 cm^{-1} may also be assigned to the asymmetric stretching of PO_4 units which has been reported to appear in crystalline fluorapatite at 1038 cm^{-1} [59].

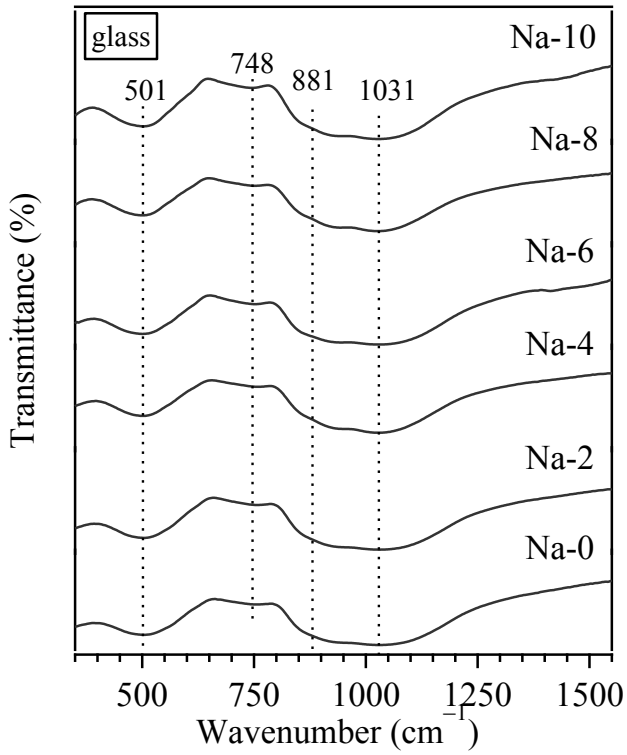

Figure 4.27 FTIR spectra of the studied glasses

Although the XRD data of glass powders after immersion in SBF solution for time period varying between 1 – 3 days exhibits a broad amorphous halo (Figure 4.28a), the FTIR spectra of these glass samples depict several changes in the glass structure that occurred due to the reaction between glass and SBF (Figure 4.29). The immersion of glass powders in SBF for 1 h resulted in the splitting of strong low frequency band in the region 350 – 650 cm^{-1} into small bands at ~465 cm^{-1}, ~570 cm^{-1} as is evident from Fig. 4.27. The band centered at 465 cm^{-1} can be ascribed to a deformation mode of silica layer that develops on the dissolving glass particles [28] while small broad bands at 570 cm^{-1} corresponds to P–O bending vibrations in a PO_4^{3-} tetrahedron implying towards the presence of non-apatitic or amorphous calcium phosphate, which is usually taken as an indication of presence of precursors to HA. The main IR band now occurs at 1060 cm^{-1} and a

nearby shoulder, centred at ~1225 cm^{-1} and attributed to Si–O–Si vibration [25] can be observed in all the glasses, due to the interfacial formation of high-area silica gel layer, as postulated in Hench's inorganic reaction set. Further, twin peaks at ~ 1420 cm^{-1} and ~ 1500 cm^{-1}, corresponding to the formation of complex carbonate species connected with the presence of Ca^{2+} ions in the surface [17], appear in all the glasses. The FTIR and XRD data are in good agreement with each other as neither of the two indicated towards the precipitation of carbonated HA on the glass surface during initial 72 h of immersion in SBF solution as is evident from Figure 4.28a and Figure 4.29. The XRD spectra of glass powders after immersion in SBF solution for 7 days exhibit broad phase reflections corresponding to the formation of HA as is evident from

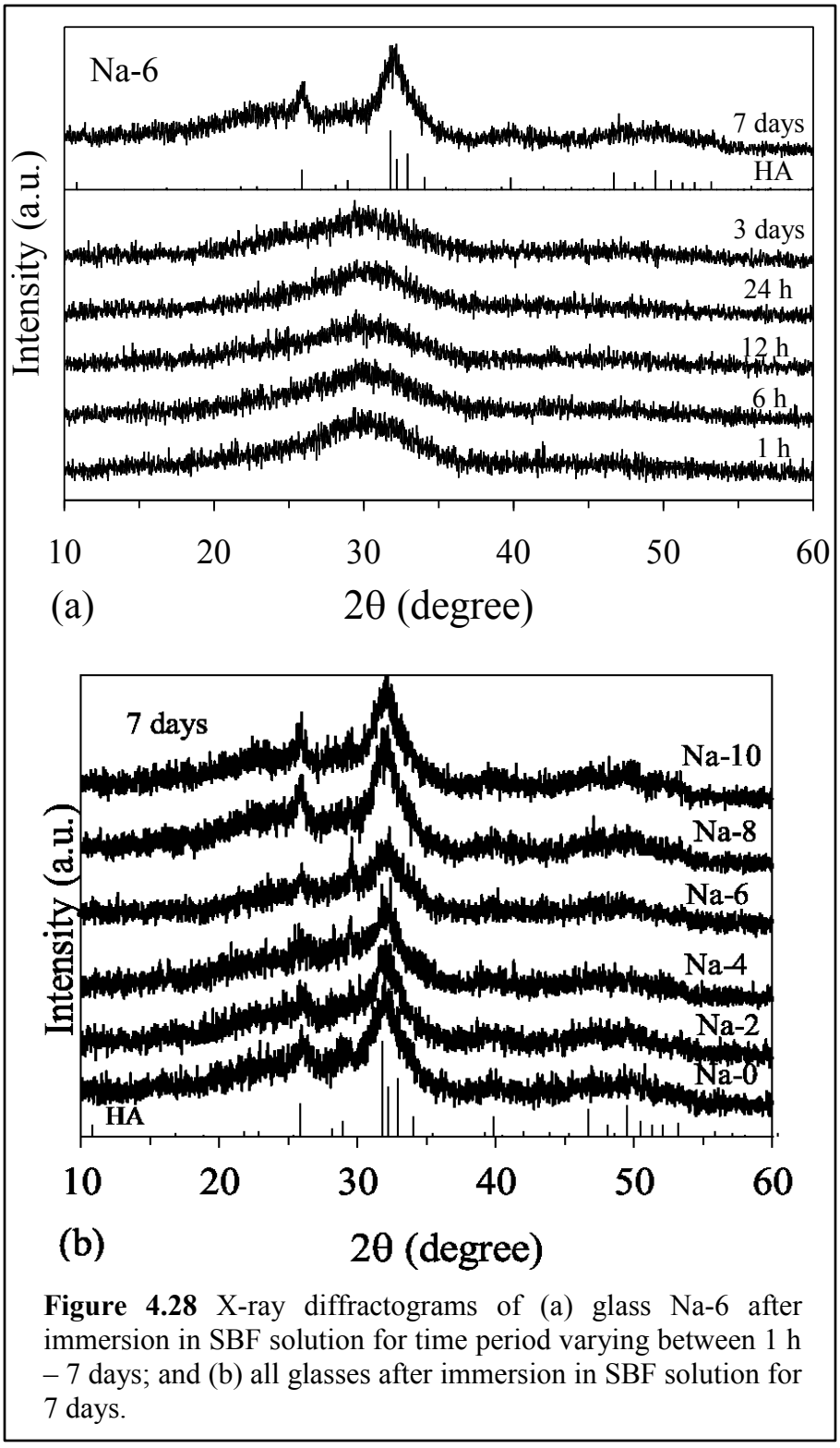

Figure 4.28 X-ray diffractograms of (a) glass Na-6 after immersion in SBF solution for time period varying between 1 h – 7 days; and (b) all glasses after immersion in SBF solution for 7 days.

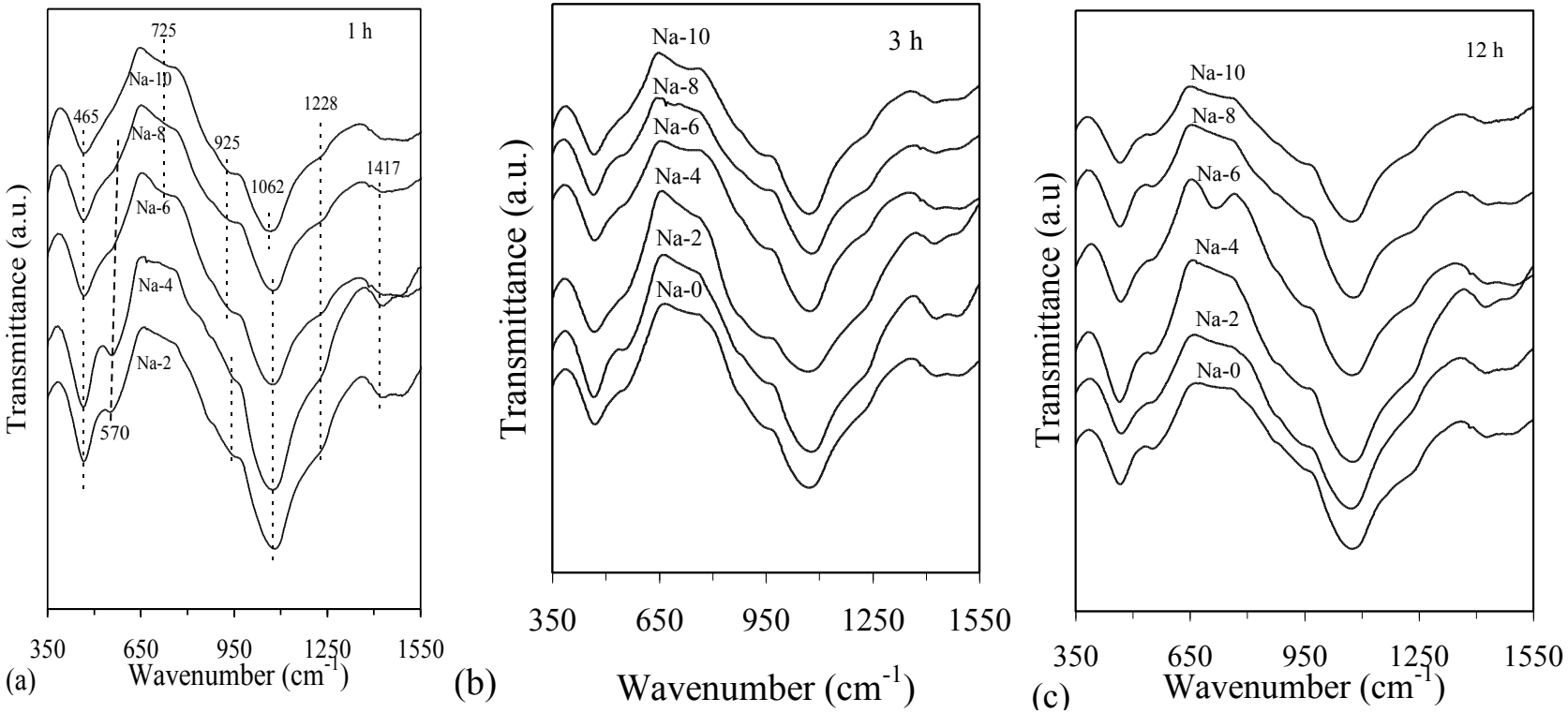

Figure 4.29 FTIR spectra of glasses after immersion in SBF solution for (a) 1 h; (b) 3 h; (c) 12 h.

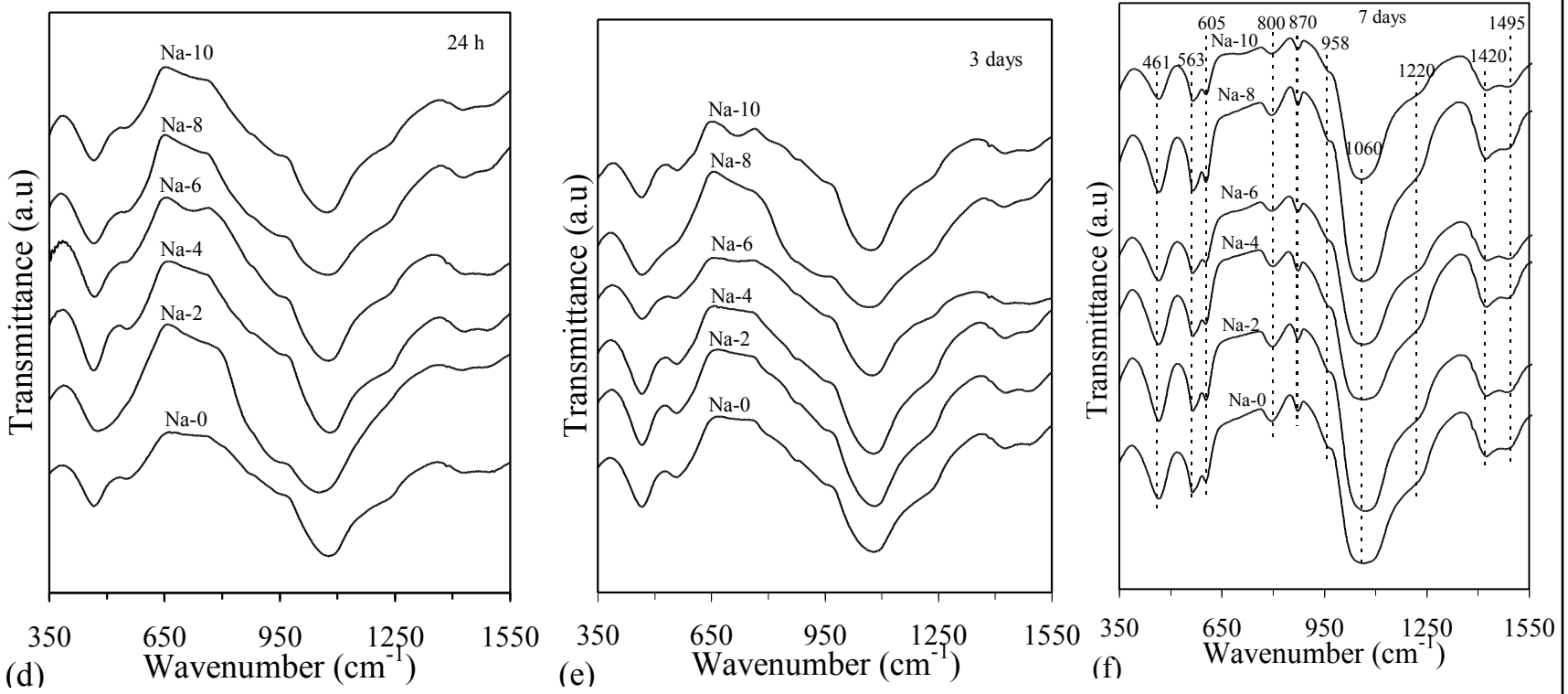

Figure 4.29 FTIR spectra of glasses after immersion in SBF solution for (a) 24 h; (b) 3 days; (c) 7 days.

Figure 4.28b. In agreement with the XRD data, the FTIR spectra of these glasses resulted in splitting of broad parent absorption bands into a number of sharp bands (Figure 4.29f). For example the bands at 563 cm^{-1} and 605 cm^{-1} along with bands at ~800 cm^{-1}, 850 cm^{-1}, 1420 cm^{-1} and 1495 cm^{-1} correspond to carbonated HA.

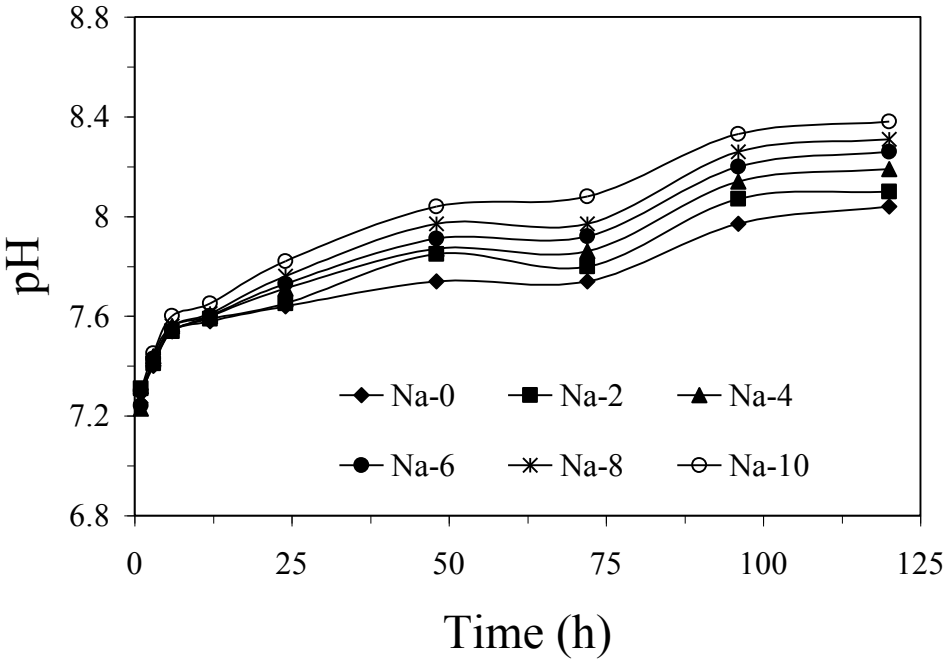

Figure 4.30 Plot demonstrating pH of Tris-HCl vs. immersion time of glass powders

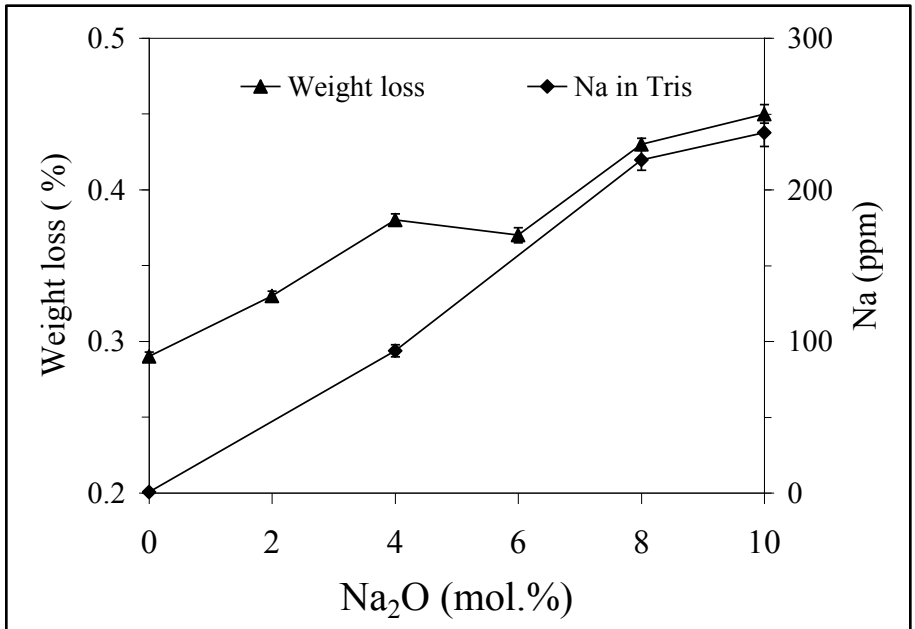

Figure 4.31 Plot depicting variation in the weight loss and sodium concentration in Tris-HCl with respect to sodium content in the investigated glasses.

The most interesting feature as observed from FTIR data of glasses immersed in SBF solution for 1 – 12 h is the diminishing intensity of band at ~570 cm^{-1} characteristic for presence of amorphous calcium phosphate layer with increasing alkali-content (Fig. 4.29a-c). This

observation may be attributed to the decreasing chemical durability of glasses with increasing alkali content which does not allow the amorphous calcium phosphate layer to adhere to the glass surface during initial hours of immersion in SBF solution. According to the results obtained from AIMD simulations on sodium migration pathways in bioactive silicate glasses conducted by Tilocca [29], the transport of sodium to the glass surface and its release are key steps leading to the biological activity of these glasses. The calcium release, needed for the later stages of interfacial bonding takes place only after most Na ions have been released. Therefore, the Na:Ca ratio and their mutual interaction play a central role in the properties of these glasses related to the ionic solubility. In case of glasses under current investigation (SiO_2<50 mol%), the low site selectivity of Na and the high flexibility of the glass network (compared to the more rigid higher silica glasses) might allow Na to move through Ca sites, temporarily vacated by hosted cation. This explains some delay in formation of the amorphous calcium phosphate layer on surfaces of glasses.

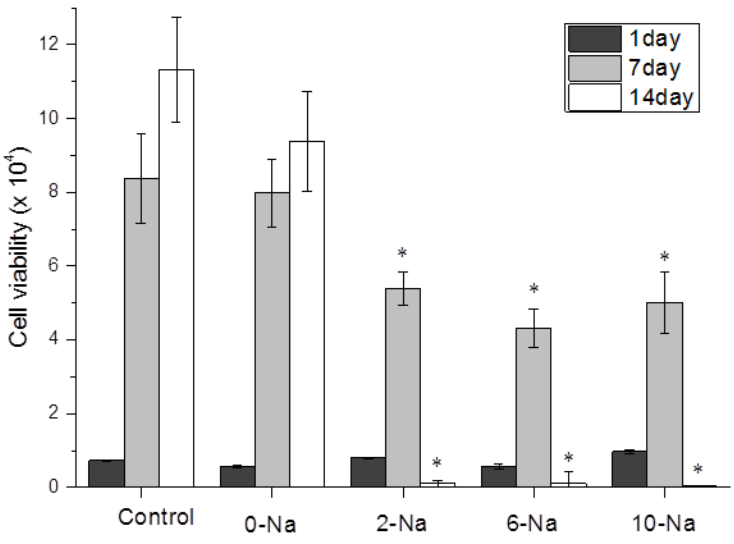

Figure 4.32 Influence of Na_2O on cell viability of MSC cultured on glass specimens as a function of time. Tissue culture plastic has been used as control. MSCs derived from rat bone marrow were used for the assay.

The variation in pH of Tris–HCl with respect to immersion time and Na_2O content in glasses is presented in Figure 4.30 while Figure 4.31 shows a comparison between weight loss and the elemental concentration of sodium released from glasses after immersion of glass powders in Tris-HCl for 5 days. An increase in pH from 8.04±0.01 to 8.38±0.05 was observed with increasing Na_2O content in glasses due to the preferential leaching of alkali ions from glasses in comparison to low mobility alkaline-earth cations as have been discussed above. All the glasses were amorphous after immersion in Tris-HCl (not shown), confirming that no

crystalline phase has been formed as a result of any chemical interaction between the dissolution products.

The preferential leaching of sodium ions from these glasses resulted in sudden release of alkali caused a cytotoxicity effect as concluded from the preliminary *in vitro* osteoblast proliferation studies performed on these glasses (Figure 4.32). Although cells initially (at day 1) adhered well on all the glass samples, with adhesion level comparable to that of the tissue culture plastic control, the cell growth for prolonged period (7 and 14 days) was significantly different. The sodium-free parent glass (Na–0) exhibited highest cell proliferation over the period of 14 days with the growth level similar to that of control, while incorporation of sodium in glasses decreased the cell viability considerably reducing it to minimal value even for the glass with lowest Na_2O concentration (Na–2). Similar results have been reported by Wallace *et al*. [60] and may be explained on the basis of faster release of alkali ions over calcium (required for cell viability and interfacial bonding) as explained by Tilocca [29].

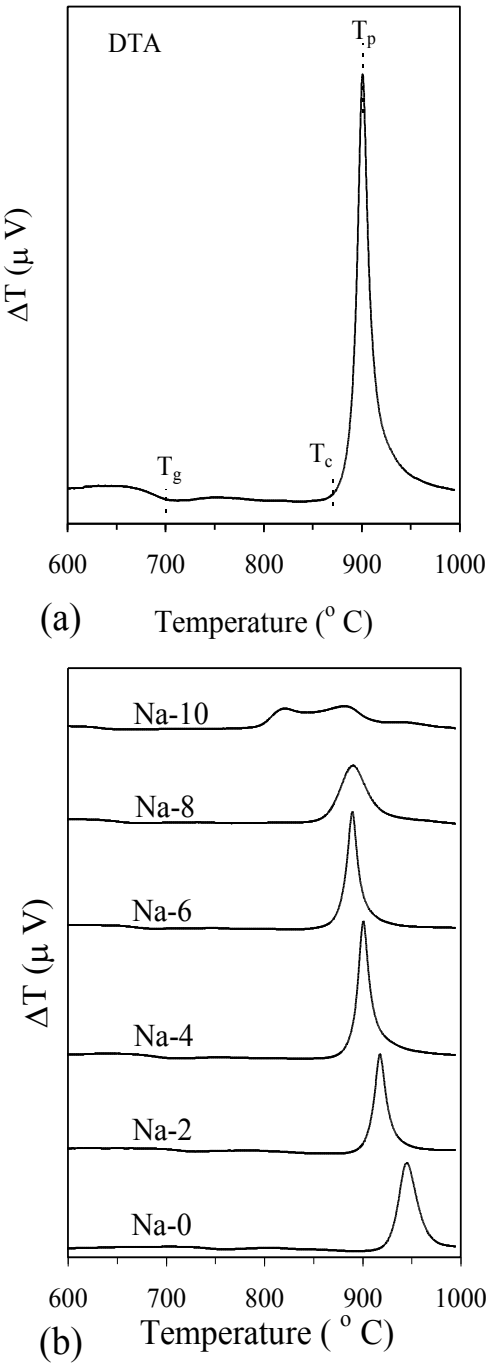

Figure 4.33 DTA thermograph of (a) glass Na-6, (b) all the glass investigated in this study. Heating rate = 20 K min^{-1}.

4. Sintering behaviour of glasses

Figure 4.33a presents DTA thermograph of glass Na-6 while Figure 4.33b presents the DTA thermographs of all the glasses investigated in the present study. Table 4.5 presents the values of thermal parameters obtained for all the glasses from DTA. The glass transition temperature (T_g) decreases with increasing Na_2O content

Table 4.5 Thermal parameters obtained from DTA at 20 K min^{-1}

Glasses	T_g	T_c	T_{p1}	T_{p2}	ΔT
Na-0	760	915	946	-	155
Na-2	725	894	918	-	169
Na-4	700	875	901	-	175
Na-6	684	862	890	-	178
Na-8	669	845	890	-	176
Na-10	645	785	822	882	140

Table 4.6 Thermal parameters obtained from DTA and HSM at 5 K min^{-1}

Glasses	T_{FS}	T_{MS1}	T_{MS2}	T_c	S_c
Na-0	758	809	893	878	69
Na-2	725	789	-	857	68
Na-4	700	770	-	845	75
Na-6	680	745	-	830	85
Na-8	673	740	830	802	62
Na-10	656	720	-	745	25

in glasses. This thermal event is then followed by onset of crystallization (T_c) and peak temperature of crystallization (T_p). The exothermic crystallization curve tends to shift gradually towards lower temperatures with increasing alkali content, further, splitting in two distinct features for glass Na-10 as shown in Figure 4.33b. The appearance of single exothermic curve implies that either the glass-ceramic formed as a result of crystallization is mono-mineral or different crystalline phases precipitate from the parent glass almost simultaneously. The addition of Na_2O decreases the viscosity of glasses leading to lowering the activation energy of crystallization due to which we can observe the decrease in crystallization temperatures. The splitting of exothermic curve in two distinct features for glass Na-10 implies towards the

formation of two or more crystalline phases in a narrow temperature interval range. Since the glass compositions have been designed in the primary crystallization field of diopside and fluorapatite, both of these phases are expected to appear in these glass-ceramics. However, owing to the lower activation energy of crystallization of fluorapatite (~350 kJ mol^{-1} [61]) in comparison to diopside (~570 kJ mol^{-1} [62]), the crystallization of former should be preferred in glass Na-10.

The characteristic thermal parameters, T_g, T_c, T_p and thermal stability, defined as $\Delta T(= T_c - T_g)$ obtained from DTA thermographs are summarized in Table 4.5. The values of ΔT varied between 140 – 178 for all the glasses and increased with initial substitution of Na_2O (0 - 4 mol%) for MgO as have been shown in Table 4.5. Further increase in Na_2O concentration in glasses between 4 – 8 mol% did not exhibit significant influence on their thermal stability as the average ΔT value for these glasses was calculated to be 176 ºC. However, increasing the Na_2O content to 10

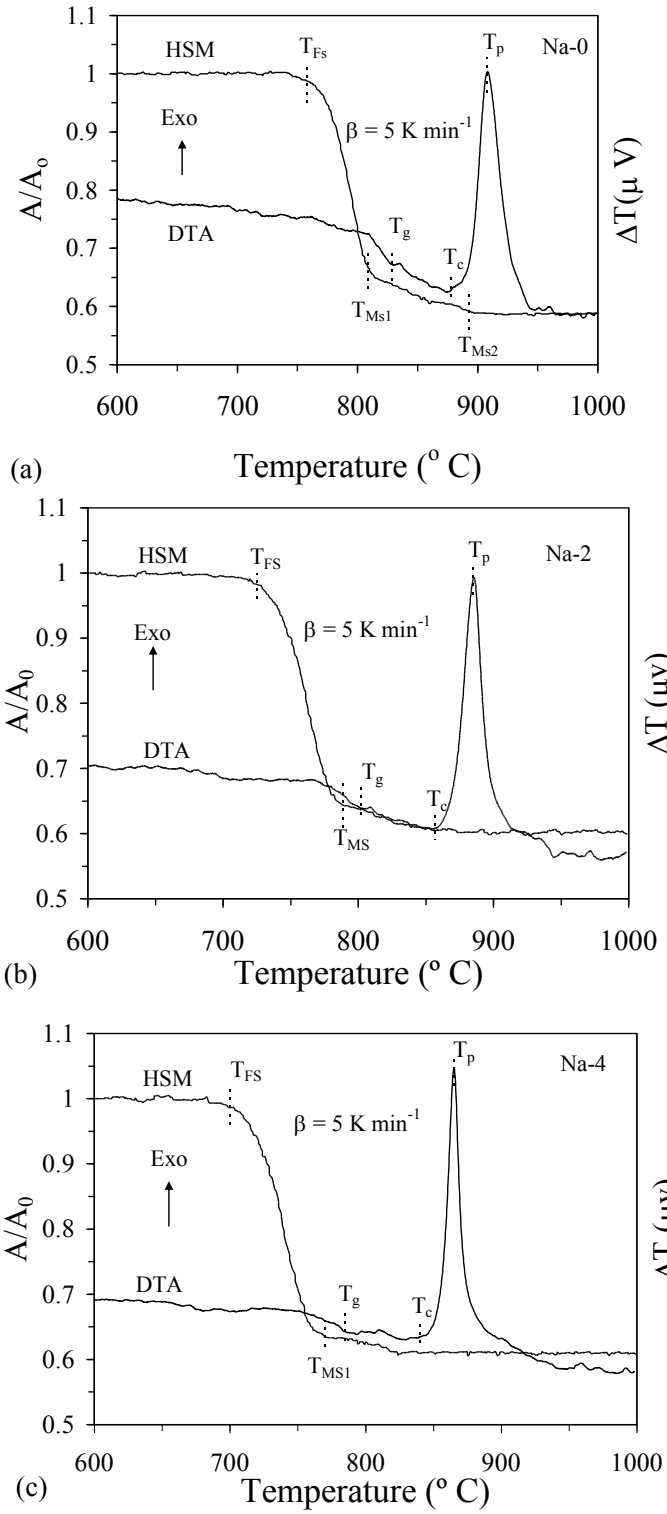

Figure 4.34 DTA and HSM curves for glasses (a) Na-0, (b) Na-2 and (c) Na-4 at 5 K min^{-1}.

mol% led to considerable decrease in the thermal stability of glass Na-10 with its ΔT = 140 ºC. The difference between T_c and T_g is an empirical and qualitative parameter that assists in deciding the processing window for glasses aimed for their application as coatings or scaffold fabrication as higher value of ΔT indicates delayed nucleation and good sintering ability [63]. A detailed analysis of sintering and crystallization behaviour of glasses has been made through DTA and HSM as discussed below.

Figure 4.34 presents DTA and HSM data at heating rate (β =5 K min^{-1}) pertaining to sintering and devitrification behaviour of glasses that allow observation of the following trends:

(i) The temperature of first shrinkage (T_{FS}; logη = 9.1 ± 0.1, η is viscosity; dPa s) decreased linearly with increasing sodium content in glasses with its value varying between 758 ºC for glass Na-0 and 656 ºC for glass Na-10 (Table 4.6).

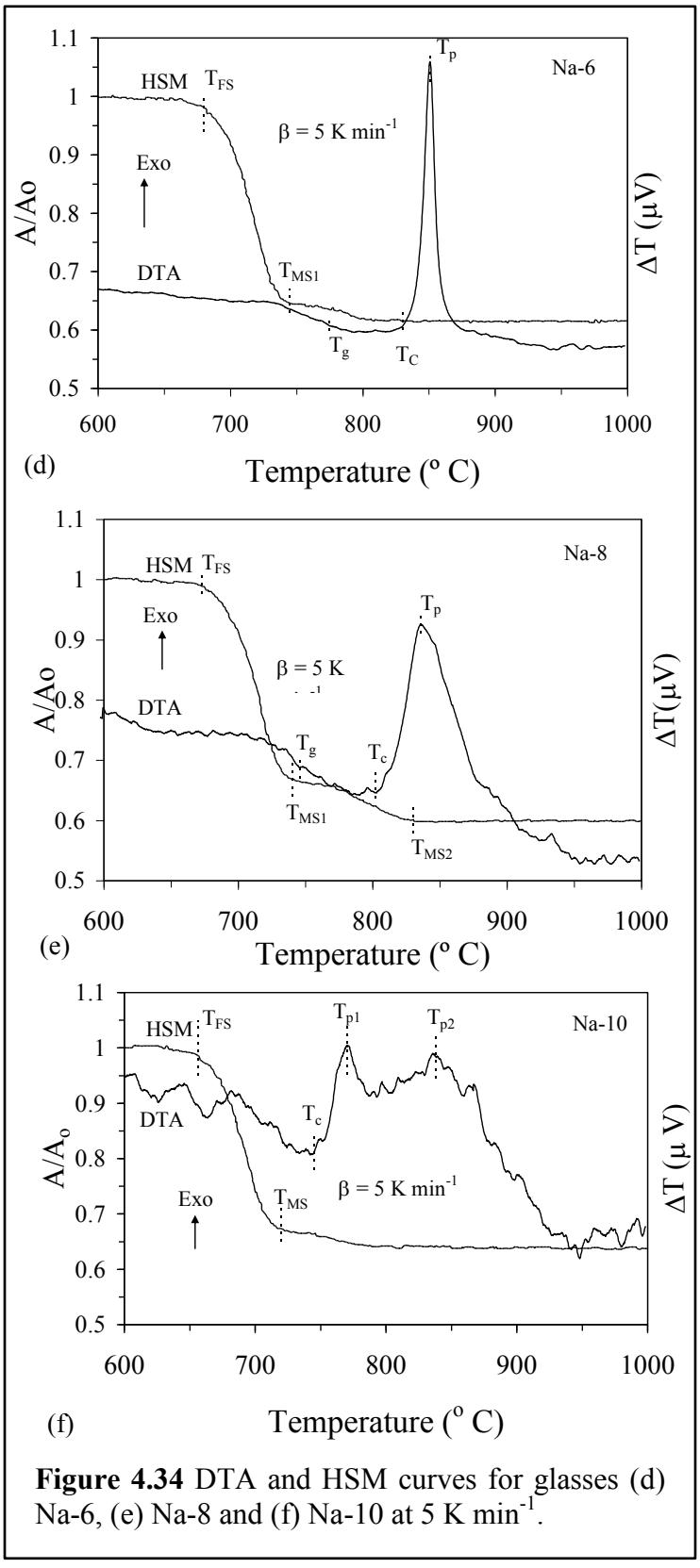

Figure 4.34 DTA and HSM curves for glasses (d) Na-6, (e) Na-8 and (f) Na-10 at 5 K min^{-1}.

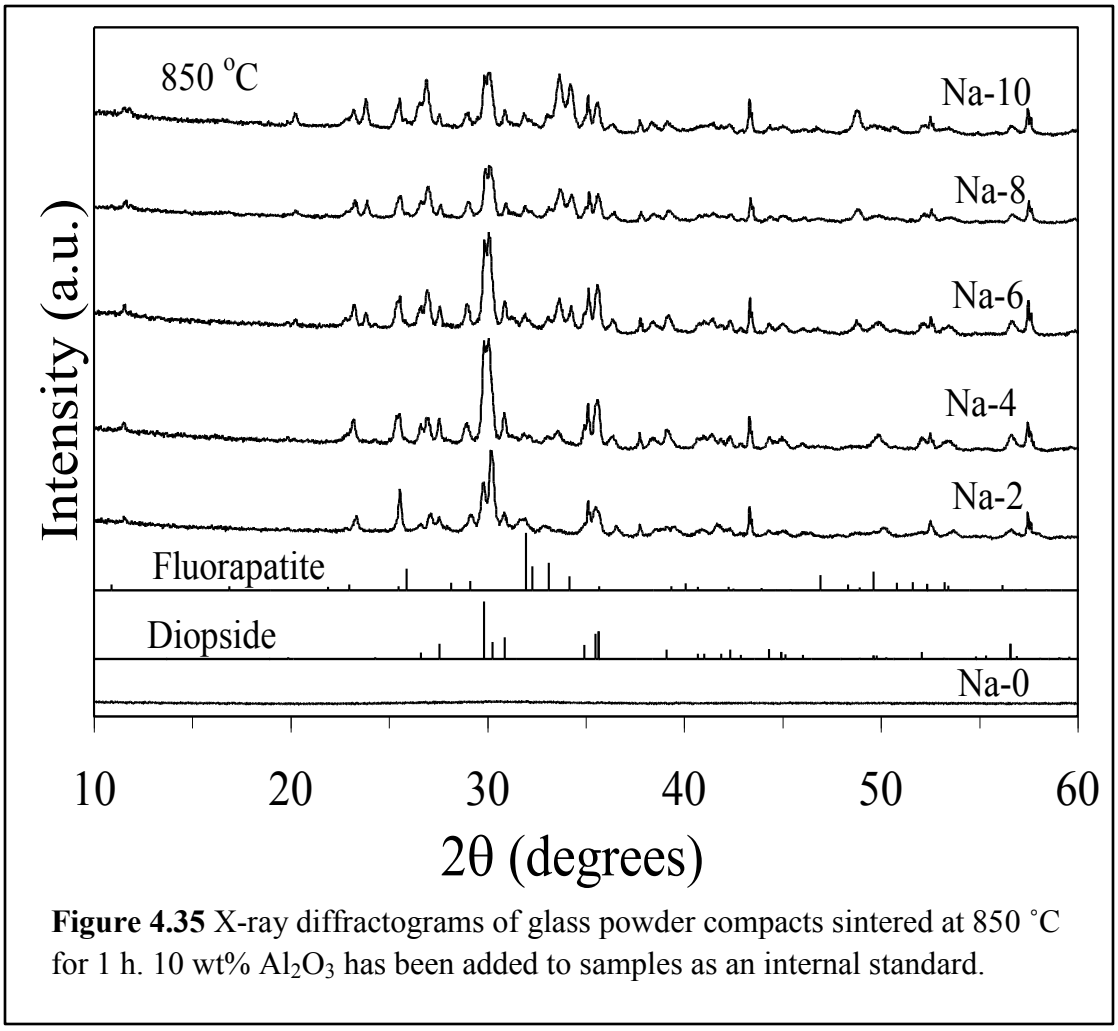

Figure 4.35 X-ray diffractograms of glass powder compacts sintered at 850 ˚C for 1 h. 10 wt% Al_2O_3 has been added to samples as an internal standard.

(ii) The temperature of maximum shrinkage (T_{MS}; $\log\eta = 7.8 \pm 0.1$), and sintering ability, S_c ($T_c - T_{MS}$) parameters have been presented in Table 4.6. The decrease in the value of S_c implies towards poor densification [13]. In concurrence with the values obtained for ΔT, the values of S_c indicate that initial incorporation of Na_2O (0 – 6 mol%) in glasses facilitated their sintering. However, further increase in Na_2O content led to the decrease in S_c values depicting the poor densification. The poor sintering ability with increasing sodium content in glasses has also been observed in other alkali-containing silicate glass systems [64] and is a major drawback for 45S5 Bioglass [65, 66]. The primary reason attributed to the poor densification of alkali-rich bioactive glasses is their high crystallization tendency [63, 64].

(iii) Two-stage shrinkage behaviour was observed for all the sodium containing glasses except Na-10 and can be attributed to the presence of glass-in-glass phase separation due to the presence of silicate and phosphate rich phases. However, increasing alkali concentration in glasses promoted crystallization of fluorapatite in glasses thus, hindering the second stage of sintering.

Table 4.7 Linear shrinkage and flexural strength of sintered glass-ceramics

	Shrinkage (%)	Flexural Strength (MPa)	Weibull *m*	Weibull $\sigma 0$ (MPa)
Na-0	12.32±0.22	137±12	11.19	142
Na-2	12.16±0.15	141±5	26.34	144
Na-4	11.73±0.12	188±18	10.19	196
Na-6	11.59±0.24	120±18	6.16	128
Na-8	0	16±1	10.63	16
Na-10	0	7±1	5.73	8

The X-ray diffractograms of the glass powder compacts sintered at 850 ^{o}C for 1 h (Figure 4.35) shows diopside ($CaMgSi_2O_6$; PDF card: 078-1390) as the main crystalline phase in all the glass-ceramics followed by fluorapatite [$Ca_5(PO_4)_3F$; PDF card: 71-880] as the secondary phase. The 11% – 12% linear shrinkage of sintered glass-ceramics (Table 4.7) with Na_2O content varying between 0 – 6 mol% depicts good sintering ability, while further increase in Na_2O content resulted in poor densification behaviour with almost negligible shrinkage. The mechanical strength results are in concurrence with the linear shrinkage data as the strength of glass-ceramics increases from 137±12 MPa (Na-0) to 188±18 MPa (Na-4) with increasing Na_2O content from 0 to 4 mol%. However, further increase in alkali content in glasses decreased their mechanical strength with glass-ceramics Na-8 and Na-10 exhibiting values of 16 MPa and 7 MPa, respectively.

5. Summary

We have studied the influence of sodium on the structure, sintering behaviour and bioactivity of phospho-silicate glasses. The incorporation of Na_2O at the expense of MgO induced slight depolymerisation in the silicate glass network as revealed by MAS NMR. Phosphorus was coordinated predominantly in orthophosphate environment and exhibited a positive chemical shift in ^{31}P NMR spectra indicating the increasing coordination of sodium with phosphate component. FTIR results depict that increasing the alkali content in glasses led to the delayed formation of amorphous calcium phosphate layer on their surface when immersed in SBF solution. This delay was mainly due to the higher mobility of sodium in comparison to calcium from glass to the body fluid. The preliminary in vitro osteoblast proliferation studies performed on these glasses suggested that the increasing alkali-concentration in glasses led to cytotoxicity in the cell culture medium.

With respect to sintering ability of glasses, incorporating Na_2O in glasses to a concentration of 4 – 6 mol% facilitates their sintering and enhances their mechanical strength. Further increase in alkali content in these glasses significantly deteriorates their thermal stability and sintering behaviour, thus rendering porous and crystallized glass-ceramics with poor mechanical properties that are unfit for scaffold fabrication.

Section 4.4

Understanding the influence of CaO/SiO_2 and CaF_2/P_2O_5 ratios on the structure, and sintering ability of bioactive glasses in diopside – fluorapatite – wollastonite system

1. Glass forming ability

The present study describes the influence of varying SiO_2/CaO and CaF_2/P_2O_5 molar ratio on the thermal behaviour of glass compositions in the CaO-MgO-SiO_2-P_2O_5-Na_2O-CaF_2 system designed in the primary crystallization field of diopside, fluorapatite and wollastonite. Table 4.8 presents the compositions of glasses investigated in the present study. The melting temperature of 1450 ºC for 1 h was adequate to obtain highly homogeneous transparent and amorphous glasses for glasses 1d, 1d-a and 1d-b, respectively. However, the melting temperature was varied between 1450-1550 ^oC for glasses 1e, 1e-a, 1e-b and 1e-c with an increment of 25 ^oC for every glass composition due to possible increase in the refractoriness with increase in P_2O_5 content in the glasses [67].

Table 4.8 Composition of glasses (mol%)

Glass	SiO_2	CaO	MgO	P_2O_5	Na_2O	CaF_2	CaO/SiO_2	P_2O_5/CaF_2
1d	45.45	30.30	12.99	2.60	4.33	4.33	0.67	0.60
1da	41.13	34.63	12.99	2.60	4.33	4.33	0.84	0.60
1db	36.8	38.96	12.99	2.60	4.33	4.33	1.06	0.60
1e	43.10	32.33	12.93	3.02	4.31	4.31	0.75	0.70
1e-a	43.10	32.33	12.93	3.88	4.31	3.45	0.75	1.12
1e-b	43.10	32.33	12.93	4.74	4.31	2.59	0.75	1.83
1e-c	43.10	32.33	12.93	5.60	4.31	1.72	0.75	3.26

2. Structure of glasses

The density of glasses, as presented in Table 4.9, increased with increase in CaO/SiO_2 ratio (1d < 1d-a < 1d-b) due to the higher density of CaO (ρ = 3.34 g cm^{-3}) in comparison to SiO_2 (ρ = 2.65 g cm^{-3}). On the other hand, it decreased with increase in P_2O_5/CaF_2 ratio in the glasses (1e > 1e-a > 1e-b > 1e-c) (Table 4.9) due to the lower density of P_2O_5 (ρ = 2.30 g cm^{-3}) in comparison with CaF_2 (ρ = 3.18 g cm^{-3}). The molar volume (V_m) values decreased with partial substitution of SiO_2 by CaO in the glasses (Table 4.9). The incorporation of network modifiers

Table 4.9 The properties of glasses as obtained from density, dilatometry, DTA and HSM.

	CaO/SiO_2			P_2O_5/CaF_2			
	1d	1d-a	1d-b	1e	1e-a	1e-b	1e-c
ρ (g cm^{-3})	2.84 ± 0.009	2.90 ± 0.003	2.93 ± 0.006	2.87 ± 0.007	2.86 ± 0.001	2.84 ± 0.002	2.82 ± 0.001
V_m (cm^3 mol^{-1})	20.85 ± 0.07	20.40 ± 0.02	20.13 ± 0.04	20.75 ± 0.05	21.03 ± 0.01	21.35 ± 0.02	21.68 ± 0.01
T_{dg} ± 2 (°C)	495	490	450	463	505	515	525
T_s ± 2 (°C)	673	673	657	674	673	680	689
CTE x 10^6 (K^{-1})	10.61	11.04	11.71	10.84	10.66	10.45	9.74
T_{FS} ± 5 (°C)	640	642	630	664	673	683	688
T_{MS} ± 5 (°C)	705	706	700	728	746	753	767
T_c ± 2 (°C)	804	800	778	805	820	837	852
T_{p1} ± 2 (°C)	831	826	794	835	844	815	799
T_{p2} ± 2 (°C)	-	-	817	-	-	853	879
A/A_0	0.69	0.65	0.65	0.79	0.66	0.64	0.78
S_c	99	94	78	77	74	84	85
E_{c1} (kJ mol^{-1})	-	-	-	406 (0.991)	450 (0.996)	299 (0.998)	309 (0.999)
E_{c2} (kJ mol^{-1})	-	-	-	-	-	303 (0.994)	285 (0.999)

ρ: density of glasses; V_m: molar volume; T_{dg}: dilatometric glass transition temperature; T_s: glass softening temperature; CTE: coefficient of thermal expansion; T_{FS}: temperature of first shrinkage; T_{MS}: temperature of maximum shrinkage; T_c: onset of crystallization; T_p: peak temperature of crystallization; A/A_0: area at maximum shrinkage/initial area; $S_c = T_c - T_{MS}$; E_c: Activation energy of crystallization (the values in parenthesis of E_c correspond to squared regression (r^2); 5 data points per linear plot were used).

alters fundamentally the glass properties due to the formation of less directed bonds, leading to the collapse of structural skeleton into a closer packing [58]. Hence, owing to the reduced degree of cross-linking, molar volume decreases, T_g is lowered and CTE increases (Table 4.9).

For glasses with varying P_2O_5/CaF_2 ratio, the values of V_m, T_g and T_s were observed to increase while CTE decreased with increasing P_2O_5 content (Table 4.9). This behaviour may be attributed to the increase in the directional bonding in the glass structure or re-polymerization in silicate glass network due to P_2O_5 addition as will be explained in next section.

The room temperature FTIR transmittance spectra of all the investigated glasses are shown in Figure 4.36a (varying CaO/SiO_2 ratio) and Figure 4.36b (varying P_2O_5/CaF_2 ratio) while the MAS-NMR spectra of selected glasses for ^{29}Si and ^{31}P nuclei are presented in Fig. 4.37. The FTIR spectra of 45S5 Bioglass® has been taken as a reference in order to make its structural comparison with the glasses under investigation (Figure 4.36a). As evident from Figure 4.36, it is noteworthy that despite of significant differences in the chemical composition of the investigated glasses in comparison to the composition of 45S5 Bioglass® the structure of all the glasses is

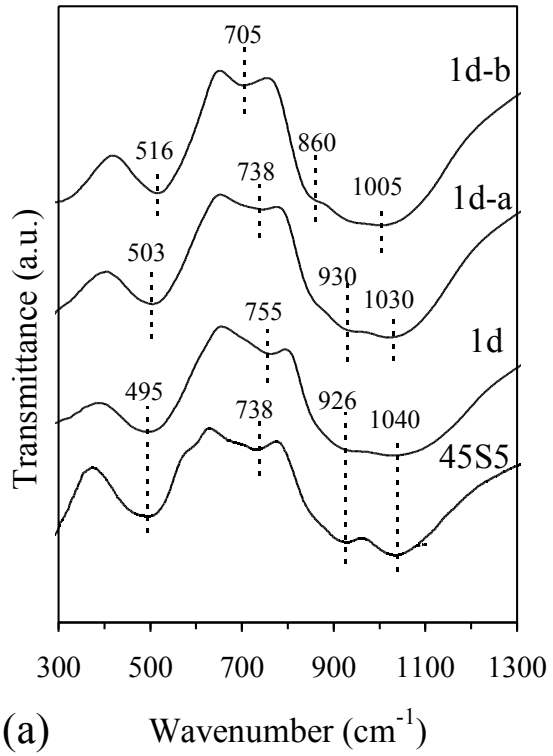

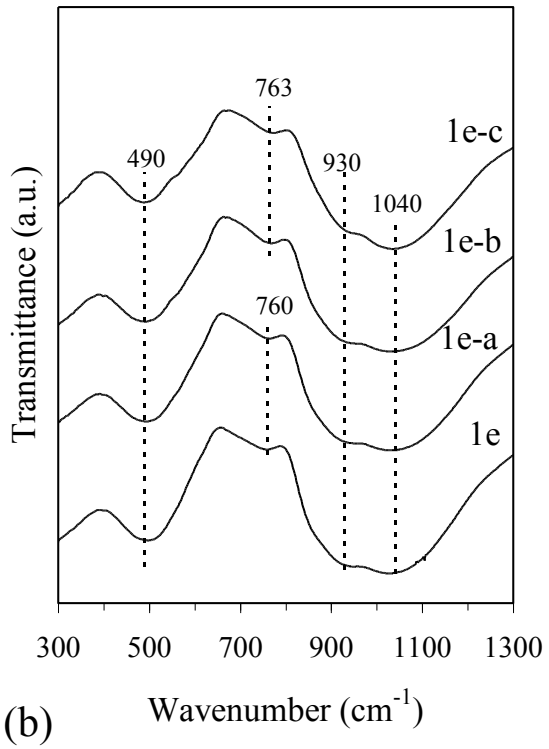

Figure 4.36 FTIR spectra of glasses (a) with varying CaO/SiO_2 ratio and (b) with varying P_2O_5/CaF_2 ratio.

similar to that of 45S5 glass. In general, infra-red spectra of all the investigated glasses exhibit three broad transmittance bands in the region of 300-1300 cm^{-1}. This lack of sharp features is indicative of the general disorder in the silicate and phosphate network mainly due to a wide distribution of Q^n (polymerization in the glass structure, where n denotes the number of bridging oxygens) units occurring in these glasses. The most intense bands in the 800–1300 cm^{-1} region correspond to the stretching vibrations of the SiO_4 tetrahedron with a different number of bridging oxygen atoms [20]. For investigated glass compositions 1d, 1d-a (Figure 4.36a) and all the glasses with varying P_2O_5/CaF_2 ratio (Fig. 4.37b), this band is around ~1040 cm^{-1} indicating the distribution of silicate Q^n units centered on Q^3 [20, 68, 69]. It should be noted that the band near ~1030 cm^{-1} (glass 1d-a) may also be attributed to PO_3 end groups due to the presence of P_2O_5 glass network former in the investigated glasses [70]. Similarly

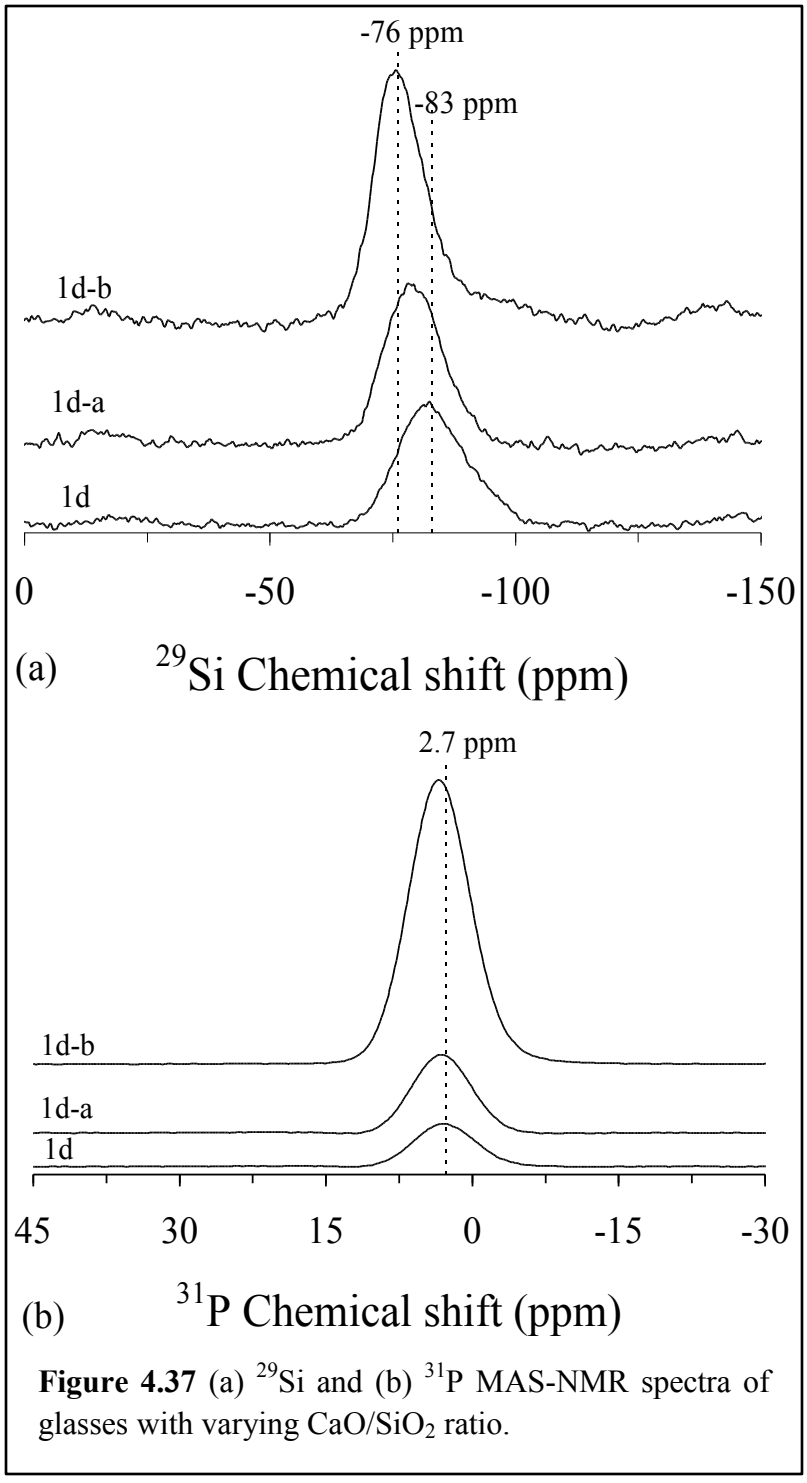

Figure 4.37 (a) ^{29}Si and (b) ^{31}P MAS-NMR spectra of glasses with varying CaO/SiO_2 ratio.

transmittance bands near 930 cm^{-1} may be attributed to the polymerization in silicate network structure with two bridging oxygens (Q^2 units) [20, 68] along with some Q^1 units.

The FTIR results are in good agreement with NMR results as presented in Figure 4.37. The peaks of ^{29}Si spectra for all the investigated glasses (Figure 4.37a and 4.37) depict the dominance of Q^2 (Si) structural units in the glasses [4]. However, increasing CaO/SiO_2 ratio in glasses led to de-polymerization in silicate glass network as is evident from shift in the peak maxima for glass 1d-a and 1d-b in Figure 4.37a while ^{31}P NMR spectra for these glasses revealed the shift in peak position from 2.7 ppm to 2.9 ppm (Figure 4.37b) with increasing CaO/SiO_2 ratio thus implying towards the formation of calcium orthophosphate groups in the glasses [4]. On the contrary, increasing P_2O_5/CaF_2 ratio in glasses led to the re-polymerization in the silicate glass structure, thus shifting the peak maxima of ^{29}Si NMR spectra

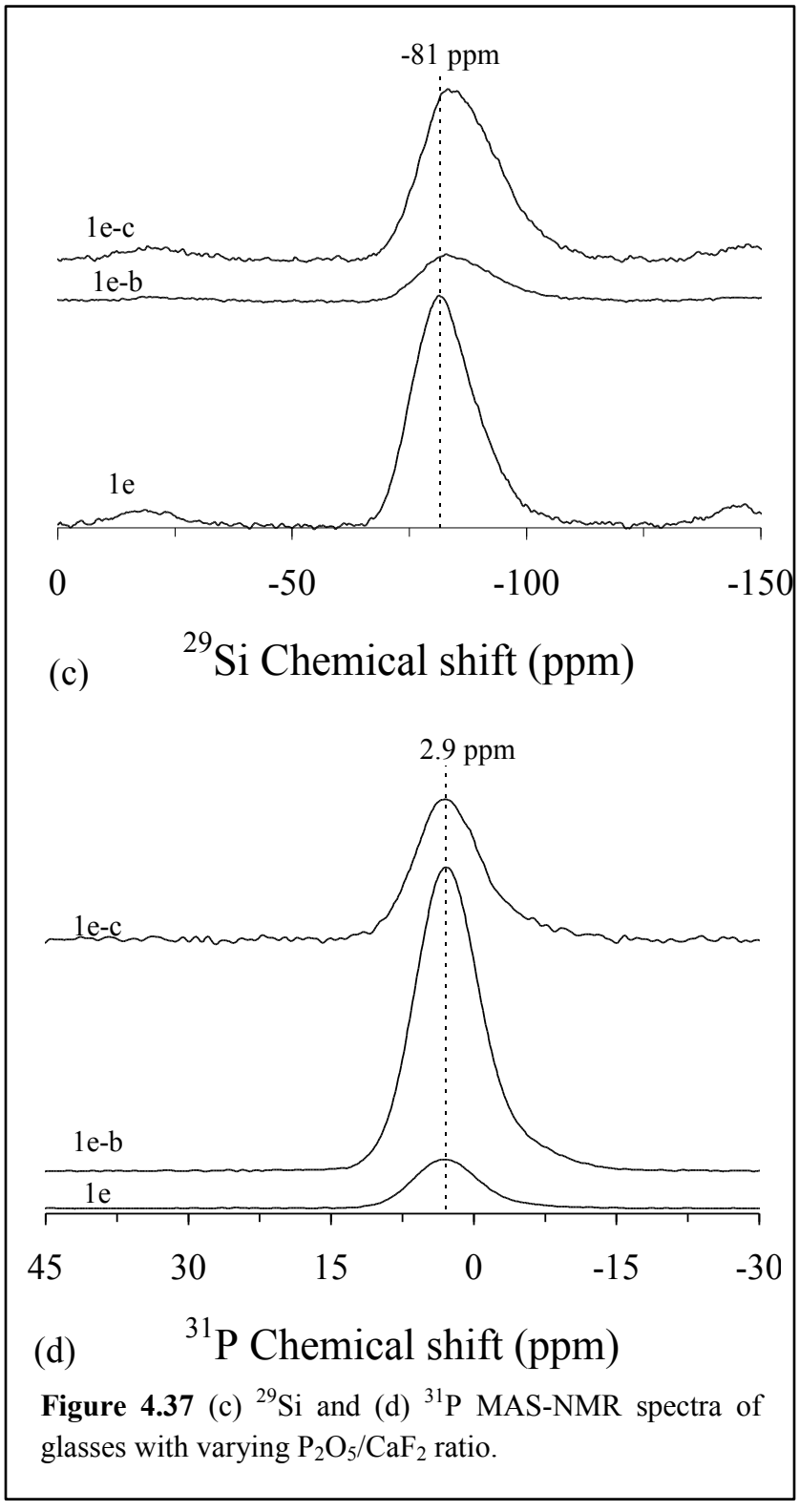

Figure 4.37 (c) ^{29}Si and (d) ^{31}P MAS-NMR spectra of glasses with varying P_2O_5/CaF_2 ratio.

(Figure 4.37c) from -82 ppm to -84 ppm which implies towards increasing number of Q^3 (Si) units. These results are in good agreement with the experimental evidence of Lockyer et al. [2] that was interpreted on the basis of higher affinity of Na and Ca cations for phosphate groups, which are able to strip the modifier cations out of the silicate network, thus inducing re-polymerization. It is noteworthy that while molecular dynamic (MD) simulations do confirm the above discussed results, they also highlight an addition factor that leads to re-polymerization in silicate glass network due to addition of P_2O_5: phosphorus can replace Na^+ or Ca^{2+} in balancing Si–NBO bonds. Therefore, the silicate network re-polymerization can occur through either Si–O–Si or Si–O–P new links. However, in the present case, we could not observe any change in peak maxima for spectra of ^{31}P nucleus (2.9 ppm) with varying P_2O_5/CaF_2 ratio (Figure 4.38d), thus neglecting the possibility of formation of Si–O–P new links. According to Tilocca [45], the highest bioactivity from a phospho-silicate glass can be expected if Q^n (Si) units are dominated by chains of Q^2 metasilicates, which are occasionally cross-linked through Q^3 units, whereas Q^1 units terminates the chains. The structure of the glasses under present investigation, specially glass 1d, glass 1d-a and all the glasses with varying P_2O_5/CaF_2 ratio exhibit these features. Therefore, high bioactivity can be expected from these glasses. Further, the influence of an increase in CaO/SiO_2 ratio is evident in the infrared spectra of glass 1d-b where the transmittance band in the region 800-1300 cm^{-1} shifts towards lower wave number, thus, depicting de-polymerization in the silicate glass network (Figure 4.36a). These results further support our molar volume and dilatometry results. A shoulder observed at 860 cm^{-1} in glass 1d-b can be attributed to vibrations of Q^0 units of silicate network structure. The bands around ~500 cm^{-1} and ~740 cm^{-1} may be attributed to vibrations of various Q^n silicate units containing NBOs, suggesting of a high modification degree of the silicate network. Nevertheless, a study of the quantitative distribution of Q^n species for silicon, phosphorus and fluorine through nuclear magnetic resonance (NMR) spectroscopy will be needed to get a better insight into the structure of these glasses.

3. Sintering and crystallization behaviour of glass powders

Figure 4.38 presents variation in the relative area and heat flow with respect to temperature as obtained from HSM and DTA, respectively, for some of the investigated glass

compositions at a heating rate of 5 K min^{-1}. In particular, photomicrographs presented in Figure 4.39 and Figure 4.40 show changes in the geometric shape of the glass powder compact with

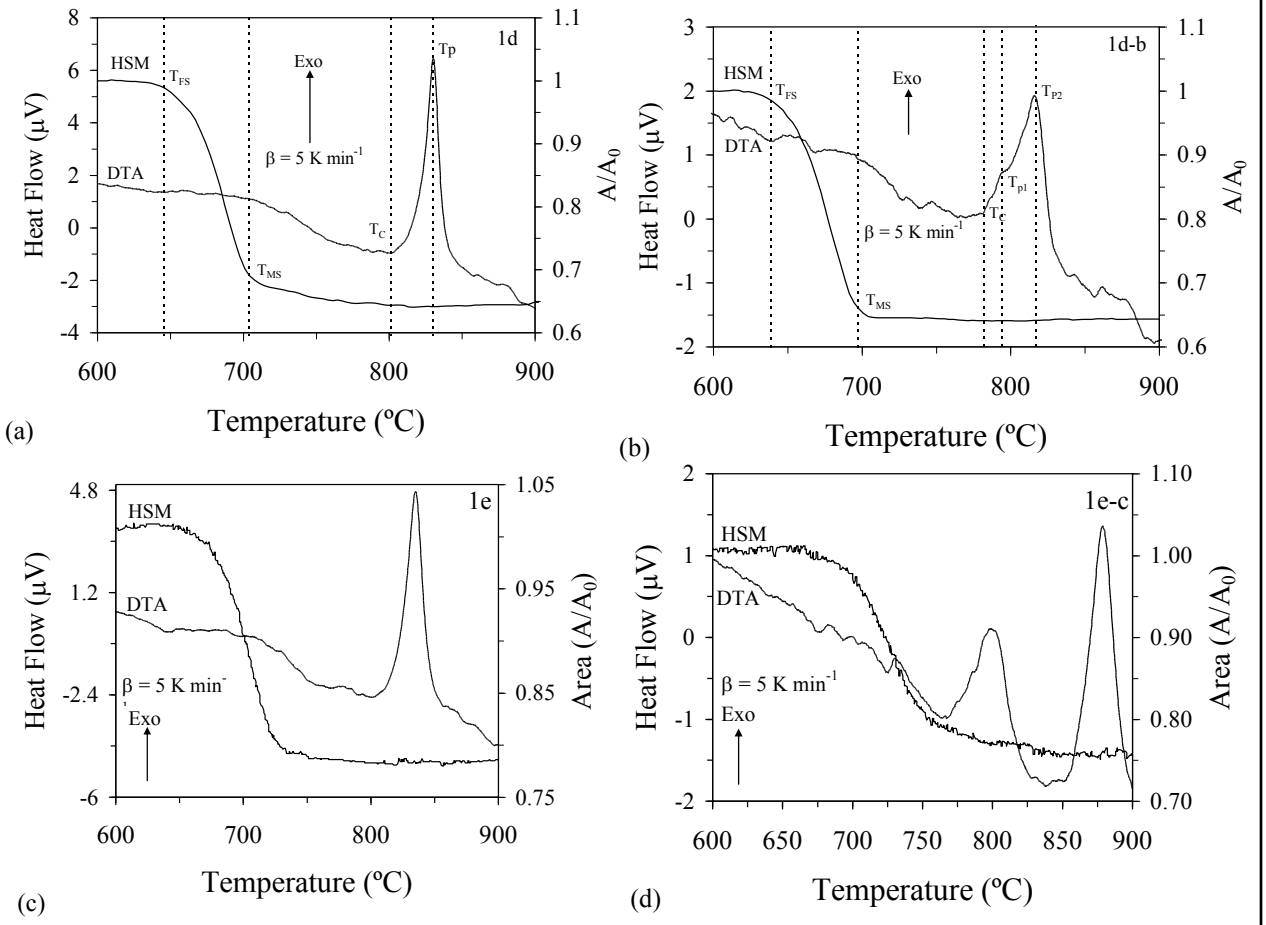

Figure 4.38 Comparison of DTA and HSM curves on the same temperature scale for compositions (a) 1d, (b) 1d-b, (c) 1e and (d) 1e-c.

respect to temperatures obtained from HSM. Table 4.9 summarizes the values of the temperature of first shrinkage (T_{FS}; log η = 9.1 ± 0.1, η is viscosity; dPa s), temperature for maximum shrinkage (T_{MS}; logη = 7.8 ± 0.1) and ratio of the final area/initial area of the glass powder compact (A/A_0) as obtained from the HSM data at T_{MS} (Figure 4.38) along with temperature for onset of crystallization (T_c) and peak temperature of crystallization (T_p), as obtained from DTA thermograph of the glasses. In all the investigated compositions, sintering preceded crystallization, thus resulting in well sintered glass-ceramics. Table 4.9 lists the values of sinterability parameter (S_c), where $S_c = T_c - T_{MS}$ [13]. The parameter S_c is the measure of ability

of sintering versus crystallization: the greater this difference, the more independent are the kinetics of both processes. In the present study, larger values of S_c (greater than 25 ºC) (74 - 99 ºC) are related with larger final densities, which indicate better sintering/crystallization behaviour. However, with respect to compositions, sintering ability degraded with increase in

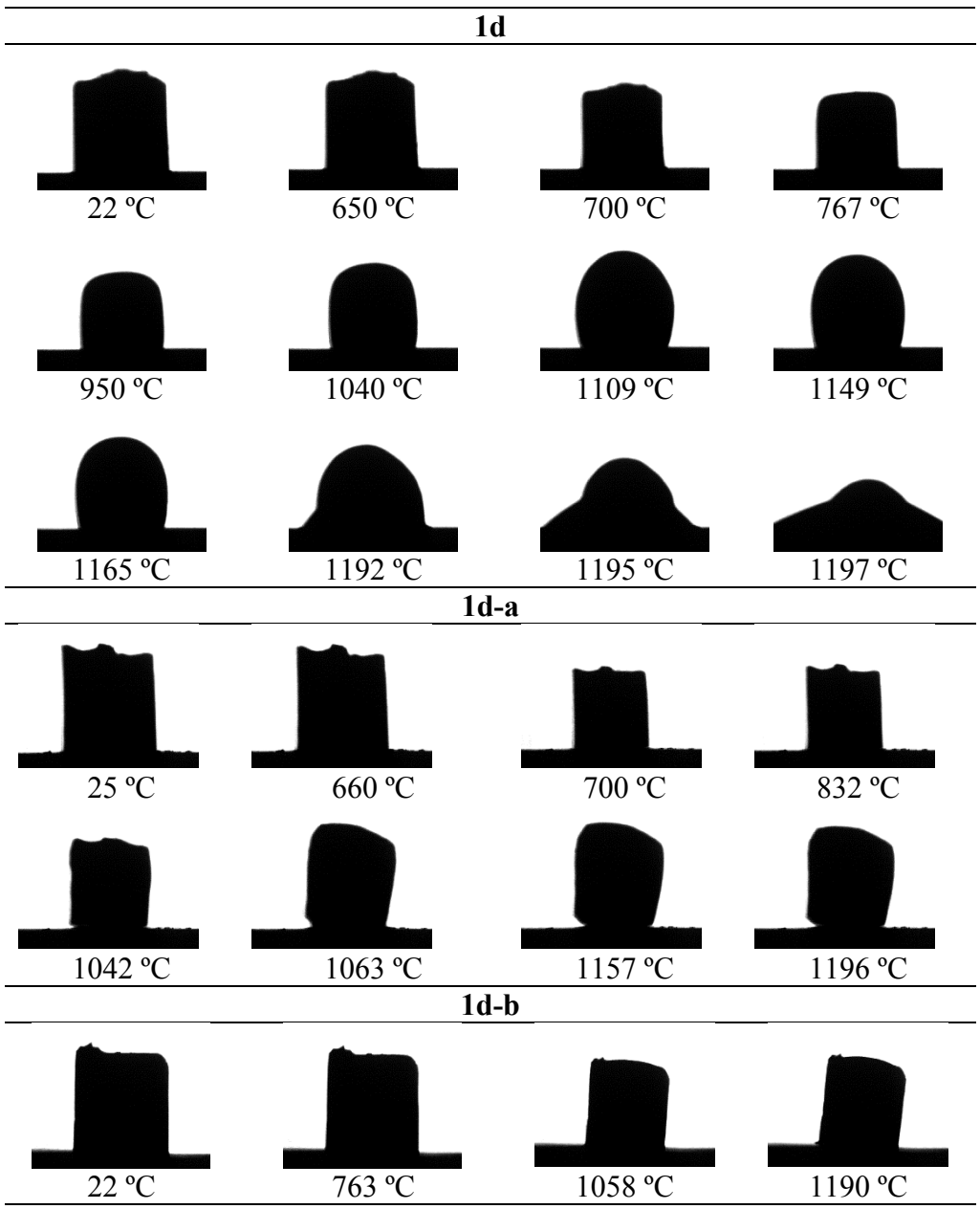

Figure 4.39 HSM images of glasses with varying CaO/SiO_2 ratio on alumina substrates at various stages of heating cycle. Heating rate: 5 K min^{-1}.

CaO/SiO_2 ratio while it improved with increase in P_2O_5/CaF_2 ratio in the glasses. Further, the values of T_c and T_p decreased with increase in CaO/SiO_2 ratio in the glasses while they increased with increase in P_2O_5/CaF_2 ratio (Table 4.9). It is noteworthy that DTA analysis of both the parent glass compositions i.e. 1d (Figure 4.38a) and 1e (Fig. 4.38c) exhibit a single exothermic curve. This anticipates that the glass-ceramic is formed either as a result of single phase crystallization or of an almost simultaneous precipitation of different crystalline phases. However, with increase in CaO/SiO_2 ratio in the glasses a shoulder appeared in the main exothermic curve of glass 1d-b, thus pointing towards the formation of two different crystalline phases (Figure 4.38b). Similarly, an increase P_2O_5/CaF_2 ratio in the glasses led to the appearance

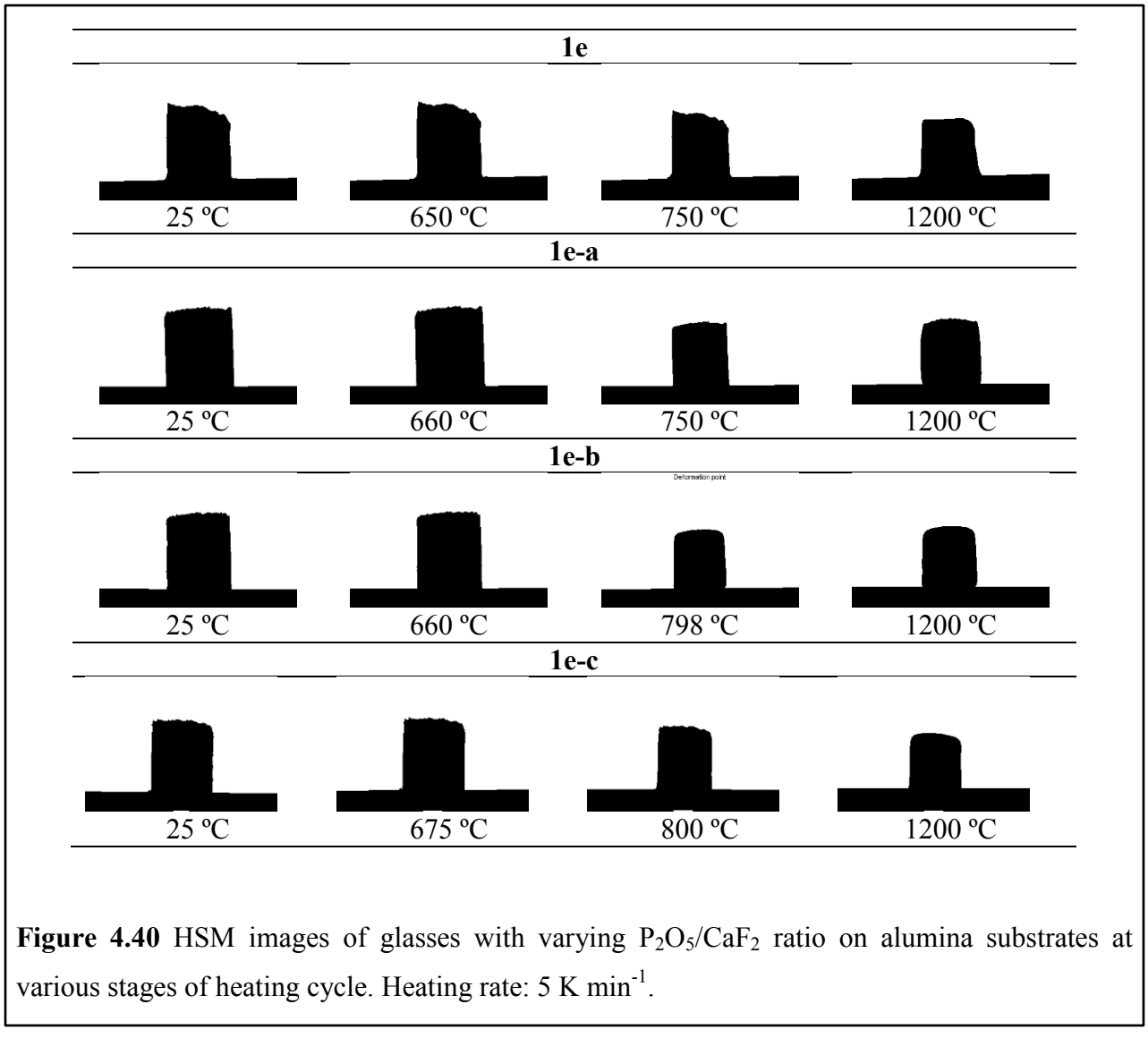

Figure 4.40 HSM images of glasses with varying P_2O_5/CaF_2 ratio on alumina substrates at various stages of heating cycle. Heating rate: 5 K min^{-1}.

of two distinct crystallization exothermic curves in glasses 1e-b and 1e-c (Figure 4.38d), respectively. The activation energy of crystallization (E_c) (as obtained in accordance with our previous study [71]) increased with increasing P_2O_5 content in the glasses due to the increasing amount of glass network former, thus, providing stability against devitrification (Table 4.9). Furthermore, as is evident from Figure 4.39, increasing CaO content in the glasses at the expense of SiO_2 increased the refractoriness of the glass compositions, thus, increasing the flow temperature (T_F; log η = 3.4± 0.1; dPa s) of the glasses 1d-a and 1d-b. The glasses from series 1e exhibited more refractory behaviour as no composition showed any deformation in the shape of the glass powder compacts until 1200 ºC, except decrease in area due to shrinkage. The increase in refractoriness of the materials with increasing P_2O_5 content is well known [67]. The half ball

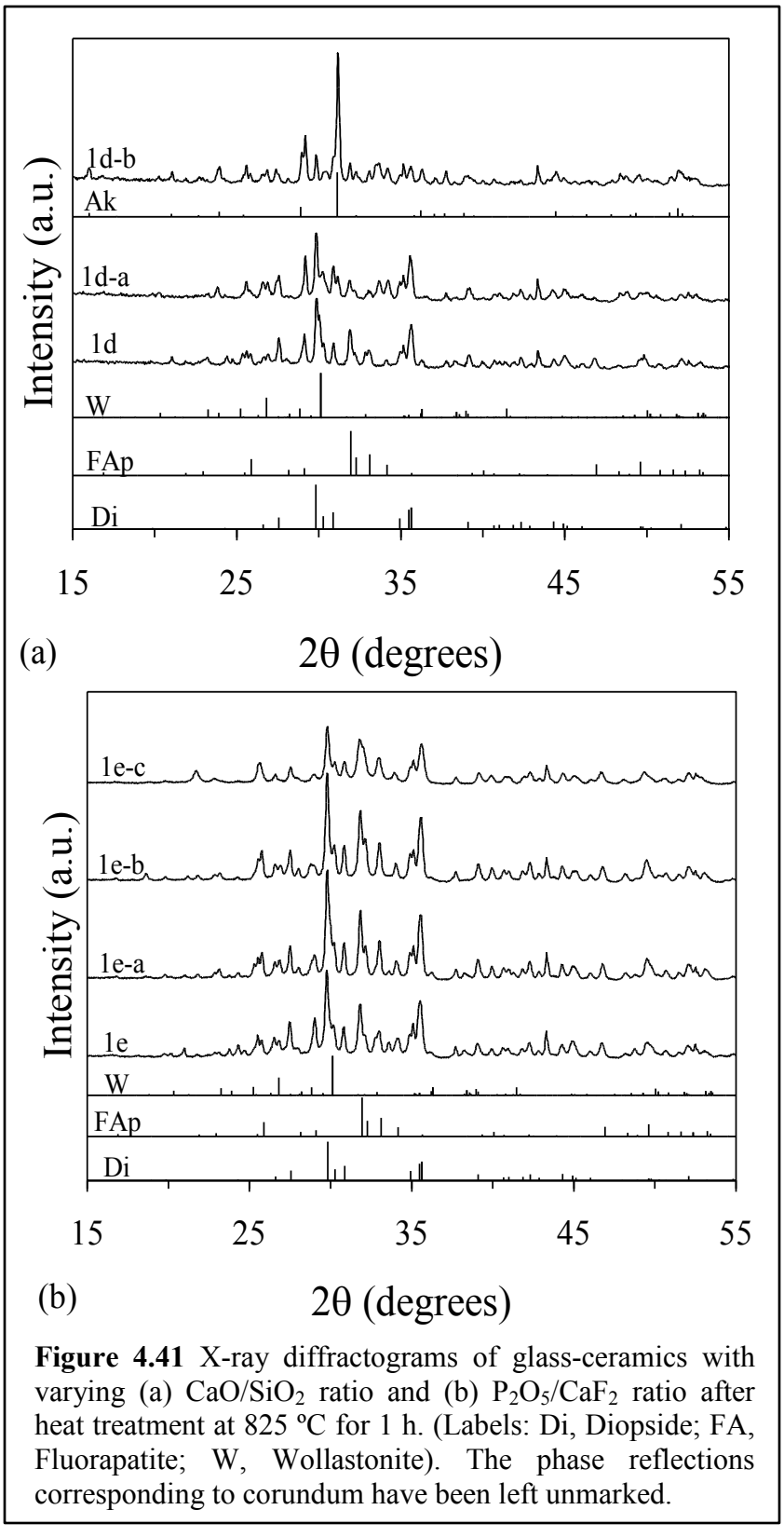

Figure 4.41 X-ray diffractograms of glass-ceramics with varying (a) CaO/SiO_2 ratio and (b) P_2O_5/CaF_2 ratio after heat treatment at 825 ºC for 1 h. (Labels: Di, Diopside; FA, Fluorapatite; W, Wollastonite). The phase reflections corresponding to corundum have been left unmarked.

temperature (T_{HB}; log η = 4.1 ± 0.1) for glass 1d, as observed from photomicrographs obtained from HSM (Figure 4.40) is 1192 ºC while the flow temperature (T_F) is 1197 ºC.

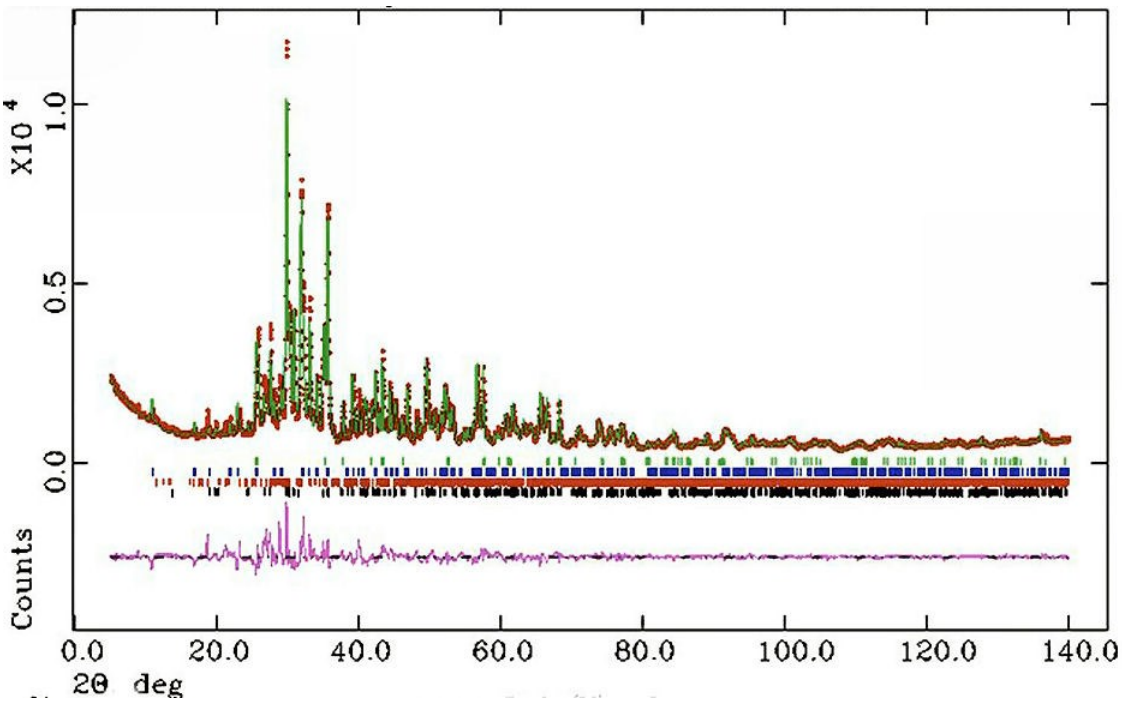

Figure 4.42 Observed (crosses), calculated (continuous line), and difference curve from the Rietveld refinement of the GC 1e-b heat treated at 825 ºC for 1 h in air. Markers representing the phase reflections correspond to corundum, fluorapatite, wollastonite and diopside (from top to bottom).

In agreement with HSM and DTA results, well sintered glass-ceramics were obtained after heat treatment of powder compacts at 825 ºC for 1 h. The qualitative analysis of XRD diffractograms of glass-ceramics presented in Figure 4.41 revealed the crystallization of diopside ($CaMgSi_2O_6$; ICDD card: 78-1390), fluorapatite ($Ca_5(PO_4)_3F$; ICDD card: 71-880) and wollastonite ($CaSiO_3$; ICDD card: 72-2297) as the only crystalline phases in all the investigated compositions except glass-ceramic 1d-b where akermanite ($Ca_2MgSi_2O_7$; ICDD card: 70-7162) also joined the crystalline phase assemblage. Table 4.10 presents the quantitative analysis of the crystalline phases present in all the investigated GCs as obtained from XRD analysis adjoined with Rietveld-R.I.R technique. Figure 4.42 shows the fit of a measured XRD pattern of a sintered GC by using the GSAS-EXPGUI software. The fitting to the measured X-ray diagram has been

Table 4.10 Results of Rietveld-R.I.R quantitative analysis (wt%)

	1d	1d-a	1d-b	1e	1e-a	1e-b	1e-c
Diopside	44.60 (3)	49.97 (3)	17.51 (1)	46.57 (1)	47.42 (1)	53.13 (1)	51.40 (1)
Wollastonite	16.07 (1)	12.60 (1)	4.95 (4)	6.82 (2)	14.03 (1)	10.55 (2)	0.92 (1)
Fluorapatite	16.94 (1)	7.12 (4)	7.70 (1)	18.70 (2)	24.42 (1)	33.21 (1)	31.79 (3)
Akermanite	-	-	37.69 (1)	-	-	-	-
Glass	22.39 (5)	30.31 (8)	32.15 (7)	27.91 (5)	14.13 (3)	3.11 (4)	15.89 (5)
Total	100	100	100	100	100	100	100
χ^2	3.07	5.26	5.38	13.18	5.90	7.57	5.731
R_{wp}	0.13	0.17	0.17	0.12	0.08	0.09	0.08
R_p	0.09	0.11	0.12	0.08	0.06	0.06	0.05

performed by a least-square calculation. The calculated diagram (Figure 4.42) is based on crystallographic structure models, which also takes into account specific instrumental and samples effects. The parameters of this model have been refined simultaneously using least-squares methods in order to obtain the best fit to all measured data. By least-squares refinement, a so-called figure-of-merit function R has been defined, which describes the residual (agreement) between observed and calculated data. It is noteworthy that many different statistical R factors have been proposed for judging the quality of a Rietveld refinement. The R factors show the mean deviation in accordance with the used model in per cent. The "profile R-factor", R_p, and "weighted profile R-factor", R_{wp}, for all the refinements are presented in Table 4.10. The values of R_{wp} as obtained in the present investigation are well in the limit of experimental accuracy. The difference plot in Figure 4.42 does not show any significant misfits. The differences under the main peaks of diopside, fluorapatite and wollastonite are caused by adjustment difficulties based on crystallinity of phases. As is evident from Table 4.10, diopside crystallized as the major crystalline phase in glass-ceramic 1d while the amount of wollastonite and fluorapatite remained almost constant. The increase in CaO/SiO_2 ratio in glass 1d-a led to an increase in diopside and wollastonite content at the expense of fluorapatite in the resultant glass-ceramics. Further

addition of CaO in the glass system at the expense of SiO_2 (1d-b) led to the crystallization of akermanite as the major phase followed by diopside, fluorapatite and wollastonite. It is noteworthy that akermanite based ceramics and glass-ceramics are potential biomaterials for bone regeneration and have been reported to exhibit excellent biocompatibility [72, 73]. The amount of glassy phase increased with increase in CaO/SiO_2 ratio in the glass-ceramics. In case of glass compositions with varying P_2O_5/CaF_2 ratio, the amount of diopside and fluorapatite increased with increase in P_2O_5 content in the glass system (Table 4.10) while the amount of amorphous glassy phase decreased until composition 1e-b. In general, all the resultant glass-ceramics exhibit high degree of crystallization (glassy phase: 10-40%).

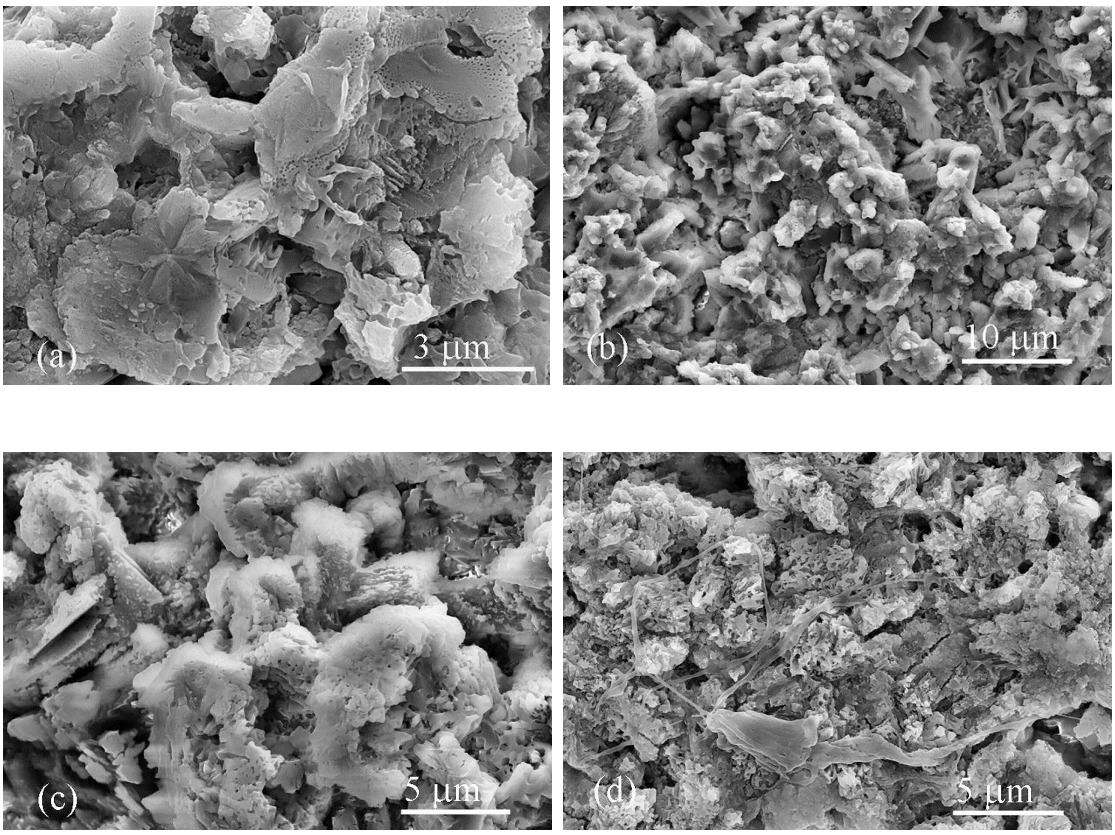

Figure 4.43 SEM images of fractured glass-ceramics after chemical etching with 2 vol.% HF solution: a) 1d, (b) 1d-a, (c) 1e, (d) 1e-b

In agreement with the XRD results, SEM images of all the glass-ceramics reveal a similar kind of microstructure (Figure 4.43) exhibiting different morphologies for different crystalline phases. Figure 4.43a presents the microstructure of the glass-ceramic 1d exhibiting rosette

morphology which is typical for diopside crystals along with the dendritic crystal growth for another phase. Figure 4.43b presents the microstructure of the glass-ceramic 1d-b at lower magnification depicting a similar morphology of crystalline phases as was observed for glass-ceramic 1d. Similar microstructure was observed for glass-ceramics 1e (Figure 4.43c), 1e-a, 1e-b (Figure 4.43d) and 1e-c, except that the size and amount of rosette shaped crystals (Figure 4.43c and 4.43d) increased, thus depicting an increase in the concentration of diopside in the glass-ceramics. It should be mentioned here that due to very similar composition of crystalline phases present in glass-ceramics and considering the semi-quantitative nature of the energy dispersive spectroscopy (EDS) technique, we could not precisely distinct the microstructure for all the crystalline phases present in the glass-ceramics.

4. Summary

An insight into the structure, sintering and crystallization behaviour of glasses in the CaO-MgO-SiO_2-P_2O_5-Na_2O-CaF_2 system with varying CaO/SiO_2 and P_2O_5/CaF_2 molar ratio has been presented. The findings from this study are summarized below:

1. The structure of the investigated glasses has some peculiar similarities with the structure of 45S5 glass since the Q^n (Si) units are dominated by Q^2 and Q^3 units.
2. Sintering preceded crystallization in all the compositions, thus resulting in well sintered glass powder compacts with diopside as the major crystalline phase followed by fluorapatite and wollastonite.
3. An increase in concentration of CaO at expense of SiO_2 led to the formation of akermanite in the glass-ceramics. In general, an increase in P_2O_5/CaF_2 and decrease in CaO/SiO_2 ratio improves the sintering ability of glass powders. All the glass-ceramics exhibited high amount of crystallinity with total amorphous phase varying between ~ 3-30 wt. %.

Finally, the structural features and properties of synthesized glasses coupled with a possibility to produce well sintered glass-ceramics from corresponding glass-powder compacts might suggest testing new materials for further applications in biomedicine.

References

[1] T. Hoche, C. Moisescu, I. Avramov, C. Russel, and W. D. Heerdegen, "Microstructure of SiO_2-Al_2O_3-CaO-P_2O_5-K_2O-F- glass ceramics. 1. Needlelike versus isometric morphology of apatite crystals," *Chemistry of Materials,* vol. 13, pp. 1312-1319, 2001.

[2] M. W. G. Lockyer, D. Holland, and R. Dupree, "NMR investigation of the structure of some bioactive and related glasses," *Journal of Non-Crystalline Solids,* vol. 188, pp. 207-219, 1995.

[3] D. U. Tulyaganov, "Phase Equilibrium in the Fluorapatite–Anorthite–Diopside System," *Journal of the American Ceramic Society,* vol. 83, pp. 3141-3146, 2000.

[4] D. S. Brauer, N. Karpukhina, R. V. Law, and R. G. Hill, "Structure of fluoride-containing bioactive glasses," *Journal of Materials Chemistry,* vol. 19, pp. 5629-5636, 2009.

[5] J. Schneider, V.R. Mastelaro, H. Panepucci, and E.D. Zanotto, "^{29}Si MAS–NMR studies of Q^n structural units in metasilicate glasses and their nucleating ability," *Journal of Non-Crystalline Solids,* vol. 273, pp. 8-18, 2000.

[6] L. Linati, G. Lusvardi, G. Malavasi, L. Menabue, M. C. Menziani, P. Mustarelli, A. Pedone, and U. Segre, "Medium-range order in phospho-silicate bioactive glasses: Insights from MAS-NMR spectra, chemical durability experiments and molecular dynamics simulations," *Journal of Non-Crystalline Solids,* vol. 354, pp. 84-89, 2008.

[7] A. Goel, S. Kapoor, A. Tilocca, R. R. Rajagopal, and J. M. F. Ferreira, "Structural role of zinc in biodegradation of alkali-free bioactive glasses," *Journal of Materials Chemistry B,* vol. 1, pp. 3073-3082, 2013.

[8] S. Kapoor, A. Goel, A. Tilocca, V. Dhuna, G. Bhatia, K. Dhuna, and J. M. F. Ferreira, "Role of glass structure in defining the chemical dissolution behavior, bioactivity and antioxidant properties of zinc and strontium co-doped alkali-free phosphosilicate glasses," *Acta Biomaterialia,* vol. 10, pp. 3264-3278, 2014.

[9] H. A. Abo-Mosallam, R. G. Hill, N. Karpukhina, R. V. Law, "MAS-NMR studies of glasses and glass-ceramics based on a clinopyroxene-fluorapatite system," *Journal of Materials Chemistry*, vol. 20, pp. 790-797, 2010.

[10] G. Lusvardi, G. Malavasi, M. Cortada, L. Menabue, M. C. Menziani, A. Pedone, and U. Segre, "Elucidation of the structural role of fluorine in potentially bioactive glasses by experimental and computational investigation," *Journal of Physical Chemistry B,* vol. 112, pp. 12730-12739, 2008.

[11] D.S. Brauer, M. Mneimne, and R. G. Hill, "Fluoride-containing bioactive glasses: Fluoride loss during melting and ion release in tris buffer solution," *Journal of Non-Crystalline Solids,* vol. 357, pp. 3328-3333, 2011.

[12] H. Taniguchi and T. Murase, "Some physical properties and melt structures in the system diopside-anorthite," *Journal of Volcanology and Geothermal Research,* vol. 34, pp. 51-64, 1987.

[13] C. Lara, M. J. Pascual, and A. Durán, "Glass-forming ability, sinterability and thermal properties in the systems RO-BaO-SiO2 (R = Mg, Zn)," *Journal of Non-Crystalline Solids,* vol. 348, pp. 149-155, 2004.

[14] J. R. Jones, P. Sepulveda, and L. L. Hench, "Dose-dependent behavior of bioactive glass dissolution," *Journal of Biomedical Materials Research,* vol. 58, pp. 720-726, 2001.

[15] K. H. Karlsson, K. Fröberg, and T. Ringbom, "A structural approach to bone adhering of bioactive glasses," *Journal of Non-Crystalline Solids,* vol. 112, pp. 69-72, 1989.

[16] P. Li, C. Ohtsuki, T. Kokubo, K. Nakanishi, N. Soga, T. Nakamura, amd T. Yamamuro, "Apatite Formation Induced by Silica Gel in a Simulated Body Fluid," *Journal of the American Ceramic Society,* vol. 75, pp. 2094-2097, 1992.

[17] M. Cerruti and C. Morterra, "Carbonate formation on bioactive glasses," *Langmuir,* vol. 20, pp. 6382-6388, 2004.

[18] I. Allan, H. Newman, and M. Wilson, "Antibacterial activity of particulate Bioglass® against supra- and subgingival bacteria," *Biomaterials,* vol. 22, pp. 1683-1687, 2001.

[19] M. Gubler, T. J. Brunner, M. Zehnder, T. Waltimo, B. Sener, and W. J. Stark, "Do bioactive glasses convey a disinfecting mechanism beyond a mere increase in pH?," *International Endodontic Journal,* vol. 41, pp. 670-678, 2008.

[20] L. Stoch and M. Środa, "Infrared spectroscopy in the investigation of oxide glasses structure," *Journal of Molecular Structure,* vol. 511–512, pp. 77-84, 1999.

[21] K. Omori, "Analysis of Infrared Absorption Spectrum of Diopside," *American Mineralogist,* vol. 56, pp. 1607, 1971.

[22] A. Aronne, V. N. Sigaev, B. Champagnon, E. Fanelli, V. Califano, L. Z. Usmanova, and P. Pernice, "The origin of nanostructuring in potassium niobiosilicate glasses by Raman and FTIR spectroscopy," *Journal of Non-Crystalline Solids,* vol. 351, pp. 3610-3618, 2005.

[23] F. L. Galeener and G. Lucovsky, "Longitudinal Optical Vibrations in Glasses: GeO_2 and SiO_2," *Physical Review Letters,* vol. 37, pp. 1474-1478, 1976.

[24] Q. Williams and E. Knittle, "Infrared and raman spectra of $Ca_5(PO_4)_3F$-fluorapatite at high pressures: Compression-induced changes in phosphate site and Davydov splittings," *Journal of Physics and Chemistry of Solids,* vol. 57, pp. 417-422, 1996.

[25] G. Lusvardi, G. Malavasi, L. Menabue, V. Aina, and C. Morterra, "Fluoride-containing bioactive glasses: Surface reactivity in simulated body fluids solutions," *Acta Biomaterialia,* vol. 5, pp. 3548-3562, 2009.

[26] L. L. Hench, "Bioceramics," *Journal of the American Ceramic Society,* vol. 81, pp. 1705-1728, 1998.

[27] D. S. Brauer, N. Karpulthina, M. D. O'Donnell, R. V. Law, and R. G. Hill, "Fluoride-containing bioactive glasses: Effect of glass design and structure on degradation, pH and apatite formation in simulated body fluid," *Acta Biomaterialia,* vol. 6, pp. 3275-3282, 2010.

[28] J. Perez-Pariente, F. Balas, and M. Vallet-Regi, "Surface and chemical study of SiO_2•P_2O_5•CaO•(MgO) bioactive glasses," *Chemistry of Materials,* vol. 12, pp. 750-755, 2000.

[29] A. Tilocca, "Sodium migration pathways in multicomponent silicate glasses: Car–Parrinello molecular dynamics simulations," *The Journal of Chemical Physics,* vol. 133, pp. 014701, 2010.

[30] I. Kansal, A. Reddy, F. Munoz, S.-J. Choi, H.-W. Kim, D. U. Tulyaganov, and J. M. F. Ferreira, "Structure, biodegradation behavior and cytotoxicity of alkali-containing alkaline-earth phosphosilicate glasses," *Materials science & engineering. C, Materials for biological applications,* vol. 44, pp. 159-65, 2014.

[31] C. Ohtsuki, T. Kokubo, and T. Yamamuro, "Mechanism of apatite formation on CaO-SiO_2-P_2O_5 glasses in a simulated body fluid," *Journal of Non-Crystalline Solids,* vol. 143, pp. 84-92, 1992.

[32] A. Tilocca, A. N. Cormack, and N. H. de Leeuw, "The formation of nanoscale structures in soluble phosphosilicate glasses for biomedical applications: MD simulations," *Faraday Discussions,* vol. 136, pp. 45-55, 2007.

[33] C. Wu, Y. Ramaswamy, and H. Zreiqat, "Porous diopside ($CaMgSi_2O_6$) scaffold: A promising bioactive material for bone tissue engineering," *Acta Biomaterialia,* vol. 6, pp. 2237-45, 2010.

[34] C. Wu and H. Zreiqat, "Porous bioactive diopside ($CaMgSi_2O_6$) ceramic microspheres for drug delivery," *Acta Biomaterialia,* vol. 6, pp. 820-9, 2010.

[35] C. P. Yoganand, V. Selvarajan, L. Lusvarghi, O. M. Goudouri, K. M. Paraskevopoulos, and M. Rouabhia, "Bioactivity of CaO–MgO–SiO_2 glass ceramics synthesized using transferred arc plasma (TAP) process," *Materials Science and Engineering: C,* vol. 29, pp. 1759-1764, 2009.

[36] I. Christodoulou, L. D. K. Buttery, P. Saravanapavan, G. P. Tai, L. L. Hench, and J. M. Polak, "Dose- and time-dependent effect of bioactive gel-glass ionic-dissolution products on human fetal osteoblast-specific gene expression," *Journal of Biomedical Materials Research Part B-Applied Biomaterials,* vol. 74B, pp. 529-537, 2005.

[37] S. Murphy, A. W. Wren, M. R. Towler, and D. Boyd, "The effect of ionic dissolution products of Ca–Sr–Na–Zn–Si bioactive glass on in vitro cytocompatibility," *Journal of Materials Science: Materials in Medicine,* vol. 21, pp. 2827-2834, 2010.

[38] I. D. Xynos, A. J. Edgar, L. D. K. Buttery, L. L. Hench, and J. M. Polak, "Gene-expression profiling of human osteoblasts following treatment with the ionic products of Bioglass (R) 45S5 dissolution," *Journal of Biomedical Materials Research,* vol. 55, pp. 151-157, 2001.

[39] T. Yamaguchi, N. Chattopadhyay, O. Kifor, R. R. Butters, T. Sugimoto, and E. M. Brown, "Mouse osteoblastic cell line (MC3T3-E1) expresses extracellular calcium (Ca-0(2+))-sensing receptor and its agonists stimulate chemotaxis and proliferation of MC3T3-E1 cells," *Journal of Bone and Mineral Research,* vol. 13, pp. 1530-1538, 1998.

[40] Z. Meleti, I. M. Shapiro, and C. S. Adams, "Inorganic phosphate induces apoptosis of osteoblast-like cells in culture," *Bone,* vol. 27, pp. 359-366, 2000.

[41] M. P. Staiger, A. M. Pietak, J. Huadmai, and G. Dias, "Magnesium and its alloys as orthopedic biomaterials: A review," *Biomaterials,* vol. 27, pp. 1728-1734, 2006.

[42] N. E. L. Saris, E. Mervaala, H. Karppanen, J. A. Khawaja, and A. Lewenstam, "Magnesium - An update on physiological, clinical and analytical aspects," *Clinica Chimica Acta,* vol. 294, pp. 1-26, 2000.

[43] J. Vormann, “Magnesium: nutrition and metabolism,” Molecular Aspects of Medicine, vol. 24, pp. 27-37, 2003.

[44] S.-A. Oh, S.-H. Kim, J.-E. Won, J.-J. Kim, U. S. Shin, and H.-W. Kim, “Effects on growth and osteogenic differentiation of mesenchymal stem cells by the zinc-added sol-gel bioactive glass granules,” *Journal of tissue engineering,* vol. 2010, pp. 475260-475260, 2011.

[45] A. Tilocca, “Structural models of bioactive glasses from molecular dynamics simulations,” *Proceedings of the Royal Society A-Mathematical Physical and Engineering Sciences,* vol. 465, pp. 1003-1027, 2009.

[46] P. G. Galliano, J. M. P. Lopez, E. L. Varetti, I. Sobrados, and J. Sanz, “Analysis by nuclear magnetic resonance and Raman spectroscopies of the structure of bioactive alkaline-earth silicophosphate glasses,” *Materials Research Bulletin,* vol. 29, pp. 1297-1306, 1994.

[47] A. Pedone, G. Malavasi, M. C. Menziani, U. Segre, and A. N. Cormack, “Role of magnesium in soda-lime glasses: insight into structural, transport, and mechanical properties through computer simulations,” *Journal of Physical Chemistry C,* vol. 112, pp. 11034-11041, 2008.

[48] A. Pedone, G. Malavasi, and M. C. Menziani, “Computational Insight into the Effect of CaO/MgO Substitution on the Structural Properties of Phospho-Silicate Bioactive Glasses,” *Journal of Physical Chemistry C,* vol. 113, pp. 15723-15730, 2009.

[49] S. J. Watts, R. G. Hill, M. D. O'Donnell, and R. V. Law, “Influence of magnesia on the structure and properties of bioactive glasses,” *Journal of Non-Crystalline Solids,* vol. 356, pp. 517-524, 2010.

[50] R. Mathew, B. Stevensson, A. Tilocca, and M. Eden, “Toward a Rational Design of Bioactive Glasses with Optimal Structural Features: Composition-Structure Correlations Unveiled by Solid-State NMR and MD Simulations,” *Journal of Physical Chemistry B,* vol. 118, pp. 833-844, 2014.

[51] R. G. Hill and D. S. Brauer, “Predicting the bioactivity of glasses using the network connectivity or split network models,” *Journal of Non-Crystalline Solids,* vol. 357, pp. 3884-3887, 2011.

[52] H. Aguiar, E. L. Solla, J. Serra, P. Gonzalez, B. Leon, N. Almeida, S. Cachinho, E. J. C. Davim, R. Correia, J. M. Oliveira, M. H. V. Fernandes, "Orthophosphate nanostructures in SiO_2-P_2O_5-CaO-Na_2O-MgO bioactive glasses," *Journal of Non-Crystalline Solids,* vol. 354, pp. 4075-4080, 2008.

[53] S. Kroeker and J. F. Stebbins, "Magnesium coordination environments in glasses and minerals: New insight from high-field ^{25}Mg MAS NMR," *American Mineralogist,* vol. 85, pp. 1459-1464, Oct 2000.

[54] T. Wilantewicz, "The effects of lithium, boron and magnesium oxides on the mechanical properties of silicate glasses," Alfred University, New York, 1998.

[55] A. Karamanov and M. Pelino, "Induced crystallization porosity and properties of sintereds diopside and wollastonite glass-ceramics," *Journal of the European Ceramic Society,* vol. 28, pp. 555-562, 2008.

[56] Z. Strnad, "Role of the glass phase in bioactive glass-ceramics," *Biomaterials,* vol. 13, pp. 317-21, 1992.

[57] P. Li, Q. Yang, F. Zhang, and T. Kokubo, "The effect of residual glassy phase in a bioactive glass-ceramic on the formation of its surface apatite layer in vitro," *Journal of Materials Science: Materials in Medicine,* vol. 3, pp. 452-456, 1992.

[58] J. W. Martin, "Concise encyclopedia of the structural materials," ed: Elsevier Science, 2006.

[59] M. R. Filgueiras, G. La Torre, and L. L. Hench, "Solution effects on the surface reactions of a bioactive glass," *Journal of Biomedical Materials Research,* vol. 27, pp. 445-453, 1993.

[60] K. E. Wallace, R. G. Hill, J. T. Pembroke, C. J. Brown, and P. V. Hatton, "Influence of sodium oxide content on bioactive glass properties," *Journal of Materials Science: Materials in Medicine,* vol. 10, pp. 697-701, 1999.

[61] I. Denry and J. Holloway, "Fluorapatite glass-ceramics," 2014.

[62] F. Branda, A. Costantini, and A. Buri, "Nonisothermal devitrifiation behavior of diopside glass," *Thermochimica Acta,* vol. 217, pp. 207-212, 1993.

[63] N. Lotfibakhshaiesh, D. S. Brauer, and R. G. Hill, "Bioactive glass engineered coatings for Ti6Al4V alloys: Influence of strontium substitution for calcium on sintering behaviour," *Journal of Non-Crystalline Solids,* vol. 356, pp. 2583-2590, 2010.

[64] A. Goel, E. R. Shaaban, J. B. Oliveira, M. A. Sa, M. J. Pascual, and J. M. F. Ferreira, "Sintering behavior and devitrification kinetics of iron containing clinopyroxene based magnetic glass-ceramics," *Solid State Ionics,* vol. 186, pp. 59-68, 2011.

[65] A. R. Boccaccini, Q. Chen, L. Lefebvre, L. Gremillard, and J. Chevalier, "Sintering, crystallisation and biodegradation behaviour of Bioglass®-derived glass-ceramics," *Faraday Discussions,* vol. 136, pp. 27-44, 2007 2007.

[66] O. Bretcanu, X. Chatzistavrou, K. Paraskevopoulos, R. Conradt, I. Thompson, and A. R. Boccaccini, "Sintering and crystallisation of 45S5 Bioglass (R) powder," *Journal of the European Ceramic Society,* vol. 29, pp. 3299-3306, 2009.

[67] H. T. Godard, C. W. Tanner, M. M. Wallen, and E. Wheeler, "Refractory Materials," US Patent#20090131241, 2009.

[68] W. L. Konijnendijk and J. M. Stevels, "Raman scattering measurements of silicate glasses and compounds," *Journal of Non-Crystalline Solids,* vol. 21, pp. 447-453, 1976.

[69] Y. Tsunawaki, N. Iwamoto, T. Hattori, and A. Mitsuishi, "Analysis of $CaO{\bullet}SiO_2$ and $CaO{\bullet}SiO_2{\bullet}CaF_2$ glasses by Raman spectroscopy," *Journal of Non-Crystalline Solids,* vol. 44, pp. 369-378, 1981.

[70] S. Agathopoulos, D. U. Tulyaganov, J. M. G. Ventura, S. Kannan, A. Saranti, M. A. Karakassides, and J. M. F. Ferreira, "Structural analysis and devitrification of glasses based on the $CaO\text{-}MgO\text{-}SiO_2$ system with B_2O_3, Na_2O, CaF_2 and P_2O_5 additives," *Journal of Non-Crystalline Solids,* vol. 352, pp. 322-328, 2006.

[71] A. Goel, D. U. Tulyaganov, A. M. Ferrari, E. R. Shaaban, A. Prange, F. Bondioli, and J. M. F. Ferreira, "Structure, sintering, and crystallization kinetics of alkaline-earth aluminosilicate glass-ceramic sealants for solid oxide fuel cells," *Journal of the American Ceramic Society,* vol. 93, pp. 830-837, 2010.

[72] H. L. Sun, C. T. Wu, K. R. Dai, J. Chang, and T. T. Tang, "Proliferation and osteoblastic differentiation of human bone marrow-derived stromal cells on akermanite-bioactive ceramics," *Biomaterials,* vol. 27, pp. 5651-5657, 2006.

[73] Y. Huang, X. Jin, X. Zhang, H. Sun, J. Tu, T. Tang, J. Chang, and K. Dai, "In vitro and in vivo evaluation of akermanite bioceramics for bone regeneration," *Biomaterials,* vol. 30, pp. 5041-5048, 2009.

…….

Chapter 5. Conclusions

Our work aimed at understanding the composition-structure-property relationships in potentially bioactive glasses designed in $CaO–MgO–P_2O_5–SiO_2–F$ system. The main emphasis was on unearthing the influence of glass composition on molecular structure, sintering ability and bioactivity of phosphosilicate glasses. The parent glass compositions were designed in alkali-free system so as to maintain compositional disparity from widely studied 45S5 Bioglass® – based alkali-rich glass compositions. The compositional disparity from alkali-rich bioactive glass compositions was necessary in order to (i) negate the possibility of competing mechanism between sodium and calcium for coordination with phosphate component in the glass structure which is known to affect structure-property relationships in these glasses significantly [1], (ii) avoid preferential leaching of sodium from glass into aqueous solutions resulting in a rapid change in pH and solution chemistry, thus, affecting the results obtained from dissolution studies, (iii) avoid high crystallization tendency in glasses so as to understand the compositional impact on the sintering ability of glass powders [2].

The initial study focussed on exploring the structure, sintering ability and bioactivity of glasses along diopside ($CaO•MgO•2SiO_2$) – fluorapatite ($9CaO•3P_2O_5•CaF_2$) join. We could obtain glasses for compositions with $(100–x)$ ($CaO•MgO•2SiO_2$) – $x(9CaO•3P_2O_5•CaF_2)$, where x varied between 0 – 40 wt.%. While silicate glass network in all the glasses was dominated by Q^2 units, phosphate component was majorly found coordinated in orthophosphate environment. While calcite formation masked the formation of carbonated-hydroxyapatite on glass surfaces when immersed in SBF (owing to the high glass powder – to – SBF ratio), increasing fluorapatite content in glasses had a marked effect on decreasing this tendency. The investigated glasses exhibited slower chemical dissolution in comparison to 45S5 Bioglass®, thus, resulting in slower pH changes in aqueous solutions. This trait is desired for aqueous colloidal processing of glass powders leading to the formation of porous glass-ceramic scaffolds.

With respect to the sintering ability of the glass powders, shrinkage behaviour of glasses shifted from single stage–to–two stage due to the possible amorphous phase separation between silicate and phosphate phase in these glasses. This resulted in well sintered glass powders compacts with high amorphous content (>60 wt.%) for compositions with x = 10 and 20 wt.%. Diopside crystallized as the primary phase in all the glass-ceramics followed by fluorapatite as secondary/minor phase. The good sintering ability of glass powders along with crystallization of diopside will provide the resultant glass-ceramics with good mechanical stability and integrity

while high residual glassy phase will ensure good bioactivity and controlled degradation. The *in vitro* biological evaluation of these glass-ceramics (x = 10 – 20 wt.%) qualify them as potential materials for scaffold fabrication as well as for coatings on biomedical implants.

Accordingly, the next studies focused on understanding the influence of compositional variations on structural, thermal and chemical properties of these glasses in an attempt to best optimize the parent compositions for their application *in vitro* and *in vivo*. While magnesium doping in glasses is best known to decrease their apatite forming ability owing to either its structural role as an intermediate oxide, thus increasing the polymerization in the glass network [3-5] or by competing with calcium for hydroxyapatite nucleation sites on the glass surface [6]; our work on influence of CaO/MgO ratio on sintering ability of diopside-fluorapatite glasses demonstrated degradation in sintering ability of investigated glasses with decreasing MgO content as the overall compositional chemistry shifted from diopside-fluorapatite binary join to diopside-fluorapatite-wollastonite ($CaO•SiO_2$) ternary system. A glass composition with 39.32 CaO – 13.60 MgO – 3.50 P_2O_5 – 42.41 SiO_2 – 1.17 CaF_2 (mol%) exhibited good sintering ability along with high residual glassy phase, thus qualifying for further experimentation as potential material for scaffold fabrication.

Alkali (Na_2O = 0 – 10 mol%) doping in these glasses at the expense of MgO resulted in interesting results where we could not observe significant influence of Na_2O on the silicate glass network but competition between sodium and calcium for coordination with orthophosphate component in glass was highly evident from ^{31}P NMR data, thus, showing the marked preference of alkali towards association with phosphate instead of silicate glass network in these glasses. Further, we experimentally validated the computational results of Tilocca [1] by demonstrating the preferential leaching of sodium over calcium from bioactive glasses in aqueous solutions and SBF, thus, inducing delayed hydroxyapatite formation and cellular apoptosis *in vitro* due to sudden outburst of alkali. Considering that conditions encountered by a biomaterial *in vitro* are significantly different than those encountered *in vivo* (static *vs* dynamic) and alkali-rich 45S5 Bioglass® has been used in >650,000 human patients [7], the concerns with cytotoxicity due to alkali-release from glasses may not be crucial for *in vivo* tissue engineering. However, they may not be the most suitable materials for application in *in vitro* tissue engineering.

With respect to the sintering ability of glasses, incorporation of sodium in glasses in small concentrations (~4 mol%) facilitates their sintering resulting in glass-ceramics with

flexural strength of ~190 MPa. Increasing alkali content in promotes crystallization which hinders their sintering, thus, resulting in poorly sintered, porous and mechanically weak glass-ceramics.

In the final study where we investigated two different series of glass compositions i.e. one with varying CaO/SiO_2 ratio and the second with varying P_2O_5/CaF_2 ratio for their molecular structure and sintering ability. In both the cases, varying network modifier – to – network former ratio did exhibit considerable impact on the glass structure. In the first series of glasses, increasing CaO/SiO_2 ratio effectively depolymerized the silicate glass network, while increasing P_2O_5/CaF_2 ratio in second series of glasses resulted in polymerizing the silicate glass network. Interestingly, phosphate component in both the glass series remained almost unaffected. While depolymerizing the silicate glass network with increasing CaO/SiO_2 ratio has been explained on the basis of increasing NBOs, increasing polymerization in silicate glass network with increasing P_2O_5/CaF_2 ratio may be attributed to the increasing amorphous phase separation in silicate and phosphate component in glasses where the latter has ability to rip off network modifying cations from the silicate glass network, thus, forcing it to re-polymerize. With respect to sintering ability of glasses, increasing network modifier – to – network former ratio in glasses (CaO/SiO_2 or CaF_2/P_2O_5) deteriorated their sintering ability and increased their crystalline content which is undesired for glass-ceramic scaffold fabrication.

In conclusion, we have tried to elucidate the fundamental science governing the chemical dissolution, thermal stability and bioactivity of phosphosilicate glasses from the perspective of their composition-structure-property relationships. In our opinion, alkali-free glass-ceramics in diopside-fluorapatite system are suitable for scaffold fabrication for their application in *in vitro* tissue engineering while the excellent biological efficacy of our glass composition 4.33 Na_2O – 30.30 CaO – 12.99 MgO – 2.60 P_2O_5 – 45.45 SiO_2 – 4.33 CaF_2 has been recently demonstrated [8].

References

[1] A. Tilocca, “Sodium migration pathways in multicomponent silicate glasses: Car–Parrinello molecular dynamics simulations,” *The Journal of Chemical Physics,* vol. 133, pp. 014701, 2010.

[2] L. Lefebvre, L. Gremillard, J. Chevalier, R. Zenati, and D. Bernache-Assolant, “Sintering behaviour of 45S5 bioactive glass,” *Acta Biomaterialia,* vol. 4, pp. 1894-1903, 2008.

[3] S. J. Watts, R. G. Hill, M. D. O'Donnell, and R. V. Law, “Influence of magnesia on the structure and properties of bioactive glasses,” *Journal of Non-Crystalline Solids,* vol. 356, pp. 517-524, 2010.

[4] A. Pedone, G. Malavasi, M. C. Menziani, U. Segre, and A. N. Cormack, “Role of magnesium in soda-lime glasses: insight into structural, transport, and mechanical properties through computer simulations,” *Journal of Physical Chemistry C,* vol. 112, pp. 11034-11041, 2008.

[5] A. Pedone, G. Malavasi, and M. C. Menziani, “Computational insight into the effect of CaO/MgO substitution on the structural properties of phospho-silicate bioactive glasses,” *Journal of Physical Chemistry C,* vol. 113, pp. 15723-15730, 2009.

[6] J. Perez-Pariente, F. Balas, and M. Vallet-Regi, “Surface and chemical study of SiO_2 center dot P_2O_5•CaO•(MgO) bioactive glasses,” *Chemistry of Materials,* vol. 12, pp. 750-755, 2000.

[7] L. L. Hench, D. E. Day, W. Holand, and V. M. Rheinberger, “Glass and Medicine,” *International Journal of Applied Glass Science,* vol. 1, pp. 104-117, 2010.

[8] D. U. Tulyaganov, M. E. Makhkamov, A. Urazbaev, A. Goel, and J. M. F. Ferreira, “Synthesis, processing and characterization of a bioactive glass composition for bone regeneration,” *Ceramics International,* vol. 39, pp. 2519-2526, 2013.

…….

Chapter 6. Future directions

In this section of the thesis, it is helpful to appreciate the fact that — though composition – structure – property relationships in bioactive glasses have been studied for long time — most of the studies published in this domain are riddled with complexity that makes a holistic understanding deceptively difficult. While significant progress has been made in the area of understanding the atomic and molecular structure of bioactive glasses—thanks to advancement in experimental and computational probes to explore glass structure—similar comments cannot be made for experimental studies describing biodegradation and chemical dissolution behaviour of bioactive glasses. While the hypothesis of 'apatite forming ability on glass surface in SBF as marker of bioactivity' is still a topic of debate, especially with the advent of concept of third generation biomaterials, most experimental studies evaluating *in vitro* bioactivity and dissolution behaviour of glasses tend to neglect some crucial aspects like thermal history, surface preparation, solution chemistry and glass/media combinations that can lead to potential complications and non-meaningful results. Based on our experience during the course of doctoral research and review of relevant literature, we have come across at least three major concerns that need to be carefully addressed for future studies in order to understand the mechanisms governing the bioactivity of glasses and to allow the design of novel glass compositions for scaffold fabrication.

(1) Surface chemistry of glasses: Since chemical dissolution (and bioactivity) of glass starts from the surface, the importance of surface chemistry in determining the dissolution kinetics of glasses cannot be neglected. However, considering the compositional complexity of multicomponent bioactive glasses, our understanding of the molecular structure of bioactive glass surfaces is very limited. In particular, it is rare to find an experimental or computational study describing the structural coordination of various moieties present on the glass surface and their impact on the macroscopic properties of bulk glass. Therefore, our future work will be focused mainly on understanding the influence of surface chemistry of glasses on their bioactivity.

(2) Influence of solution chemistry – While the relevance of apatite forming ability in SBF is still controversial, the protocols for studying chemical degradation of bioactive glasses and ceramics as defined in various ISO standards need to be reviewed. Most of the ISO standards (for example, ISO 10993-14:2001 – Biological evaluation of medical devices: Identification and quantification of degradation products from ceramics; ISO 23317:2014 – Implants for surgery –

In vitro evaluation for the apatite-forming ability of implant materials) recommend the usage of buffered solutions in order to: (i) resist pH changes in the solution media due to glass dissolution; (ii) simulate the buffered fluids encountered by a biomaterial in human body. However, considering that (i) most of these experiments are conducted in static media and (ii) buffered aqueous solutions comprise mixture of both organic and inorganic salts, these experiments can be subject to complications that lead to significant error. Since the human physiological system is a dynamic system, the results obtained in static conditions do not simulate the actual conditions encountered by a biomaterial *in vivo* primarily due to errors generated by solution feedback effect. Further, organic ions in buffered solutions tend to chelate with silicate and aluminium ions (released from the glass into contact solution) while alkali ions already present in the solution tends to slow down the process of chemical dissolution by shifting the equilibrium of ion exchange reaction ($\equiv Si - O - Na + H_3O^+ \leftrightharpoons \equiv Si - OH + Na^+ + H_2O$) towards the left, thus, affecting the overall dissolution kinetics and chemical degradation of the system. Therefore, new experimental protocols need be defined where solution chemistry has minimal impact on the dissolution kinetics of glasses. Our future work will also be focused in this direction.

(3) Fabrication of glass-ceramic scaffolds by rapid prototyping: With respect to fabrication of 3D porous glass-ceramic scaffolds for tissue engineering applications, recent advancements in the field of rapid prototyping (particularly with direct write assembly) have paved the way for fabrication of scaffolds with hierarchical pore structure. As discussed in this dissertation, we are at a stage where we have designed suitable glass composition with requisite properties desired for a scaffold. Further research in this domain will be focused on understanding the rheology of suspensions prepared from these glass compositions in order to create inks for direct write assembly.

…….